Title
Mechanisms of the Human Telomerase Catalytic Cycle

Author
Wu, Robert Alexander

Publication Date
2016

Peer reviewed|Thesis/dissertation

Mechanisms of the Human Telomerase Catalytic Cycle

By

Robert Alexander Wu

A dissertation submitted in partial satisfaction of the

requirements for the degree of

Doctor of Philosophy

in

Molecular and Cell Biology

in the

Graduate Division

of the

University of California, Berkeley

Committee in charge:

Professor Kathleen Collins, Chair
Professor Donald C. Rio
Associate Professor Andreas Martin
Professor David E. Wemmer

Spring 2016

Abstract

Mechanisms of the Human Telomerase Catalytic Cycle

by

Robert Alexander Wu

Doctor of Philosophy in Molecular and Cell Biology

University of California, Berkeley

Professor Kathleen Collins, Chair

At the ends of every linear chromosome, genomic integrity is threatened by incomplete DNA synthesis by the replisome and the potential for inappropriate DNA break repair. Eukaryotic cells control these reactions through the function of telomeres. Maintenance of the characteristic DNA repeat tracts that form telomeres requires the specialized reverse transcriptase telomerase, with its active site in the protein subunit TERT and the template for DNA synthesis in the integral RNA subunit. Many telomerases can extend a chromosome 3' end by processive addition of single-stranded repeats. This processive telomeric repeat synthesis requires a specialized telomerase catalytic cycle, involving nucleic acid handling specificities not found in any other polymerase. Developing new approaches of subunit fluorescence labeling for single-molecule analysis, I show that human telomerase reconstitution generates mixtures of complexes of varying TERT subunit stoichiometry but activity requires a complex containing only one TERT molecule. This establishes conservation of active telomerase subunit architecture across phylogeny. Using TERT and RNA domain-complementation assays to sensitize for primer-template duplex use by the telomerase active site and a direct footprinting assay for telomerase association with product DNA, I uncover mechanisms by which TERT domains and RNA motifs interact to specify telomeric repeat synthesis. This work develops a new model for specialized primer-template duplex sensing during the human telomerase catalytic cycle.

In memory of Robert Mowshyoung Wu

TABLE OF CONTENTS

LIST OF FIGURES

LIST OF ABBREVIATIONS

^{32}P	phosphorus-32
ATM	ataxia telangiectasia mutated
ATP	adenosine triphosphate
ATR	ataxia telangiectasia and Rad3-related protein
bp	base pair
CHAPS	3-[(3-Cholamidopropyl)dimethylammonio]-1-propanesulfonate hydrate
Ci (mCi, mCi)	curie (microcurie, millicurie)
C-terminus	carboxyl-terminus
Cy3, Cy5	cyanine 3, cyanine 5
Da (kDa)	dalton (kilodalton)
ddNTP	dideoxynucleotide
DNA	deoxyribonucleic acid
dATP	deoxyadenosine triphosphate
dCTP	deoxycytidine triphosphate
ddATP	dideoxyadenosine triphosphate
ddCTP	dideoxycytidine triphosphate
ddGTP	dideoxyguanosine triphosphate
ddTTP	dideoxythymidine triphosphate
dGTP	deoxyguanosine triphosphate
dNTP	deoxynucleoside triphosphate
DTT	dithiothreitol
dTTP	deoxythymidine triphosphate
EDTA	ethylene diamine tetraacetic acid
EGTA	ethylene glycol tetraacetic acid
g (ng, μg, mg)	gram (nanogram, microgram, milligram)
HEK	human embryonic kidney
HEPES	4-(2-Hydroxyethyl)piperazine-1-ethanesulfonic acid
HIV	human immunodeficiency virus
K_d	dissociation constant
K_M	Michaelis-Menton constant
l (μl, ml)	liter (microliter, milliliter)
LTR	long terminal repeat
M (nM, μM, mM)	molar(ity) (nanomolar, micormolar, millimolar)
N-terminus	amino-terminus
NP-40	nonidet P-40
NTP	nucleoside triphosphate
PAGE	polyacrylamide gel electrophoresis
PMSF	phenylmethane sulfonyl fluoride
RNA	ribonucleic acid

RNase	ribonuclease
SDS	sodium dodecyl sulfate
Tris	tris(hydroxymethyl)aminomethane

ACKNOWLEDGMENTS

I am privileged to have met many people who have made doing science not only possible but also a great pleasure. I am exceedingly indebted to my advisor and mentor, Kathy Collins. It seems impossible to express just how fortunate I feel to have had the opportunity to work with and learn from Kathy. Of course, her intelligence, knowledge and passion about telomerase biochemistry and science generally are unmatched. These traits are obvious to anyone who meets her. But what I've discovered after facing many challenges over many years with Kathy is that her formidable scientific skill is matched with her great compassion. She gave encouragement when I felt depressed or tired and toughness when I instead slipped into sloppiness or self-pity. The discerning way she interacts with all of her students is perhaps what has impressed me most. I know that I would have been lost during and after graduate school without her wise guidance and I am grateful beyond words for the greatest teacher I could ever hope to have found.

Being a Collins "Labbite" has also meant that I have been blessed with many wonderful colleagues. On occasions so numerous it is senseless to give specific examples, this talented and dedicated group of people has helped me with my experiments, generously provided materials and protocols, asked the right question at the right time or given a key insight into a confusing experiment, gifted me their food, graciously listened to me complain, picked me up from the airport and taken me to the doctor. It is traditional in this section to list ones labmates individually with a tidbit or two about each one. However, this seems needlessly limiting because I can certainly say that each of them has done all of these things for me. You are all my true friends.

I have also received great support from my thesis committee members Don Rio, Andy Martin and Dave Wemmer, as well as Dirk Hockemeyer. I am grateful for their continued interest in my projects, valuable questions and suggestions, encouragement and support.

Finally, I wish to thank my family and friends outside of the lab. I imagine I would have given up a long time ago without the steady and loyal support each has given me. Most of all, every good thing I have been able to do in my life is possible through the love and caring of my mother and sister. I cannot thank them enough.

CHAPTER ONE

Telomeric Repeat Synthesis by the Telomerase Ribonucleoprotein

The Ends of Linear Chromosomes: Problems and Solutions

The evolution of linear chromosomes has been suggested to be a prerequisite for the diversification of the eukaryotic chromosome by facilitating genetic exchange between DNA molecules (Volff and Altenbuchner, 2000) and meiosis (Ishikawa and Naito, 1999). But despite this advantage, chromosome linearity poses significant difficulties for the cell. One set of challenges, collectively called the end-protection problem, arises from how cells typically respond to free DNA ends. These processes are essential to preserve genome integrity at sites of damage but have the opposite effect at linear chromosome ends. For example, the breakage of both strands of DNA is a serious form of damage that triggers the activation of the DNA damage response (Ciccia and Elledge, 2010). The cell possesses diverse pathways for repairing double stranded breaks, which all lead to the rejoining of the free ends (Chapman et al., 2012). However, cells possessing linear chromosomes must distinguish the natural chromosome ends from damage-induced double stranded breaks to prevent these pathways from fusing chromosome ends (Muller, 1938; McClintock, 1941; McClintock, 1942; Doksani and de Lange, 2014), a severely detrimental event that would ultimately result in chromosomal instability, aneuploidy, and cell death (Tusell et al., 2010; Murnane, 2012). Free DNA ends may also be processed by a host of nucleases which, if allowed to act unregulated, would threaten to erode essential genetic information (Mimitou and Symington, 2009).

Another challenge, known as the end-replication problem, stems from the fact that all natural DNA polymerase enzymes are unidirectional, extending a DNA strand only at its free 3'-hydroxyl group (Steitz, 1999). Thus while the replicative DNA polymerases are competent to copy (almost) the entire genome, they cannot replicate beyond the position of the last RNA primer placed closest to the chromosome end on the lagging strand. Every round of DNA replication therefore results in the loss of terminal sequence which eventually leads to the loss of essential genetic information. The end-replication problem was originally predicted for blunt-ended DNA molecules (Watson, 1972; Olovnikov, 1973). It has since been observed that the ends of eukaryotic chromosomes in fact have single-stranded 3' overhangs (Henderson and Blackburn, 1989; Wellinger et al., 1993; McElligott and Wellinger, 1997). Insufficient replication has been shown to lead to loss of sequence with leading strand synthesis when the new 3' overhang is generated (Soudet et al., 2014).

With very limited exceptions, eukaryotes manage these challenges through the function of telomeres, nucleoprotein complexes at the ends of linear chromosomes. The nucleic acid component typically consists of a repetitive sequence of short tandem repeats. Across eukaryotes, there are variations in telomeric repeat sequence, length, number, and how precisely they are defined (Blackburn, 1990). However, in general the strand constituting the single-stranded 3' overhang is G-rich, as exemplified by the vertebrate telomeric repeat sequence, 5'-TTAGGG-3' (Moyzis et al., 1988). Telomere function also

requires protein complexes that associate specifically with telomeric DNA repeats. A high degree of diversity exists among the telomere-associated proteins across organisms (Linger and Price, 2009). In mammals, the telomere-specific six-protein complex called shelterin is essential to the function of telomeres (Palm and de Lange, 2008) and exemplifies how the DNA and protein components of the telomere function together to counteract the end-protection and end-replication problems. For example, adverse DNA repair and processing events are prevented at chromosome ends by shelterin-mediated repression of nucleases and the DNA damage response-activating kinases, ATM and ATR (d'Adda di Fagagna et al., 2004; Palm and de Lange, 2008). Higher-order architectures, mediated by shelterin interactions and/or adopted by telomeric DNA, including t-loops (lariat structures formed via duplex invasion by the single-stranded 3' overhang), may also contribute to the inhibition of unwanted repair or processing events (Griffith et al., 1999; de Lange, 2004), although their precise roles and mechanisms remain less well understood. Telomeres also provide a solution to the end-replication problem provided they can be elongated to counterbalance the gradual shortening resulting from conventional replication. In fact, it would be shown that telomere maintenance requires de novo enzymatic synthesis (see below).

Enzymatic Addition of Telomeric Repeats

Several lines of evidence emerging from the physical characterization of chromosome ends suggested that telomeres are synthesized and maintained by a mechanism distinct from general genome replication. First, telomeres appeared to be subject to lengthening and shortening processes. The telomeres across a diversity of organisms were found to be heterogeneous in length, consisting of a varying number of telomeric repeats (Blackburn and Gall, 1978; Johnson 1980; Emery and Weiner, 1981; Szostak and Blackburn, 1982) and trypanosome telomeres were observed to gradually elongate over multiple cell divisions (Bernards, et al., 1983). In addition, it was found that new telomere sequences are generated on macronuclear DNA molecules of the ciliate *Tetrahymena thermophila* during the development of the macronucleus (Blackburn et al., 1983). Various models for telomere synthesis were proposed, including pathways involving terminal hairpin structures (Blackburn and Gall, 1978; Bernards et al., 1983) and recombination (Heumann, 1976; Goldbach et al., 1979). However, these hypotheses proved insufficient to explain the observation that a linear plasmid derived from *T. thermophila* ribosomal DNA was appended with yeast telomeres when maintained in *Saccharomyces cerevisiae* (Szostak and Blackburn, 1982; Shampay et al., 1984).

These observations prompted the prediction of a telomeric repeat terminal transferase (Shampay et al., 1984). The activity of this hypothetical enzyme was subsequently detected in *T. thermophila* extract, capable of adding tandem telomeric repeats to single-stranded oligonucleotide primers that resemble the single-stranded 3' overhang at telomeres (Greider and Blackburn, 1985). The newly discovered enzyme was named “telomerase” (Greider and Blackburn, 1987). Telomerase activity is not detected in non-immortalized human cell lines experiencing gradual telomere shortening (Counter et al., 1992) and ectopic expression of telomerase in cells lacking telomerase activity induces telomere elongation (Bodnar et al., 1998), establishing the link between telomere

maintenance and telomerase activity. While alternative mechanisms for telomere maintenance that do not require telomerase have been identified (for example, retrotransposition in dipteran insects including *Drosophila melanogaster* (Biessmann and Mason, 1997) and recombination-mediated pathways in *S. cerevisiae* (Lundblad and Blackburn, 1993) and some human tumors (Bryan et al., 1997)), the vast majority of eukaryotic organisms have proven to rely on the action of telomerase at chromosome ends for telomere maintenance.

Telomerase: A Ribonucleoprotein Reverse Transcriptase

Telomerase was quickly identified as a ribonucleoprotein (RNP) complex, as demonstrated by the presence of a specific RNA species copurifying in *T. thermophila* fractions with telomerase activity and the sensitivity of the enzymatic activity to both proteinase K and RNase A (Greider and Blackburn, 1987). Surprisingly at the time, the RNA subunit was found to contain the sequence 5'-CAACCCCAA-3' which was recognized as the potential template of the telomeric repeats (5'-TTGGGG-3') synthesized by the enzyme (Greider and Blackburn, 1989). Mutation of the 5'-CAACCCCAA-3' sequence in *T. thermophila* resulted in the synthesis of new telomere sequences in vivo (Yu et al., 1990), confirming that telomerase is in fact a reverse transcriptase. Notably, telomerase carries its template internally within an integral RNA subunit, generally termed Telomerase RNA (TER).

Given its activity of DNA synthesis directed by an internal RNA template, telomerase was labeled a "specialized reverse transcriptase" (Shippen-Lentz and Blackburn, 1990). However, knowledge of the nature of the telomerase active site was much slower to emerge. Indeed, early speculation proposed that TER might act as a ribozyme (Gall 1990), reminiscent of the catalytic *T. thermophila* self-splicing intron. However, cloning of the p123 protein subunit of the *Euplotes aediculatus* telomerase RNP and analysis of Est2p, its homolog in *S. cerevisiae,* led to the revelation that these telomerase protein subunits share conserved reverse transcriptase-specific motifs with LTR-retrotransposable element, mobile group II intron-encoded and HIV-1 reverse transcriptases (Lingner et al., 1997). This established that telomerase catalyzes deoxyribonucleotide transfer by a mechanism similar to other reverse transcriptases in an active site contained within the protein subunit. Therefore, the telomerase protein subunit has been given the general name Telomerase Reverse Transcriptase (TERT).

In the following years, the TERT and TER subunits of telomerases from a broad range of species have been identified, including those of the human telomerase RNP (Podlevsky et al., 2008). In all telomerases studied so far, TERT contains the active site that catalyzes reverse transcription of a template internal within TER, synthesizing single-stranded telomeric repeats. Therefore, it is perhaps unsurprising that TERTs and TERs from organisms ranging from fungi to ciliates to vertebrates share several general features (Blackburn and Collins, 2011). As mentioned above, sequence alignment of diverse TERTs to other reverse transcriptases reveal seven shared motifs which are critical for catalytic function (Lingner et al., 1997; Nakamura and Cech, 1998). In addition, TERTs also possess an RNA-binding domain N-terminal to the reverse transcriptase domain

which binds TER and a C-terminal extension which is involved in interaction with the template-primer duplex in conjunction with the reverse transcriptase motifs (Podlevsky and Chen, 2012). The RNA-binding domain and the C-terminal extension form protein-protein interactions that, possibly with contributions from protein-RNA interactions with TER, close these three domains into a ring-shaped RNP, termed the ring RNP (Gillis et al., 2008; Robart and Collins, 2011). Most TERTs also have a telomerase-specific domain N-terminal to the RNA-binding domain, known as the TEN domain (Podlevsky et al., 2008). The TEN domain plays roles in several important features of telomerase function, including catalysis (Jurczyluk et al., 2010; Wyatt et al., 2010; Bairley et al., 2011; Eckert and Collins, 2012; Wu and Collins, 2014a), repeat addition processivity (Moriarty et al., 2004; Robart and Collins, 2011; Wu and Collins, 2014a) and telomerase recruitment to the telomere via interaction with shelterin (Zaug et al., 2010; Sexton et al., 2012; Schmidt et al., 2014). The TEN domain is connected to the ring RNP by a linker region, which varies dramatically in length and sequence among species (Podlevsky et al., 2008) and has no apparent catalytic contribution (Wu et al., 2015). The domain architecture of human TERT is illustrated in Figure 1.1A.

Despite substantial sequence and size divergence, TERs across species share several general features required for catalysis (Blackburn and Collins, 2011). The obvious feature common to all TERs is the template for telomeric repeat synthesis. Additionally, a pseudoknot with a common fold is found adjacent to the template in TERs from ciliates, yeasts and vertebrates (Blackburn and Collins, 2011; Zhang et al., 2011). The precise function of the conserved pseudoknot is not fully understood, but its presence is required for interactions with TERT that are important for establishing an RNP architecture competent for telomerase activity (Robart and Collins, 2011; Wu and Collins, 2014a). Thus its involvement may be in positioning TERT domains and the TER template in the proper positions relative to one another. TERs also feature a stem loop or stem junction that provides the high-affinity binding site for the TERT RNA-binding domain (Mitchell and Collins, 2000; Lai et al., 2001; Livengood et al., 2002). Finally, additional TER elements also stimulate catalytic activity, as exemplified by *T. thermophila* loop IV (Mason et al., 2003) or human TER (hTR) P6.1 (Chen et al., 2002). These elements act in a manner independent of TERT binding, but like the pseudoknot may instead be important for creating the precise RNP architecture required for catalysis. The secondary structure of hTR is illustrated in Figure 1.1B.

In vivo, telomerases function as holoenzymes containing subunits in addition to TERT and TER. As a result, TERs also contain motifs that are not required for catalysis but instead are critical for the formation of the holoenzyme (Egan and Collins, 2012a). The holoenzyme proteins and the associated TER motifs that they bind are very diverse across phylogenetic groups, but in general they function in telomerase RNP assembly, localization, and recruitment to the telomere. The human telomerase holoenzyme contains two sets of H/ACA proteins (dyskerin, NHP2, NOP10 and GAR1) and the Cajal body localization factor TCAB1 (Egan and Collins, 2012a; Podlevsky and Chen, 2012; Schmidt and Cech, 2015).

The Unique Specificities of Telomerase Activity

A variety of reverse transcriptases besides telomerase are found throughout nature, including those encoded by retrotransposons, group II introns, and retroviruses (Eickbush and Jamburuthugoda, 2008). Like DNA-dependent DNA polymerases, these reverse transcriptases generate double-stranded product via monotonous progression along their templates (Xi and Cech, 2015). In contrast, the immediately observable in vitro activity of most telomerase enzymes is the addition of single-stranded tandem telomeric repeats to substrates resembling the 3' overhang that exists at chromosome ends (Collins, 2011), most simply single-stranded DNA oligonucleotide primers with the G-rich telomeric sequence characteristic of the particular species. For most telomerases, including the human and ciliate enzymes, each encounter with the DNA substrate can result in the addition of multiple repeats (Blackburn and Collins, 2011). That is, these telomerases synthesize the addition of telomeric repeats processively, a property known as repeat addition processivity (RAP). That these multiple repeats are added processively and not as the product of multiple telomerase enzymes encountering the same substrate molecule sequentially has been demonstrated by the synthesis of multiple repeats on an individual primer molecule even when the primer is present in vast molar excess relative to the enzyme (Greider, 1991). The significance of RAP for the maintenance of human telomere length homeostasis is not completely understood due to the challenge of specifically inhibiting RAP without simultaneous alteration of overall telomerase activity and the likelihood that whether telomeric repeat synthesis in a cell is processive or distributive is influenced by the level of telomerase expression. With these caveats, partial RAP inhibition in human telomerase by a chemical inhibitor (Damm et al., 2001; Pascolo et al., 2002) or disease-associated TERT mutation (Robart and Collins, 2010) leads to telomere shortening, suggesting that in vivo RAP is necessary for telomerase-mediated telomere length maintenance.

Consequently, the biochemical activities of telomerase that distinguish it from the other known reverse transcriptases are the generation of single-stranded instead of double-stranded product and reiteratively copying a short template rather than continuous progression along RNA (Collins, 2011). Repeat addition processivity by telomerase implies a telomerase catalytic cycle (Figure 1.2). This catalytic cycle comprises features common to other DNA polymerases (e.g. catalysis of deoxyribonucleotide transfer to the primer strand 3' hydroxyl group) or other reverse transcriptases (e.g. active site handling of an RNA template-DNA primer duplex) as well as multiple unique specializations for nucleic acid handling not found in other polymerases:

1. Separating the Primer and Template Strands

Upon completion of a telomeric repeat (Figure 1.2, Step 1), RAP obliges a mechanism for the separation of the completed DNA product from the RNA template strand (Figure 1.2, Step 2). To date, detailed description of the mechanism of this thermodynamically unfavorable transaction remains elusive. However, models invoking the contribution of compressing and stretching of template-flanking RNA (Berman et al., 2011), forming secondary structure within product DNA (Yang and Lee, 2015), escape of the primer-

template duplex from the active site (Qi et al., 2012; Wu and Collins, 2014a) or DNA-protein interactions (Wu and Collins, 2015) have been proposed and await further testing. The precise number of base-pairs that must be melted is unknown for human telomerase, but studies in yeast telomerase (Förstemann and Linger, 2005) suggest that the telomerase active site may only permit the formation of less than maximal length of primer-template duplex at any point during repeat synthesis, due to product dissociation at the 3' end of the template during synthesis across the template.

2. DNA Product Handling Independent of Template Base-Pairing

During the process of strand separation, DNA product must be retained by the enzyme to avoid complete substrate dissociation. Since the DNA is unpaired from the template during this step of the catalytic cycle, the enzyme-product interaction must be distinct from primer-template Watson-Crick base-pairing (Collins and Greider, 1993). This interaction defines the telomerase "anchor site," although this functional definition does not imply the nature of the interaction (for example, whether it involves an interaction between the DNA and TERT and/or TER or whether it involves a specific location with respect to the DNA or the telomerase RNP). An additional putative function of the anchor site may be to control when (at which step of the catalytic cycle) and how (by nucleotide or by repeat) the product DNA is released by the enzyme.

3. Defining a TER Region for Primer Interaction

The function of the telomerase anchor site permits the repositioning of the unpaired template relative to the active site (Figure 1.2, Step 3), which is followed by the formation of a new primer-template duplex (Figure 1.2, Step 4). The new duplex is now poised for re-engagement by the active site for synthesis of the next repeat (Figure 1.2, Step 2). Primer-template duplex reformation necessitates that the TER region used for primer interaction, usually referred to as the "template," actually consist of two regions: a 5' region that directs deoxyribonucleotide addition and a 3' region that aligns the primer by base-pairing (Chen and Greider, 2003; Drosopoulos et al., 2005). Indeed, the template regions of most TERs consist of the complementary sequence of one and a half to two times the telomeric repeat sequence, and nucleotide substitutions within the non-templating alignment region can negatively impact RAP (Drosopoulos et al., 2005). Optimal primer-template duplex reformation also requires strict definition of the TER region that is used as template. If synthesis is allowed to bypass the template boundary, realignment with the 3' alignment region may become inefficient. Studies performed in ciliate and yeast telomerases indicate that a stem 5' of the template region enforces the template boundary by sterically preventing template-flanking RNA from traversing the active site (Tzfati et al., 2000; Lai et al., 2002; Chen and Greider, 2003). Within the vertebrate enzymes, human telomerase also possesses an RNA stem 5' of the template region while mouse telomerase does not (Podlevsky et al., 2008). Signals within the template sequence itself may also contribute to catalytic specificity, as substitutions within the templating region of TER have been shown to impact a range of telomerase enzymatic properties including efficiency of catalysis (Gilley and Blackburn, 1996), rate

of enzyme turnover (Hardy et al., 2001), fidelity (Lin et al., 2004), or primer dissociation (Drosopoulos et al., 2005; Brown et al., 2014).

Physical Determinants of the Telomerase Catalytic Cycle

The studies presented here aim to understand the mechanisms by which human telomerase achieves its catalytic cycle. In vivo, telomerases across species function as holoenzymes consisting of TERT, TER and other proteins. In some telomerases, these holoenzyme proteins can profoundly impact characteristics of telomerase catalysis, such as rate and processivity. This can be the result of product DNA handling by holoenzyme proteins (Min and Collins, 2010) and/or allosteric influence on the TERT-TER catalytic RNP (Eckert and Collins, 2012; Hong et al., 2013). However, the basic features of the human telomerase catalytic cycle are fully reconstituted by a complex consisting only of TERT and hTR as evidenced by the detection of RAP products in heterologously expressed complexes in rabbit reticulocyte lysates (RRL; Weinrich et al., 1997) or *Escherichia coli* (Hansen et al., 2016). Therefore, the physical determinants of the individual biochemical specificities that produce the telomerase catalytic cycle must be contained within TERT and hTR.

As described in the previous section, the telomerase catalytic cycle comprises both features in common with and distinct from other reverse transcriptases. Reverse transcriptases and TERT share seven motifs which are required for primer and template strand interaction within the active site and magnesium-ion coordination involved in deoxyribonucleotide transfer (Steitz and Steitz, 1993; Lingner et al., 1997; Nakamura and Cech, 1998). The reverse transcriptases encoded by HIV-1, L-1 non-LTR retrotransposable element, and mobile group II intron act as complexes containing two copies of the reverse transcriptase protein (Kohlstaedt et al., 1992; Yang and Eickbush, 1998; Rambo and Doudna, 2004). Answering the question of whether the functional human telomerase active site similarly obliges dimerization of TERT subunits is fundamental toward understanding all other aspects of telomerase catalytic cycle mechanism. Unfortunately, biochemical approaches have not yielded a satisfying answer due to their inherent limitations when used with heterogeneous populations. In Chapter Two, we employ a single-molecule fluorescence imaging approach to resolve this issue. This allows us to understand the telomerase catalytic cycle as the function of one TERT with one hTR.

Biochemical specificities unique to telomerase are expected to require TERT domains or motifs that are specific to telomerase, TER domains, or functional interactions between these. For example, the telomerase-specific TERT TEN domain has received much attention for its potential role in mediating anchor site function. Substitutions within the TEN domain alter RAP (Moriarty et al., 2004; Romi et al., 2007; Zaug et al., 2008). The high-resolution structure of the *T. thermophila* isolated TEN domain reveals a charged groove speculated to accommodate single-stranded DNA product (Jacobs et al., 2006). Functionally, a human telomerase RNP lacking the TEN domain is capable of synthesizing one repeat but is incompetent for RAP while complementation with a TEN domain in trans restores RAP activity (Robart and Collins, 2011). On the other hand,

direct evidence for a site within the TEN domain that binds product DNA is lacking. Within TER, the pseudoknot may also contribute to the mechanism of RAP, as evidenced by impact of substitutions within the hTR pseudoknot on RAP (Ly et al., 2003; Chen and Greider, 2005; Robart and Collins, 2010). Interestingly, a substitution within the hTR pseudoknot prevents TEN domain trans-complementation of RAP (Robart and Collins, 2011), indicating that a network of protein-RNA and/or protein-protein interactions in the telomerase RNP are crucial for catalytic cycle mechanisms. However, understanding these interactions at a mechanistic level has been challenging. One difficulty is that standard methods such as mutagenesis may have multiple simultaneous effects in the context of a network of interactions. As described in Chapter Three, these caveats can be avoided by reconstituting the enzyme in a manner that allows for the isolated assay of the contributions of individual domains or interactions. These studies provide insight into the mechanisms of the human telomerase catalytic cycle.

Figure 1.1 Schematic of human telomerase subunits TERT and hTR.

(**A**) Schematic of the domain architecture of human TERT. The residues at the domain boundaries are indicated. The seven conserved reverse transcriptase motifs 1, 2, A, B, C, D, and E are shown in green.
(**B**) Secondary structure of hTR. The sequence of the region that specifies the template is boxed.

Figure 1.1

A

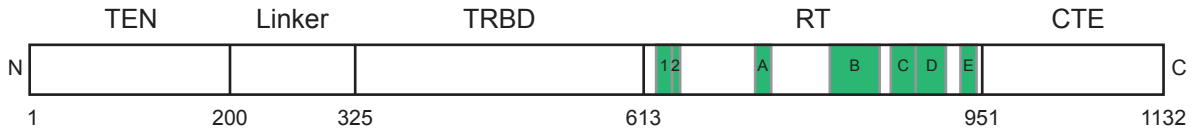
TEN
Linker
TRBD
RT
CTE
N
C
1 2
A
B
C
D
E
1
200
325
613
951
1132

B

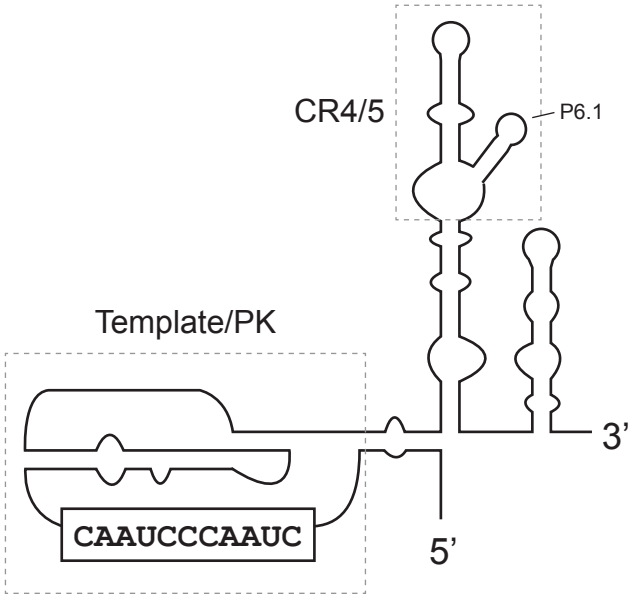
CR4/5
P6.1
Template/PK
3’
CAAUCCCAAUC
5’

Figure 1.2 The telomerase catalytic cycle.

Schematic of the telomerase catalytic cycle. After primer (blue) extension directed by the RNA template (green box) synthesizes a telomeric repeat (Step 1), enforcement of the template 5' boundary is followed by separation of primer and template strands (Step 2). The template is recycled by repositioning relative to the active site while the DNA product remains associated with the enzyme (Step 3). A new primer-template duplex can form (Step 4), allowing for processive addition of multiple repeats.

Figure 1.2

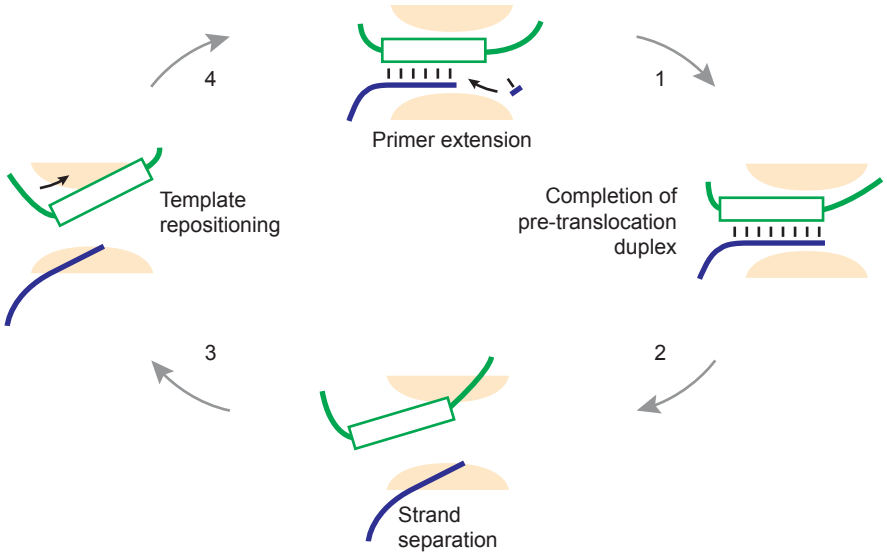
Primer extension
1
Completion of
pre-translocation
duplex
2
Strand
separation
3
Template
repositioning
4

CHAPTER TWO

Single-Molecule Imaging of Telomerase Reverse Transcriptase in Human Telomerase Holoenzyme and Minimal RNP Complexes

Based on Wu et al., *eLife*, 2015

Abstract

A fundamental question concerning human telomerase mechanism is whether catalytic activity requires cooperation across two TERT subunits. In this chapter, I describe studies that use new approaches of subunit labeling for single-molecule imaging, applied to determine the TERT content of complexes assembled in cells or cell extract. Surprisingly, telomerase reconstitutions yielded heterogeneous DNA-bound TERT monomer and dimer complexes in relative amounts that varied with assembly and purification method. Among the complexes, cellular holoenzyme and minimal recombinant enzyme monomeric for TERT had catalytic activity. Dimerization was suppressed by removing a TERT domain linker with atypical sequence bias, which did not inhibit cellular or minimal enzyme assembly or activity. I thus define human telomerase DNA binding and synthesis properties at single-molecule level and establish conserved telomerase subunit architecture from single-celled organisms to humans.

Introduction

The active human telomerase RNP includes TERT, which provides the enzyme active site, and hTR containing a reiteratively copied internal template. As introduced in Chapter One, unique repeat addition processivity of telomerase requires conserved domains in both TERT and hTR that distinguish telomerases from other polymerase families (Blackburn and Collins, 2011; Podlevsky and Chen, 2012). The TERT N-terminal (TEN) domain allows retention of single-stranded DNA during the template repositioning required for tandem repeat synthesis. TEN-domain-truncated TERT, designated "TERT ring" based on *Tribolium castaneum* TERT structure (Gillis et al., 2008), supports only single-repeat synthesis that can be complemented to high repeat addition processivity by the TEN domain as a separate polypeptide (Robart and Collins, 2011; Wu and Collins, 2014a). In addition to these and other catalytic activity requirements for TERT and hTR, a biologically functional human telomerase holoenzyme contains two sets of H/ACA proteins (dyskerin, NHP2, NOP10 and GAR1) bound to hTR to direct RNP biogenesis and TCAB1 to redistribute the RNP from nucleoli to Cajal bodies (Egan and Collins, 2012a; Podlevsky and Chen, 2012; Schmidt and Cech, 2015). Telomerase holoenzyme must also assemble with the shelterin protein TPP1 for telomere recruitment and extension of chromosome ends (Nandakumar and Cech, 2013; Lue et al., 2013; Sexton et al., 2014).

Endogenous human telomerase is scarce, with the number of TERT-hTR complexes per cell estimated as only ~35 (Cohen et al., 2007) or ~250 (Xi and Cech, 2014) in even the most highly telomerase-positive tumor cell lines. Consequently, biochemical investigations of human telomerase have been greatly facilitated by enzyme reconstitution. Enzyme reconstitution in cells exploits transiently introduced plasmids to overexpress TERT and the 451-nucleotide mature hTR, which must be 3'-processed from an appropriate precursor (Mitchell et al., 1999; Fu and Collins, 2003). Telomerase complexes reconstituted in cells have a diversity of substoichiometric associated factors (Egan and Collins, 2012a; Nandakumar and Cech, 2013; Schmidt and Cech, 2015). As an alternative reconstitution approach, a minimal-subunit catalytically active RNP can be assembled by expressing TERT in RRL with in vitro transcribed full-length hTR (Weinrich et al., 1997) or a half-sized RNA such as hTRmin used here (Wu and Collins, 2014a), which lacks the two-hairpin H/ACA motif that assembles the holoenzyme subunits dyskerin, NHP2, NOP10, GAR1 and TCAB1. Only two hTR domains are critical for telomerase catalytic activity: a domain containing the template and adjacent pseudoknot and a branched stem-junction domain containing stem-loop P6.1 (Mitchell and Collins, 2000; Chen et al., 2002). Importantly, human telomerase enzymes reconstituted in cells or in RRL can interact with the same length of single-stranded DNA, have similar specific activity and have only minor differences in other enzyme properties such as repeat addition processivity (Jurczyluk et al., 2010; Zaug et al., 2013; Wu and Collins, 2014a).

Central to defining telomerase RNP architecture is a delineation of the number of TERT and hTR subunits that assemble together to generate an enzyme active site. RNP affinity purification and structural studies indicate a single RNA and single TERT per

biologically functional telomerase holoenzyme of single-celled eukaryotes (Livengood et al., 2002; Witkin and Collins, 2004; Cunningham and Collins, 2005; Jiang et al., 2013; Hong et al., 2013; Bajon et al., 2015). This subunit stoichiometry is recapitulated by the minimal *T. thermophila* telomerase RNP assembled in RRL (Bryan et al., 2003). However, the subunit stoichiometry of an active human telomerase RNP is unresolved: some assays suggest TERT and hTR function as monomeric subunits, without dominant-negative inhibition of a wild-type subunit by coexpressed mutant subunit (Errington et al., 2008; Egan and Collins, 2010) while other assays suggest obligate co-dependence of active site function across TERT and hTR subunits (Wenz et al., 2001; Sauerwald et al., 2013). Size fractionation of human telomerase holoenzyme has been suggested to establish TERT dimerization based on molecular mass by gel filtration of ~600 kDa (Wenz et al., 2001) or by glycerol gradient sedimentation of 550 kDa (Schnapp et al., 1998) or 670 kDa (Cohen et al., 2007) relative to protein standards, but similar fractionation would be predicted for a holoenzyme with a single TERT, single hTR, single TCAB1 and a complex of dyskerin, NHP2, NOP10 and GAR1 bound to each of two H/ACA-motif hairpin stems (Egan and Collins, 2012a). Analysis using single-molecule fluorescence correlation spectroscopy detected one TERT and one hTR per RRL-reconstituted minimal RNP (Alves et al., 2008). On the other hand, cellular subunit overexpression, purification and crosslinking yielded particles observed by electron microscopy that were proposed to be active dimeric TERT RNPs, based on detection of two bound single-stranded DNAs (Sauerwald et al., 2013). Unfortunately, all of the experiments above suffer from the caveat that individual complexes are inferred to have the activity measured only for a bulk population.

Single-molecule fluorescence microscopy can detect the number of subunits in individual macromolecular complexes. We therefore developed a single-molecule TERT labeling strategy to determine the TERT subunit content of human telomerase RNPs assembled and purified using methods typical in previous studies. We exploited the preserved function of N-terminally tagged human TERT to introduce the acyl carrier protein (ACP) tag for covalent labeling by prosthetic group transfer from derivatives of Coenzyme A (CoA). ACP and ACP-based tags are well suited to the applications developed here because they are small, monomeric and expose the conjugated prosthetic group as a conformationally dynamic extension from the protein surface (Byers and Gong, 2007; Chan and Vogel, 2010). We applied previously developed tag labeling methods (Yin et al., 2006; Zhou et al., 2007) to investigate the TERT content of individual complexes from purifications of cellular telomerase holoenzyme reconstituted by assembly in human 293T cells and minimal recombinant RNP reconstituted by assembly in RRL. Surprisingly, different affinity purifications yielded different mixtures of complexes monomeric or variously multimeric for TERT. TERT complexes were also heterogeneous in catalytic activity and DNA binding properties. Complexes with TERT monomer supported DNA synthesis. Apparently non-productive TERT self-association occurred through a low-complexity region of the protein dispensable for RNP catalytic activity. Overall these studies support the function of human telomerase holoenzyme and minimal recombinant RNPs with a single subunit of TERT and demonstrate an evolutionarily conserved telomerase subunit architecture.

Materials and Methods

Telomerase reconstitution in cells

HEK 293T cells were transiently transfected with pcDNA3.1 TERT expression plasmid(s), the hTR expression plasmid pBS-U3-hTR-500 (Fu and Collins, 2003) and, where indicated, the N-terminally triple Myc-tagged TPP1 OB-fold domain (residues 88-249) expression plasmid pcDNA3.1-3xMyc-TPP1(88-249) using calcium phosphate. After 48 h, cells were resuspended in HLB buffer (20 mM HEPES at pH 8, 2 mM $MgCl_2$, 0.2 mM EGTA, 10% glycerol, 0.1% NP-40, 1 mM DTT and 0.1 mM PMSF) and lysed by three freeze-thaw cycles. NaCl was adjusted to 400 mM and the whole-cell extract was cleared by centrifugation.

Telomerase reconstitution in RRL

TNT T7 coupled transcription/translation reactions were assembled according to manufacturer's instructions (Promega) with 40 ng/μl TERT expression plasmid and 100 ng/μl purified in vitro transcribed hTRmin added prior to TERT synthesis (Wu and Collins, 2014a). Reactions were incubated at 30°C for 3.5 h.

Enrichment of complexes by tagged TERT, tagged TPP1 or hTR template for activity assays

HEK 293T cell extracts (200 μl per precipitation) or RRL reconstitution reactions (37.5 μl per precipitation) were adjusted to 150 mM NaCl and bound to 10 μl FLAG M2 monoclonal antibody resin (Sigma-Aldrich), 10 μl c-Myc antibody resin (Sigma-Aldrich) or 10 μl streptavidin agarose resin (Sigma-Aldrich) coated with 5'-biotinylated template-antisense oligonucleotide (CTAGACCTGTCATCAGUUAGGGUUAG, where the underlined nucleotides are 2'OMe RNA; (Schnapp et al., 1998)) by end-over-end rotation at room temperature for 2 h. Following binding, the resin was washed three times at room temperature with HLB containing 150 mM NaCl, 0.1% Triton X-100 and 0.2% CHAPS. Resin-bound telomerase was then used in activity assay reactions (see below).

Immunoblots

Immunoblotting for TERT detection was performed using mouse anti-TERT polyclonal primary antibody 1A4 raised against the TERT C-terminus at 1:3,000 dilution. FLAG was detected using mouse anti-FLAG monoclonal primary antibody M2 (Sigma-Aldrich) at 1:5,000 dilution. Tubulin was detected using mouse anti-alpha-tubulin monoclonal primary antibody DM1A (Calbiochem) at 1:500 dilution. Biotin was detected using goat anti-biotin polyclonal primary antibody ab6643 (Abcam) at 1:5,000 dilution. Myc was detected using rabbit anti-c-Myc polyclonal primary antibody A-14 (Santa Cruz Biotechnology) at 1:3,000 dilution. Immunoblots using mouse primary antibodies were detected with goat anti-mouse IR 800 secondary antibody (Rockland Immunochemicals) at 1:20,000 dilution. Immunoblots using goat primary antibodies were detected with donkey anti-goat Alexa Fluor dye 680 secondary antibody (Life Technologies) at

1:15,000 dilution. Immunoblots using rabbit primary antibodies were detected with goat anti-rabbit IR 800 secondary antibody (Rockland Immunochemicals) at 1:20,000 dilution. All incubations were performed in 3% nonfat milk in TBS buffer (50 mM Tris pH 7.5, 150 mM NaCl). Membranes were washed with TBS buffer prior to visualization on a LI-COR Odyssey imager.

Telomerase activity assays

Primer extension assays with radiolabeled nucleotide incorporation were performed in 20 μl reactions containing 10 μl resin-bound telomerase, 500 nM $(T_2AG_3)_3$ telomeric primer and >0.1 μM α-^{32}P dGTP (3,000 Ci/mmol, 10 mCi/ml, Perkin-Elmer) in telomerase activity assay buffer (50 mM Tris-acetate at pH 8, 3 mM $MgCl_2$, 1 mM EGTA, 1 mM spermidine, 5 mM DTT and 5% glycerol) with 5 μM dGTP, 250 μM dTTP and dATP for detection of repeat addition processive synthesis or 250 μM dTTP and 500 μM ddATP for detection of single repeat synthesis. Reactions were incubated at 30°C for 40 min. For the 5'-end labeled primer extension pulse-chase assay, 10 μl resin-bound telomerase was incubated with 20 nM ^{32}P 5'- end labeled $(T_2AG_3)_3$ telomeric primer for 30 min, then washed twice with HLB containing 150 mM NaCl and 0.1% NP-40 to remove unbound primer. The assay was initiated by addition of 20 μl of telomerase activity assay buffer with 250 μM dGTP, dTTP and dATP. The reactions were incubated at 30°C for 5 min followed by addition of unlabeled $(T_2AG_3)_3$ telomeric primer to a final concentration of 5 μM and further incubated at 30°C to reach the indicated total reaction time.

The products of all activity assay reactions were then extracted, precipitated and resolved on 12% polyacrylamide/7 M urea/0.6x Tris borate-EDTA gels. An end-labeled oligonucleotide was added prior to product precipitation to serve as a recovery control (RC) and end-radiolabeled primer was loaded separately from product DNA as a size marker (migration is indicated in Figures by ►). Dried gels were visualized by phosphorimaging on a Typhoon Trio system (GE Healthcare) and quantified using ImageQuant TL (GE Healthcare). Activity was quantified on the combined intensities of all product DNA.

ACP/MCP labeling with CoA derivatives

Complexes bound to an affinity purification resin were washed into 50 mM HEPES at pH 8, 1 mM DTT and 10 mM $MgCl_2$. CoA-conjugated biotin was purchased (New England Biolabs) and CoA-conjugated Cy3 or Cy5 was prepared as described (Yin et al., 2006) and added to a final concentration of 10 μM. Labeling reactions were carried out by addition of ACP or SFP synthase (New England Biolabs) to 1 μM final concentration and incubation at room temperature for 2 h. Following the labeling reaction, the resin was washed three times at room temperature with HLB containing 150 mM NaCl, 0.1% Triton X-100 and 0.2% CHAPS. For samples sequentially labeled with two dyes, the labeling reactions were repeated with the second dye and synthase. After the final labeling reaction and wash, complexes were eluted by incubation with 200 nM FLAG peptide or 30 μM 3'-terminal 2',3'-dideoxyguanosine-modified displacement oligonucleotide (CTAACCCTAACTGATGACAGGTCTAG; (Schnapp et al., 1998)) for

1 h at room temperature. Complexes bound to FLAG antibody or 2'OMe RNA oligonucleotide resin were eluted in 14 μl or 70 μl buffer, respectively. These volumes were required to normalize activity and fluorescent spot count among preparations from the same amount of input. Labeled bulk samples were analyzed by 10% SDS-PAGE and imaged on a Typhoon Trio system (GE Healthcare).

Labeled TERT depletion

Telomerase was reconstituted with ACP- and/or MCP-TERT as described above, with the RRL reaction supplemented with ^{35}S-methionine. Following FLAG purification, complexes were labeled with CoA or CoA-biotin with ACP or SFP synthase. Samples were eluted from the affinity purification resin with 200 nM FLAG peptide and bound to streptavidin agarose or Myc antibody agarose (Sigma-Aldrich) for 1 h. For depletion in denaturing conditions, samples were eluted from affinity purification resin in buffer adjusted to 2 M urea. The streptavidin-agarose unbound fraction was analyzed by 10% SDS-PAGE or activity assay.

Microscopy

A prism-type total internal reflection fluorescence microscope was built using a Nikon Ti-E Eclipse inverted fluorescence microscope equipped with a 60X 1.20 N.A. Plan Apo water objective (Nikon). A 532 nm laser (Coherent, 350 mW) was used for Cy3 excitation and a 633 nm laser (JDSU, 35 mW) was used for Cy5 excitation. For two-color colocalization experiments, Cy3 and Cy5 fluorescence were split into two channels and imaged separately on a single charge-coupled device (CCD) chip using an Optosplit II image splitter (Cairn Instruments). Fluorescence signal was collected with a 512x512 pixel electron-multiplied CCD camera (Andor Technology). All data collection was conducted at 22°C.

Slide preparation

Quartz coverslips were coated with a mixture of 99% PEG and 1% biotinylated-PEG. Airtight sample chambers were constructed by sandwiching double-sided tape between the coverslips and quartz slides (MicroSurfaces, Inc.). To prepare the slides for molecule deposition, the surface was pre-blocked by sequential 15 min incubations with 20% Biolipidure 203/206 (NOF Corporation) and 10 mg/ml casein (Sigma-Aldrich). Following each incubation, the sample chamber was washed with telomerase slide buffer (50 mM Tris-HCl at pH 8, 10% glycerol, 2 mM $MgCl_2$ and 0.2 mM EGTA). The surface was then incubated with 1 mg/ml streptavidin (Sigma-Aldrich) for 10 min and washed twice with telomerase slide buffer.

Two-color colocalization and photobleaching analyses

Streptavidin-coated slides were incubated with 40 nM 5'-biotinylated telomeric primer (Tel2, T_{15}TTAGGGTTAGGG) in telomerase activity assay buffer for 10 min and washed with telomerase slide buffer. The slide was then incubated for 30 min with 1 μl labeled

telomerase supplemented with 1 mg/ml casein followed by two washes with telomerase slide buffer to remove excess unbound sample. After washing, imaging buffer (1 mg/ml glucose oxidase, 0.34 mg/ml catalase, 0.8% w/v D-glucose and 2 mM Trolox in telomerase slide buffer) was flowed into the sample chamber.

The fraction of two-color colocalization was experimentally determined considering only complexes with Cy5 signal and measuring the percentage of the spots that also had Cy3 signal. This was done because initial Cy5 labeling of the ACP tag by ACP synthase is selective for ACP versus MCP tag, whereas the subsequent SFP synthase labeling used to add Cy3 can label both MCP and ACP tags. By only considering complexes that labeled with Cy5, we avoided the possibility of counting two-TERT single-color Cy3 labeled complexes as TERT monomers rather than dimers. Samples were excited with the 633 nm laser throughout the experiment and imaged at 100 ms time resolution. After the first 10-20 frames, samples were excited with the 532 nm laser for ~20 additional frames. For photobleaching, the 633 nm laser was used for excitation and 500-1000 frames were collected at 100 ms time resolution.

Activity-dependent elution

Tel2-bound slides were incubated with 1 μl Cy5-labeled telomerase in telomerase activity assay buffer for 30 min, and then washed twice. Antisense Tel2 oligonucleotide (Anti-Tel2, CCCTAACCCTAA) was then introduced at 100 nM final concentration and incubated for 15 min to block any unbound immobilized Tel2. The slide was washed twice, and imaging buffer was flowed into the sample chamber. The samples were excited at 633 nm to collect 30 frames at 100 ms time resolution to determine the initial number of complexes bound to immobilized Tel2. For assays of elution, after initial imaging the slide was washed and incubated with either 20 μl dNTP elution buffer (10 nM Anti-Tel2, 500 μM dATP and 500 μM dTTP in telomerase activity assay buffer) or mock elution buffer (10 nM Anti-Tel2 in telomerase activity assay buffer). After 15 and 30 min the slide was then washed with telomerase activity assay buffer, imaging buffer was flowed into the imaging chamber and the remaining number of bound complexes was determined by collecting 30 frames at 100 ms time resolution with 633 nm excitation. For photobleaching step quantification after elution, no initial imaging or imaging at 15 min was performed. For quantification of RNase sensitivity, Cy5-labeled MCP-TERT reconstitutions were pre-incubated with 0.1 mg/ml RNase A at room temperature for 1 h immediately prior to introduction to the flow cell.

Determination of DNA K_d

Streptavidin-coated slides were incubated with 1 μl biotin-labeled sample diluted in telomerase activity assay buffer for 10 min. The sample chamber was washed with telomerase slide buffer and incubated with 500 nM nonspecific blocking oligonucleotide (AAATGATAACCATCTCGC) for 15 min, followed by two washes with telomerase slide buffer. Telomeric oligonucleotide (TTAGGGTTAGGG) 5'-end labeled with Cy5 was incubated for 15 min. Excess DNA was washed away and imaging buffer was

flowed into the sample chamber. Bound DNA was detected by collecting 30 frames at 100 ms time resolution with 633 nm excitation.

Northern blots

RNA was purified using TRIzol reagent (Life Technologies) and resuspended in 2 μl of water. The RNA was spotted onto Hybond N+ nylon membrane (GE Healthcare) and detected using ^{32}P end-labeled probe complementary to hTR positions 51-72 (Fu and Collins, 2003).

Results

Purification-biased TERT subunit content of DNA-bound complexes

To quantify the TERT subunit content of reconstituted human telomerase complexes, we developed a strategy to label individual TERT molecules with a Cy3 or Cy5 fluorophore. The 8 kDa ACP and MCP tags derive from bacterial proteins that accept covalent transfer of the CoA phosphopantetheinyl (Ppant) group to a serine on the protein surface (Figure 2.1A, left). In endogenous bacterial context, the Ppant group serves as a 20 Å swing-arm tether for subsequent transient attachment of the acyl groups that are the carrier proteins' cargo. For labeling ACP/MCP in vitro, the Ppant group of CoA can be pre-conjugated to diverse labels including Cy3, Cy5 or biotin prior to the prosthetic group transfer reaction, such that the Ppant swing-arm becomes a spacer between the label and the protein (Belshaw et al., 1999; George et al., 2004; Yin et al., 2006). ACP synthase catalyzes transfer from a derivatized CoA to the ACP tag but does not label the MCP tag, while either tag is labeled by SFP synthase (Zhou et al., 2007). Labeling of a tagged fusion protein by SFP synthase in vitro occurred with >80% efficiency (Yin et al., 2005).

Human TERT tagged at the N-terminus supports telomere elongation, whereas telomerase assembled with C-terminally tagged TERT does not (Counter et al., 1998; Wong and Collins, 2006). Therefore, we fused the human TERT N-terminus to a triple FLAG peptide and either the ACP or MCP tag (Figure 2.1A, right). To assemble telomerase holoenzyme, TERT was overexpressed in 293T cells along with full-length hTR overexpressed using the U3 small nucleolar RNA promoter (Fu and Collins, 2003). To reconstitute catalytically active minimal RNP, TERT was expressed in RRL pre-supplemented with vast molar excess of purified recombinant hTRmin (Wu and Collins, 2014a). TERT complexes from each reconstitution method were enriched by each of two purification approaches: TERT binding to FLAG antibody resin followed by peptide elution (F purification) or RNA template base-pairing to a resin-immobilized 2'O-methyl RNA (2'OMe) oligonucleotide followed by displacement oligonucleotide elution (O purification; Figure 2.2, panels A,B; Schnapp et al., 1998). The 3'-modified displacement oligonucleotide used in this work did not compete with DNA primer for telomerase elongation (Figure 2.2, panel C). 293T cell lysates or RRL expression reactions were split and purified in parallel using the F and O purification approaches (Figure 2.1B). ACP- and MCP-tagged TERTs expressed at equivalent level and assembled active telomerase, quantified by radiolabeled dGTP incorporation in reactions also containing dTTP and ddATP (Figure 2.1C). CoA-Cy5 labeling of ACP-TERT using ACP synthase and CoA-Cy3 labeling of MCP-TERT using SFP synthase were confirmed by SDS-PAGE and fluorescence scanning, with no labeling of TERT lacking an ACP or MCP tag (Figure 2.1D). Importantly, the profile of telomerase product synthesis was not affected by the labeling reaction for fluorophore conjugation (Figure 2.1E).

While purification by either tagged TERT or RNA template yields active telomerase, these purification strategies also enrich either TERT not assembled with hTR or hTR without TERT, respectively. To investigate the amounts of tagged TERT versus active RNP, we compared the levels of TERT protein and enzyme activity across the four

combinations of reconstitution and purification, subsequently designated 293T-F, 293T-O, RRL-F and RRL-O (Figure 2.1B,F). TERT was detected by an antibody raised against its C-terminal region (Figure 2.2, panel D). Activity was quantified from reactions with dTTP, ddATP and radiolabeled dGTP. O-purification by the hTR template enriched more telomerase activity relative to TERT than did F-purification (Figure 2.1F), as would be expected based on template hybridization versus antibody binding to TERT. Comparison between the pair of 293T or RRL purifications suggests that most of the TERT in 293T-F and RRL-F was not assembled as telomerase RNP. This was anticipated for the 293T-F purification, because cellular expression of hTR is limited by inefficient co-transcriptional H/ACA RNP assembly (Darzacq et al., 2006; Egan and Collins, 2012b). However RRL reconstitution exploits the use of pre-transcribed hTR added at very high final concentration relative to TERT. Nonetheless, even optimized RRL expression produced hTR-free TERT enriched by F-purification.

To investigate the TERT content of individual complexes within a bulk fraction, we used total internal reflection fluorescence microscopy to image labeled TERT complexes bound to immobilized single-stranded $T_{15}(T_2AG_3)_2$ DNA primer. This 5'-biotinylated primer was anchored to a polyethylene glycol-coated coverslip surface via biotin-streptavidin attachment (Figure 2.3A, left). Primers with this 3' permutation of the telomeric repeat have exceptionally stable binding to human telomerase (Wallweber et al., 2003), due to the finely tuned recognition of template-paired primer 3' ends in the enzyme active site (Brown et al., 2014; Wu and Collins, 2014b). Optimal DNA binding by human telomerase requires a primer length of two telomeric repeats (Wallweber et al., 2003), which is the same length that active human telomerase protects from nuclease digestion (Wu and Collins, 2014a).

We applied two parallel approaches to determine the number of TERT subunits per complex. In the first method (Fig 2.3A, left), we assembled telomerase by coexpression of ACP-TERT and MCP-TERT and labeled the TERTs sequentially, first labeling ACP-TERT with ACP synthase and CoA-Cy5 then labeling MCP-TERT with SFP synthase and CoA-Cy3. Fields of individual complexes were imaged to detect both dyes, and images were scored for the fraction of Cy5-labeled ACP-TERT that colocalized a Cy3-labeled MCP-TERT. In the second TERT subunit counting method (Figure 2.3B, left), we assembled telomerase complexes containing only MCP-TERT and labeled using SFP synthase and CoA-Cy5. Fields of individual complexes were imaged, and each Cy5 "spot" in the flow cell was analyzed for the number of dye photobleaching steps that occurred before the spot vanished. In the parallel approaches, the fraction of two-color colocalized spots and the number of photobleaching steps are both readily related to the sample fractional content of TERT monomer and dimer considering all possible two-subunit combinations (see Equations 1 and 2). Fluorescently labeled TERT complexes were diluted to obtain 1-4 spots per 100 μm^2 of the slide surface, and unbound protein was removed before imaging. To attain similar spot count per field across samples, labeled O-purification complexes required dilution relative to F-purification complexes isolated from an equal amount of the same extract, consistent with the greater yield of active RNP for O-purification (Figure 2.1F).

Both two-color colocalization and photobleaching assays revealed the presence of more than one labeled TERT in a subset of the DNA-bound TERT complexes (Figure 2.3A,B). In the two-color colocalization assay, there was no statistically significant difference in TERT colocalization comparing DNA-bound 293T-O, RRL-F and RRL-O complexes (Figure 2.3A; 17-23%, $p = 0.58$). In contrast, 293T-F complexes had much more TERT colocalization (46%, $p = 0.0015$). This distinction was consistent across a range of fluorescent spot density per field and different 293T cell extracts used for purifications (Figure 2.4). Results from the photobleaching method of TERT subunit counting also indicated no statistically significant difference in TERT subunit content across the population of DNA-bound complexes from 293T-O, RRL-F and RRL-O (Figure 2.3B; 19-27% bleaching in multiple steps, $p = 0.33$). In contrast, 293T-F complexes had much more multistep photobleaching (43%, $p = 0.0066$) including a substantial fraction of complexes that photobleached in three or even more than three steps (12%). We analyzed whether the results from the methods of subunit counting were consistent with each other, assuming a mixed population of TERT monomer and TERT dimer complexes (Equation 3, and see below). There is excellent correlation of two-color colocalization to two-step photobleaching results for 293T-O, RRL-F and RRL-O but not 293T-F (Figure 2.3C). The abundance of 293T-F TERT complexes that photobleached in three or more steps is likely responsible for this discord, as this population of complexes was distinguished from TERT dimer complexes in the count of photobleaching steps but would be lumped together with TERT dimer complexes in the count of two-color colocalization. Together, the findings above reveal a surprising diversity of TERT subunit content in DNA-bound complexes. Furthermore, it is evident that this heterogeneity varies across the methods of telomerase reconstitution and purification (Figure 2.3D).

Quantification of the TERT monomer fraction of DNA-bound complexes

The subunit colocalization and multistep photobleaching values measured above are related to the number of TERTs within each complex but are also influenced by the labeling efficiency of the MCP tag. Therefore, in order to calculate the fraction of complexes with TERT monomer or TERT dimer for each method of reconstitution and purification, it was necessary to establish MCP-TERT labeling efficiency. Labeling of 293T- and RRL-reconstituted, F-purified MCP-TERT complexes was to saturation within 30 min of a reaction with CoA-Cy3 or CoA-Cy5 (Figure 2.5A), well within the standard 2-hour labeling protocol. Also, labeling efficiency was not dependent on the reconstitution and purification method (Figure 2.5B). We adapted a previously developed approach to quantify a minimum lower bound of labeling efficiency without assumptions from fluorescence intensity (Yin et al., 2005). Using CoA-biotin as the synthase substrate results in covalent target protein biotinylation, which can be used as the basis for protein depletion by binding to streptavidin resin. The minimum lower bound of labeling efficiency can be calculated from the amount of protein remaining in the unbound fraction. First we confirmed that CoA-biotin is used equivalently to CoA-fluorophore by measuring competition between CoA-biotin and CoA-Cy3. If RRL-reconstituted F-purified MCP-TERT was labeled to saturation with CoA-Cy3 and then labeled with CoA-biotin, no biotinylation of TERT could be detected (Figure 2.5C). Similarly, labeling with CoA-biotin drastically reduced subsequent labeling with CoA-Cy3 (Figure 2.5C).

Therefore, biotin labeling provides a surrogate for quantification of dye labeling efficiency.

To preclude the depletion of unlabeled TERT as part of a TERT multimer, biotin-labeled TERT complexes were bound to streptavidin in 2 M urea. Complexes of RRL-reconstituted TERT synthesized with ^{35}S-methionine were F-purified and labeled with biotin, biotinylated TERT was depleted using streptavidin agarose, and the fraction of unbound TERT was quantified by radiolabel detection after SDS-PAGE (Figure 2.5D). Depletion was an indistinguishable 54.9 ± 0.7% or 50.6 ± 5.9% of ACP-TERT or MCP-TERT, respectively, quantified from the unbound ~45% or ~49% (Figure 2.5D, lanes 3-6). As a negative control, TERT from labeling reactions with underivatized CoA was not depleted (Figure 2.5D, lanes 1-2). Also, MCP-TERT was not depleted after a labeling reaction with ACP synthase (Figure 2.5D, lanes 7-8). When ACP- and MCP-TERT were coexpressed, CoA-biotin labeling of ACP-TERT by ACP synthase resulted in half the depletion attained when ACP-TERT alone was expressed (Figure 2.5D, lanes 9-10 versus 3-4), confirming equal coexpression of the two tagged TERTs. Similar depletion was observed for biotin-labeled F-purified MCP-TERT expressed in 293T cells, detected by immunoblot (Figure 2.5D, lanes 11-12). Also, ~50% depletion was observed for the catalytic activity of MCP-TERT RNPs labeled with CoA-biotin bound to streptavidin in native rather than denaturing conditions, independent of the reconstitution or purification method or enzyme repeat addition processivity (Figure 2.5E).

To measure how efficiently biotinylated TERT was depleted by streptavidin in the 2 M urea condition that converts the entire population of protein to monomer, we determined the fraction of biotinylated TERT that was depleted compared to the fractional depletion of total TERT. For maximal immunoblot detection sensitivity, the 293T-expressed F-purified MCP-TERT was biotin labeled, allowed to bind streptavidin then analyzed by immunoblot with antibodies specific for TERT and biotin (Figure 2.5F). Streptavidin depleted 49% of the TERT protein (Figure 2.5F), consistent with the previous TERT depletions (Figure 2.5D). However, 38% of biotinylated TERT remained unbound (Figure 2.5F), revealing that streptavidin binding in 2 M urea did not completely deplete the labeled TERT. Therefore the MCP-TERT labeling efficiency was much higher than 51%. Correcting the quantified total TERT depletion for depletion efficiency of biotin-TERT gives an MCP-TERT labeling efficiency of 82% (Figure 2.5G). This matches the labeling efficiency determined for a related tag in similar reactions with SFP synthase and CoA-biotin (Yin et al., 2005).

We determined the fraction of TERT monomer versus dimer in each population using the colocalization quantifications (Figure 2.3A, Equation 1) or the photobleaching quantifications (Figure 2.3B, Equation 2) by modeling the DNA-bound complexes as having either one or two TERTs. We set labeling efficiency as 82% but also modeled a range of labeling efficiency from 51% to 100% as lower and upper bounds (indicated as "Low L" and "High L" limits). Colocalization and photobleaching quantifications support modeling of DNA-bound 293T-O, RRL-F and RRL-O populations as a mixture of complexes with one or two TERT subunits (Figure 2.5H,I). The 293T-F population of DNA-bound TERT could not be modeled as a mixture of TERT monomer and dimer

across the full range of labeling efficiency using the colocalization quantification (Figure 2.5H), likely due to the substantial fraction of complexes with three or more TERT subunits (Figure 2.3B). TERT monomer complexes exceeded TERT dimer complexes in the DNA-bound 293T-O, RRL-F and RRL-O populations across almost the entire range of modeled labeling efficiencies (Figure 2.5H,I). Overall these analyses establish that TERT complexes competent for DNA binding can have a single subunit of TERT.

Assessing the active RNP fraction of DNA-bound TERT complexes

The heterogeneity of TERT subunit content in DNA-bound complexes described above raised the question of whether only a subset of the DNA-bound complexes corresponds to active RNP. To investigate this question, we exploited the permutation-dependent telomeric-repeat DNA binding affinity of the human telomerase active site. The single-stranded $T_{15}(T_2AG_3)_2$ DNA primer used to bind TERT complexes to the flow cell surface has extremely slow dissociation from the telomerase holoenzyme active site (Wallweber et al., 2003). Introducing dTTP + dATP into the imaging chamber would support primer extension to a GGGTTA-3' end (Figure 2.6A), which disengages from the active site with k_{off} at least ~100-fold greater than the TTAGGG-3' end (Wallweber et al., 2003). Thus, Cy5-labeled MCP-TERT complexes with DNA bound in a functional active site would exhibit activity-dependent elution in buffer with dTTP + dATP (Figure 2.6A). Inactive RNP and hTR-free TERT would remain bound as well as some active RNP not dissociated from product (Figure 2.6A), and also any 293T TERT bound to DNA indirectly through an associated shelterin complex. To control for activity-independent dissociation of TERT complexes from DNA we performed parallel incubations without dTTP + dATP. We also assayed complexes reconstituted with the catalytic-dead TERT D868A (Weinrich et al., 1997). Elution of Cy5-labeled MCP-TERT was monitored by spot count per field over 30 minutes in buffer with or without dNTPs (Figure 2.6B).

Reproducibly more elution of wild-type TERT complexes occurred in the presence of buffer with dTTP + dATP versus buffer alone (Figure 2.6C, compare black and gray). In contrast, D868A TERT complexes showed the same amount of dissociation with or without dNTPs (Figure 2.6C, compare dark and light blue). Curiously, the fraction of wild-type TERT complexes with activity-dependent elution varied widely across the TERT populations from different reconstitution and purification conditions (Figure 2.6C). RRL-F and RRL-O complexes showed predominantly activity-dependent elution. About half of the DNA-bound 293T-O complexes also showed activity-dependent elution, but a surprisingly low percentage of 293T-F complexes eluted with the opportunity for DNA synthesis. The non-eluting fraction of TERT complexes roughly correlated with the fraction of complexes that could bind slide-immobilized DNA after sample pre-treatment with RNase A (Figure 2.6C, gray bars).

Importantly, the fraction of DNA-bound 293T-O, RRL-F and RRL-O TERT complexes with nucleotide-dependent "specific" elution (Figure 2.6C) overlaps the fraction of DNA-bound complexes with monomeric TERT (Figure 2.5H,I). This overlap establishes that at least some TERT monomer RNPs have catalytic activity. To directly measure the contribution of TERT monomer RNPs to specific elution, we used RRL-reconstituted O-

purified Cy5-labeled MCP-TERT complexes to quantify TERT spot count per field and steps of photobleaching for samples after incubation in parallel for 30 minutes in buffer with or without dNTPs (Figure 2.6D). Approximately one third as many labeled TERT complexes were present in samples incubated with dNTPs (Figure 2.6E), consistent with the elution time course (Figure 2.6C). The reduction of TERT spot count by activity-based elution occurred entirely in complexes with single-step photobleaching (Figure 2.6E, $p = 0.0006$). The conditions of elution altered the relative representation of TERT monomer and dimer complexes, calculated by adjusting the photobleaching step quantifications for TERT labeling efficiency (Figure 2.6F). Consistent with specific elution of TERT monomer complexes, the DNA-bound TERT complexes remaining after specific elution were enriched for TERT dimer. Overall the findings above strongly suggest that human telomerase catalytic activity requires only a single TERT subunit per RNP.

Assessing the DNA binding affinity of TERT complexes

The heterogeneity of DNA-bound TERT complex elution was surprising. We therefore investigated whether the bulk populations of TERT complexes from different reconstitution and purification conditions had heterogeneous DNA binding affinities as well. Towards this goal, we quantified the DNA binding affinity of TERT complexes anchored directly to the flow cell surface. To do this, we labeled MCP-TERT with CoA-biotin, bound the biotin-labeled TERT complexes to streptavidin on the flow cell surface, and assayed the immobilized TERT complexes for retention of Cy5-labeled $(T_2AG_3)_2$ (Figure 2.7A). This direct TERT immobilization captured the full TERT heterogeneity of the bulk purification fractions, which we monitored separately by SDS-PAGE of MCP-TERT labeled with Cy5 (Figure 2.7B). Bulk 293T-F purifications of MCP-TERT contained a large amount of a proteolytic product corresponding to the MCP-tagged TERT TEN domain alone (Figure 2.7B). TEN domain expressed in *E. coli* has barely detectable if any DNA binding activity (O'Connor et al., 2005; Sealey et al., 2010), suggesting that it would not form a stable complex with the Cy5-labeled $(T_2AG_3)_2$. None of the other bulk purification fractions contained TEN domain alone, but curiously the 293T-F and 293T-O bulk purifications contained TERT proteolytic products corresponding to the TEN domain plus adjacent linker (Figure 2.7B; see below).

We quantified the amount of Cy5-labeled $(T_2AG_3)_2$ bound to immobilized TERT complexes using a range of DNA concentration. DNA binding across a titration from 0.3 to 30 nM DNA yielded K_d calculations in nM of 4.9 ± 0.7 for 293T-O, 5.4 ± 1.1 for 293T-F, 8.7 ± 2.0 for RRL-O and 14.7 ± 5.4 for RRL-F (Figure 2.7C). The ~5 nM K_d of holoenzyme and ~10 nM K_d of minimal RNP are consistent with the holoenzyme K_m for elongation of similar primers measured, under different conditions, as 2 nM or 8 nM (Wallweber et al., 2003; Jurczyluk et al., 2010). In parallel, immobilized TERT complexes were assayed for DNA binding using 100 nM $(T_2AG_3)_2$. DNA binding by 293T-F TERT complexes increased ~4-fold with 100 nM compared to 30 nM DNA (Figure 2.7D). In contrast, at 100 nM compared to 30 nM DNA concentration 293T-O TERT complexes showed no additional DNA binding and RRL-F and RRL-O complexes showed only limited additional association with DNA (Figure 2.7D). These findings

suggest that 293T-O, RRL-F and RRL-O TERT complexes competent for DNA binding have a relatively homogeneous DNA binding affinity matching the expectation for catalytically active human telomerase.

A TERT linker region not required for telomerase RNP assembly or activity

Next we sought to create a homogeneous pool of TERT monomer or dimer complexes. Many variations of reconstitution method had surprisingly little impact on the DNA-bound TERT monomer/dimer ratio, with one exception: elimination of the 125 amino acid linker between the TERT ring and TEN domain. Phylogenetic comparison revealed that this domain linker is particularly long in vertebrate TERTs (Podlevsky et al., 2008), approximately 100 amino acids longer than in the ciliate and budding yeast TERTs that assemble only TERT monomer RNPs (Livengood et al., 2002; Bryan et al., 2003; Witkin and Collins, 2004; Cunningham and Collins, 2005; Jiang et al., 2013; Bajon et al., 2015). Scanning six-residue substitutions of human TERT linker sequence did not uncover any significance of the region for telomerase catalytic activity or telomere maintenance (Armbruster et al., 2001), but this approach did not alter the atypical amino acid composition of the linker region overall. Human TERT amino acids 201-325 are 18% proline, 14% arginine and 12% glycine. When subject to bioinformatical analysis for amino acid content (Harbi et al., 2011), this region is identified as having high compositional bias. We also used SEG analysis (Wootton and Federhen, 1993) to search for low-complexity sequence within the human TERT linker. SEG analysis identified two segments of the linker, residues 213-248 and 313-323, as low complexity. Low-complexity regions can mediate diverse protein-protein interactions including concentration-dependent self-association (Coletta et al., 2010; Kato et al., 2012). Thus, the TERT low-complexity proline/arginine/glycine-rich linker (termed the PAL) is a candidate region for mediating self-association of overexpressed TERT.

Whether the length of the human TERT PAL influences RNP assembly or activity has not been tested. Previous assays that separated the TEN domain from the TERT ring retained the PAL on either the TEN domain or TERT ring (Robart and Collins, 2011; Wu and Collins, 2014a). We therefore removed TERT residues 201-325 from the N-terminally F-tagged full-length protein, either by simply deleting the region (TERT-ΔPAL; Figure 2.8A) or replacing it with 5, 10 or 20 repeats of the sequence NAAIRS (TERT-5N, -10N, -20N; Figure 2.8A), the six amino acid motif used previously in the non-disruptive scanning mutagenesis (Armbruster et al., 2001). The PAL-mutant TERT proteins expressed at levels similar to wild-type TERT in 293T cells and in RRL (Figure 2.8A), and binding of wild-type and PAL-mutant TERT complexes to FLAG antibody resin enriched similar amounts of catalytic activity (Figure 2.8B). Although direct fusion of the TEN domain to the TERT ring did not substantially affect the quantified overall activity it appeared to reduce the amount of the longest product DNAs (Figure 2.8B). This change in product profile was rescued by NAAIRS repeat insertion (Figure 2.8B). Since the number of radiolabeled dGTP nucleotides incorporated into a product DNA is proportional to length, products elongated by many repeats are detected with disproportionately high sensitivity relative to their actual abundance. To more accurately profile the repeat addition processivity of the reconstituted enzymes, we assayed

telomerase activity using a primer radiolabeled at its 5' end rather than by extension with radiolabeled dNTPs. This also allowed the use of a non-limiting concentration of dGTP in the activity assay reaction (see Materials and Methods). A five-minute pulse of primer extension was followed by a chase period with excess unlabeled primer to eliminate telomerase reinitiation on released product DNA. Under these conditions, primer extension was highly processive for complexes of wild-type TERT, TERT-ΔPAL and TERT-20N assembled in 293T cells (Figure 2.8C). Similar results were obtained with RRL-reconstituted enzymes (data not shown). We conclude that human TERT linker length and linker sequence have a very limited influence on the catalytic activity of reconstituted holoenzyme or minimal RNPs.

Telomerase-mediated telomere synthesis is strictly dependent on TEN domain interaction with the oligonucleotide/oligosaccharide-binding (OB) fold domain of the shelterin component TPP1 (Xin et al., 2007; Sexton et al., 2014; Schmidt et al., 2014). To test whether sequence substitutions of the PAL compromise catalytically active telomerase association with TPP1, we co-overexpressed N-terminally 3xMyc-tagged TPP1 OB-fold domain (TPP1 residues 88-249) with F-tagged wild-type TERT, TERT-ΔPAL or TERT-20N in 293T cells. Within a two-fold difference, the TPP1 OB-fold domain copurified active telomerase regardless of TERT linker length or sequence (Figure 2.8D).

As additional characterization prior to single-molecule imaging, we analyzed Cy5-labeled O-purified MCP-tagged wild-type TERT, TERT-ΔPAL and TERT-20N complexes by SDS-PAGE. Curiously, the 293T TERT-ΔPAL and TERT-20N bulk purification fractions lacked the TERT proteolysis products coenriched by wild-type TERT (Figure 2.8E). The wild-type TERT proteolysis products correspond to the TEN domain fused to lengths of PAL ending at the two computationally identified low-complexity regions. A simple hypothesis to explain these findings is that an hTR-bound full-length TERT can copurify a TERT fragment dimerized through the PAL. This would account for the detection of some PAL-containing TEN domain in the 293T-O bulk purification, which unlike the bulk F-purification should not directly enrich TERT fragments compromised for hTR binding. Bulk purification fractions of RRL-reconstituted wild-type TERT lacked the TERT proteolysis products detected in the 293T bulk purifications (Figure 2.7B and data not shown), suggesting that the TERT PAL may be a target of protease cleavage in cells. Furthermore, this proteolysis is specific for wild-type PAL sequence because no TEN domain fragments were observed the TERT-ΔPAL and TERT-20N purifications (Figure 2.8E). We note that although TERT proteolysis products are present in the 293T wild-type TERT bulk purifications, they may not be represented in the DNA-bound subset of TERT complexes assayed by single-molecule imaging.

TERT dimer requirement for the PAL

To investigate the TERT subunit content of PAL-mutant TERT complexes bound to DNA, we first O-purified 293T- and RRL-reconstituted complexes of coexpressed ACP- and MCP-tagged wild-type TERT, TERT-ΔPAL or TERT-20N. A dramatic decrease in TERT colocalization was observed for TERT-ΔPAL and TERT-20N relative to wild-type TERT (Figure 2.9A; 21% versus 5% colocalization in 293T samples, $p = 0.0008$, and

22% versus 2-3% in RRL samples, $p < 0.0001$). By calculations using a value of 82% TERT labeling efficiency, RRL-reconstituted TERT-ΔPAL and TERT-20N complexes were 98% and 96% TERT monomer, respectively (Figure 2.9B). Even by modeling using the lower-bound underestimate of TERT labeling efficiency, TERT monomer complexes were 93-96% of the DNA-bound RRL-reconstituted TERT complex total (Figure 2.9B). For 293T-reconstituted TERT-ΔPAL and TERT-20N complexes, TERT monomers were 94% of the population with a lower-bound underestimate of 89-90% (Figure 2.9B).

Parallel results were obtained by quantifying TERT subunit content using Cy5-labeled MCP-TERT steps of photobleaching. MCP-tagged TERT-ΔPAL and TERT-20N complexes assembled in 293T cells or RRL were dramatically depleted for multistep photobleaching compared to wild-type TERT complexes (Figure 2.9C; 24% versus 8-9% multistep bleaching in 293T samples, $p = 0.0036$, or 22% versus 4-7% in RRL samples, $p = 0.0073$). By calculations using a value of 82% TERT labeling efficiency, RRL-reconstituted TERT-ΔPAL and TERT-20N complexes were 92% and 95% TERT monomer, respectively (Figure 2.9D; 86-96% across the modeled range of TERT labeling efficiency). Similarly, 293T-reconstituted TERT-ΔPAL and TERT-20N complexes were 90% and 88% TERT monomer, respectively (Figure 2.9D; 80-92% across the modeled range of TERT labeling efficiency).

To determine whether RNPs assembled with TERT-ΔPAL and TERT-20N retained the characteristic permutation dependence of human telomerase DNA binding, we tested Cy5-labeled MCP-tagged TERT-ΔPAL and TERT-20N complexes for activity-dependent elution. More elution of TERT-ΔPAL and TERT-20N complexes occurred in buffer + dNTPs than in buffer alone (Figure 2.9E). As observed for wild-type TERT complexes, the TERT-ΔPAL and TERT-20N complexes assembled in 293T cells showed less specific elution than complexes assembled in RRL. Nevertheless, specific elution of 293T and RRL complexes of TERT-ΔPAL or TERT-20N uniformly exceeded the fraction of TERT dimer complexes in each population, determined using subunit colocalization or photobleaching (Figure 2.9B,D,E).

We conclude that although PAL disruption drastically reduced TERT dimerization, RNPs assembled with PAL-mutant TERTs retained catalytic activity and even the permutation-dependent release of product DNA characteristic of the human telomerase active site. TERT dimerization was as effectively suppressed for telomerase holoenzyme assembled in cells as for minimal RNP assembled in RRL, suggesting that the TERT subunit content of reconstituted complexes has no dependence on any holoenzyme protein other than TERT. We speculate that in physiological context, protein interaction(s) mediated by the TERT PAL could chaperone hTR-free TERT from its synthesis in the cytoplasm to nuclear sites of RNP assembly (Figure 2.9F, left). TERT overexpression may bypass this chaperoning requirement and promote a TERT self-association disfavorable for TEN domain positioning relative to TERT ring in an active RNP (Figure 2.9F).

Equations

Equation 1

Here, we derive an expression for the probability of a complex containing one TERT molecule as a function of labeling efficiency and measured two-color colocalization. Below "monomer" and "dimer" are used to indicate TERT subunits within complexes.

We model the telomerase complexes as having either one or two TERT molecules. Let M = probability of monomer and D = probability of dimer:

$$M + D = 1$$
$$\text{Therefore, } D = 1 - M$$

The probability of a monomeric complex containing ACP- or MCP-TERT is assumed to be equivalent. Furthermore, we considered the ACP and MCP tags to label at the same efficiency L. Therefore, the probability of a monomeric TERT complex labeled with Cy5 (Red, *R*) or Cy3 (Green, *G*) expressed as a function of *M* and *L* is:

$$P(R) = P(G) = 0.5ML$$

Complexes containing two TERTs could have two copies of ACP-TERT or two copies of MCP-TERT (denoted as *same*) or one of each (denoted as *mixed*). The ACP_{same}, MCP_{same} and ACP/MCP_{mixed} populations exist in a ratio of 0.25:0.25:0.5, respectively. Below, the ACP tag labeled with Cy5 is denoted as *R* and the MCP tag labeled with Cy3 is denoted as *G*.

Considering complexes with two copies of ACP-TERT or two copies of MCP-TERT, the probability that both subunits are labeled is:

$$P(RR) = P(GG) = 0.25DL^2 = 0.25(1 - M)L^2$$

The probability that one of the subunits is labeled while the other is unlabeled (0) is:

$$P(R0_{same}) = P(0R_{same}) = P(G0_{same}) = P(0G_{same})$$
$$= 0.25D(1 - L)L = 0.25(1 - M)(1 - L)L$$

Complexes with one copy of ACP-TERT and one copy of MCP-TERT can be labeled on both subunits:

$$P(RG|GR) = 0.5DL^2 = 0.5(1 - M)L^2$$

or labeled on one subunit only:

$$P(R0|0R_{mixed}) = P(G0|0G_{mixed}) = 0.5D(1 - L)L = 0.5(1 - M)(1 - L)L$$

The fraction of colocalization was experimentally determined considering only complexes with Cy5 signal (*R*) and measuring the percentage of the spots that also had Cy3 signal (*G*). This was done because initial Cy5 labeling of the ACP tag by ACP synthase is selective for ACP versus MCP tag, whereas the subsequent SFP synthase labeling used to add Cy3 can label both MCP and ACP tags. By only considering complexes that labeled with Cy5, we avoided the possibility of counting two-subunit single-color Cy3 labeled complexes as monomers rather than dimers.

The probability of colocalization, *C*, is therefore the probability of a dimer with one Cy5-labeled subunit and one Cy3-labeled subunit (*RG*|*GR*) normalized to all complexes with a Cy5-labeled subunit (*Any R*).

$$C = \frac{P(RG|GR)}{P(Any\ R)} = \frac{P(RG|GR)}{\sum P(R),P(RG|GR),P(R0_{same}),P(0R_{same}),P(R0|0R_{mixed}),P(RR)}$$

$$= \frac{0.5(1-M)L^2}{0.5ML+0.5(1-M)L^2+0.25(1-M)(1-L)L+0.25(1-M)(1-L)L+0.5(1-M)(1-L)L+0.25(1-M)L^2}$$

$$= \frac{-2(M-1)L}{M(L-2)-L+4}$$

Solving for *M*:

$$M = \frac{L(C+2)-4C}{L(C+2)-2C}$$

Equation 2

Here, we derive an expression for the probability of a complex containing one labeled TERT as a function of labeling efficiency and measured one-step photobleaching.

We model the telomerase complexes as having either one or two TERT molecules. Let *M* = probability of monomer and *D* = probability of dimer:

$$M + D = 1$$
Therefore, $D = 1 - M$

For photobleaching experiments, telomerase was reconstituted with MCP-TERT labeled with Cy5. The probability of a monomeric complex with Cy5 (Red, *R*) in terms of the labeling efficiency *L* is:

$$P(R) = ML$$

Complexes with two TERT molecules could have one or both subunits labeled. The probability that both subunits are labeled is:

$$P(RR) = DL^2 = (1-M)L^2$$

The probability that one subunit is labeled while the other is unlabeled (0) is:

$$P(R0) = P(0R) = D(1-L)L = (1-M)(1-L)L$$

The probability of one-step photobleaching, B_1, as a function of M and L is the probability of any complex with exactly one Cy5-labeled subunit normalized to all complexes with a Cy5-labeled subunit (*Any R*):

$$B_1 = \frac{\sum P(R),P(R0),P(0R)}{P(Any\ R)} = \frac{\sum P(R),P(R0),P(0R)}{\sum P(R),P(RR),P(R0),P(0R)}$$

$$= \frac{ML+(1-M)(1-L)L+(1-M)(1-L)L}{ML+(1-M)L^2+(1-M)(1-L)L+(1-M)(1-L)L}$$

$$= \frac{2ML-2L-M+2}{ML-L-M+2}$$

Solving for M:

$$M = \frac{L(B_1-2)-2B_1+2}{L(B_1-2)-B_1+1}$$

Equation 3

Here, we determine the probability of two-step photobleaching as a function of the fraction of colocalization. This gives an indication for how cross-consistent colocalization and multistep bleaching results are with each other.

Combining Equation 1, where C = probability of colocalization:

$$M = \frac{L(C+2)-4C}{L(C+2)-2C}$$

and Equation 2, where B_1 = probability of one-step photobleaching:

$$M = \frac{L(B_1-2)-2B_1+2}{L(B_1-2)-B_1+1}$$

it follows that:

$$\frac{L(C+2)-4C}{L(C+2)-2C} = \frac{L(B_1-2)-2B_1+2}{L(B_1-2)-B_1+1}$$

Therefore, the probability of one-step photobleaching as a function of the fraction of two-color colocalization is:

$$B_1 = \frac{3C-2}{C-2}$$

Since it is assumed that the telomerase complexes have either one or two TERT molecules, all labeled complexes should photobleach in either one or two steps. Let B_2 = probability of two-step photobleaching:

$$B_1 + B_2 = 1$$
$$\text{Therefore, } B_2 = 1 - B_1$$

The probability of two-step photobleaching as a function of the fraction of two-color colocalization is:

$$B_2 = 1 - B_1 = 1 - \frac{3C-2}{C-2}$$

$$B_2 = \frac{-2C}{C-2}$$

Discussion

Understanding telomerase mechanism and regulation requires knowledge of the subunit stoichiometry of an active RNP. Whether assembled in vivo or in vitro, we show that human telomerase complexes monomeric for TERT are catalytically active. Monomeric TERT was abundant in the populations of DNA-bound complexes from at least three of the four bulk purification samples examined here, particularly from any purification using a template-complementary oligonucleotide. These results establish the phylogenetic conservation of a TERT-monomer telomerase active site. Also our results support TERT haploinsufficiency rather than dominant-negative inhibition as the mechanism accounting for human disease from heterozygous TERT mutation (Armanios et al., 2005; Armanios and Blackburn, 2012). We note that although the budding yeast telomerase holoenzyme has a TERT monomer (Bajon et al., 2015), multiple telomerase RNPs can transiently colocalize as a cluster (Gallardo et al., 2011). Similarly in human cells, Cajal bodies and/or shelterin interactions could dynamically cluster telomerase RNPs within a general nuclear area. The biological significance of this clustering remains to be determined (Hockemeyer and Collins, 2015).

The biased amino acid composition, low sequence complexity and predicted lack of structure of the TERT PAL all may promote overexpressed TERT formation of dimers and aggregates. The similar TERT monomer/dimer ratio observed for DNA-bound O-purified 293T versus RRL complexes suggests that TERT self-association accounts for the vast majority of dimer formation, since 293T and RRL TERT complexes differ in all components other than TERT (full-length hTR and H/ACA proteins versus hTRmin). TERT complexes with multistep photobleaching appeared to support little if any activity-dependent elution from DNA. It remains possible that active RNP dimers form under reconstitution conditions other than the standard protocols used in this work. Also, not all TERT monomer complexes had efficient activity-dependent elution: a larger fraction of 293T-O complexes than RRL-O complexes failed to elute with the opportunity for DNA synthesis, even when these complexes were converted to nearly homogeneous TERT monomer content by PAL deletion. We speculate that this difference arises from the greater heterogeneity of TERT structure, modification and interaction partners produced by expression in cells. All of the findings above raise the need for caution in the interpretation of biochemical assays conducted using bulk purifications of TERT complexes. Surprisingly, even selection for single-stranded DNA binding activity did not fully discriminate against inactive TERT.

We pinpoint a proline/arginine/glycine-rich human TERT domain linker as the major site of TERT dimerization. Although the PAL mediates dimerization of overexpressed TERT, at lower endogenous TERT expression level we propose that the PAL has other biological roles. To address this hypothesis it will be important to determine PAL interaction partners using approaches that recapitulate a physiological TERT expression level. Also it will be of interest to understand which features of the TERT PAL are functionally significant. Because the PAL is present in vertebrate but not ciliate or budding yeast TERTs, we predict that it has biological function(s) related to the assembly of the vertebrate telomerase holoenzyme as an H/ACA RNP.

Figure 2.1 Reconstitution, purification and labeling of human TERT.

(**A**) *Left:* Derivatized CoA Ppant prosthetic group transfer to ACP or MCP tag by ACP or SFP synthase. The MCP tag is a modified version of the ACP tag, containing two amino acid substitutions, D36T and D39G. CoA can be modified with dye or biotin groups (R) for enzymatic labeling of a fusion protein. *Right:* Schematic of two ACP- and/or MCP-TERT labeling strategies using Cy5 (red) and Cy3 (green). An ACP or MCP tag is N-terminal to the TERT TEN domain, which is connected to the TERT ring by a linker region (L). Numbering refers to the full-length TERT amino acid sequence. A 3xFLAG tag is N-terminal to the ACP or MCP tag.
(**B**) Schematic of telomerase holoenzyme reconstitution by overexpression of TERT with full-length hTR in cells (293T) or minimal RNP reconstitution by TERT expression with hTRmin in vitro (RRL) followed by FLAG antibody purification for the TERT N-terminal tag (FLAG antibody purification, F) or purification using a 2'OMe RNA oligonucleotide complementary to the hTR template (Template oligo purification, O). Only the template of hTR or hTRmin is illustrated (blue).
(**C**) TERT and telomerase activity measured for O-purified, eluted complexes. Various N-terminally tagged TERT proteins were detected by TERT antibody immunoblot. The hTR Δtemp reconstitutions used template-less hTR or hTRmin with a 5' end at hTR position 64. Elution fractions were assayed for telomerase activity by primer extension with dTTP, ddATP and α-^{32}P dGTP, followed by denaturing gel electrophoresis. End-radiolabeled oligonucleotide was added prior to product precipitation to serve as a recovery control (RC), here and in subsequent panels. End-radiolabeled primer is a size marker (►), here and in subsequent panels. Specific activity in this panel indicates product DNA normalized to amount of TERT.
(**D**) SDS-PAGE analysis of RRL-expressed TERT in telomerase reconstitutions of ACP-, MCP- or only F-TERT in the presence of hTRmin, labeled with ^{35}S-methionine and any additional label as indicated. ACP synthase was used for ACP-TERT dye labeling and SFP synthase was used for MCP-TERT dye labeling.
(**E**) Activity of telomerase reconstituted with ACP-, MCP- or F-TERT in RRL with hTRmin and labeled as indicated. Activity was detected in reactions containing dATP, dGTP, dTTP and α-^{32}P dGTP, followed by denaturing gel electrophoresis.
(**F**) TERT content and telomerase activity in bulk purifications of MCP-TERT reconstituted in 293T cells or RRL, assayed as described in (**C**). TERT immunoblot with input extracts used 3% of the total purification input. Half of the post-purification sample was used for activity assays and half for TERT immunoblot. For single-molecule detection, O-purifications were diluted relative to F-purifications from the same extract.

Figure 2.1

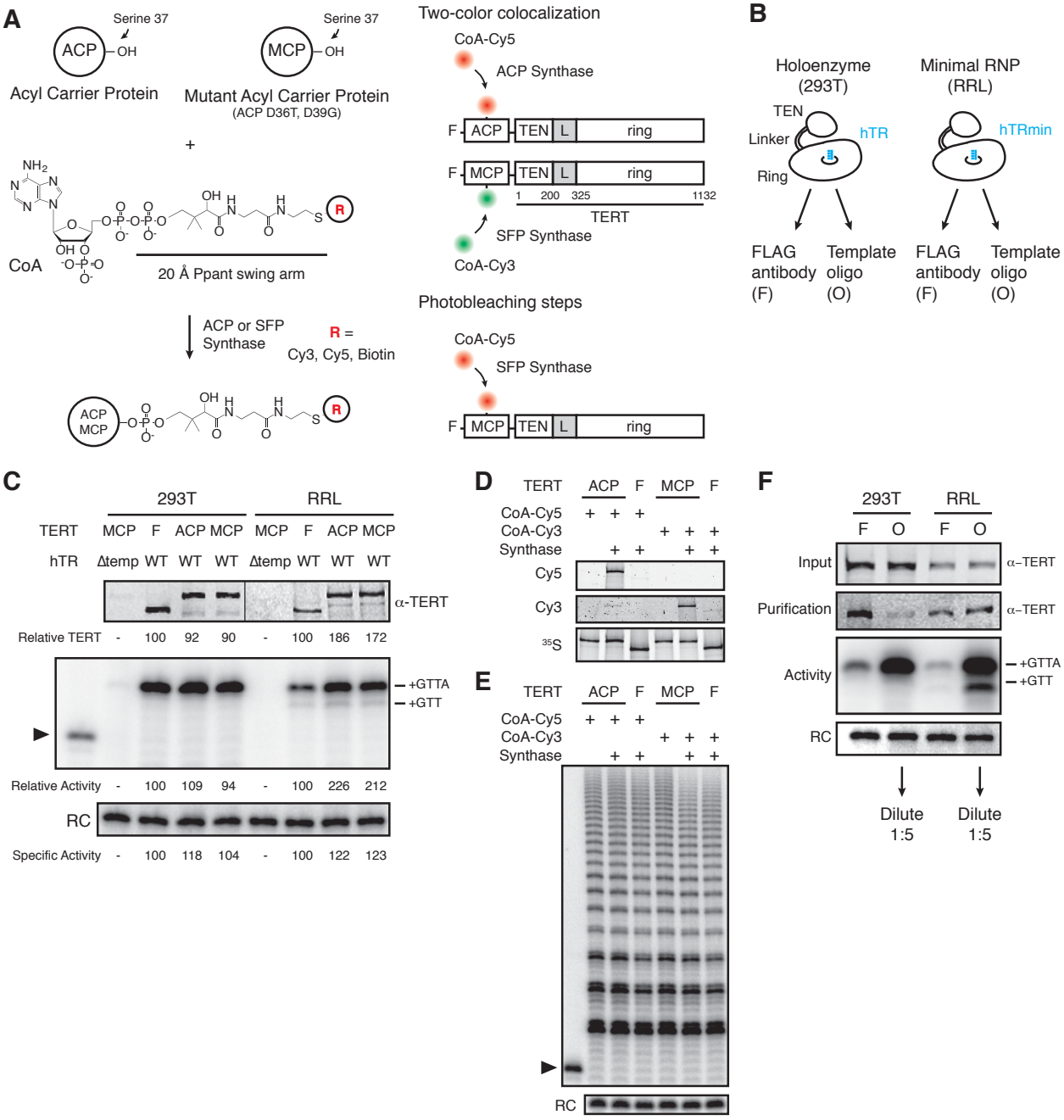
A
Serine 37
ACP
OH
Acyl Carrier Protein
Serine 37
MCP
OH
Mutant Acyl Carrier Protein
(ACP D36T, D39G)
+
CoA
20 Å Ppant swing arm
ACP or SFP
Synthase
R =
Cy3, Cy5, Biotin
ACP
MCP
Two-color colocalization
CoA-Cy5
ACP Synthase
F
ACP
TEN
L
ring
MCP
1
200
325
1132
TERT
SFP Synthase
CoA-Cy3
Photobleaching steps
CoA-Cy5
SFP Synthase
B
Holoenzyme
(293T)
Minimal RNP
(RRL)
TEN
Linker
Ring
hTR
hTRmin
FLAG
antibody
(F)
Template
oligo
(O)
C
293T
RRL
TERT
MCP
F
ACP
MCP
hTR
Δtemp
WT
α-TERT
Relative TERT
100
92
90
186
172
+GTTA
+GTT
Relative Activity
109
94
226
212
RC
Specific Activity
118
104
122
123
D
CoA-Cy5
CoA-Cy3
Synthase
Cy5
Cy3
35S
E
F
Input
Purification
Activity
RC
Dilute
1:5

Figure 2.2 Methods of human telomerase reconstitution and purification.

(**A**) Telomerase reconstitutions in cells with full-length hTR or in RRL with hTRmin generate hTR-free TERT, TERT RNPs and TERT-free hTR. These are differentially enriched by TERT-based versus template-based affinity purification. The template region is boxed as an overlay on RNA secondary structure overall (position numbering is from full-length hTR). Reconstituted complexes are schematized with only part of the RNA, and proteins other than TERT are not depicted. Telomerase RNP is shown with template in the active site. Relative elution of TERT RNP versus TERT-free hTR or hTR-free TERT was not determined.
(**B**) Sequence of the template affinity oligonucleotide and displacement oligonucleotide used for RNA-based purification. Only the template/pseudoknot (t/PK) domain of hTR is illustrated; the template region primary sequence is shown maximally base-paired to the template affinity oligonucleotide.
(**C**) Activity of RRL-reconstituted, F-purified TERT RNP with displacement oligonucleotide added directly to the activity assay reaction at the concentration indicated.
(**D**) Detection of overexpressed (OE) 293T F-TERT in unpurified cell extract by immunoblot with TERT antibody or FLAG antibody. Cell extract lacking overexpressed TERT was used as the negative control, and detection of tubulin was used as a loading control.

Figure 2.2

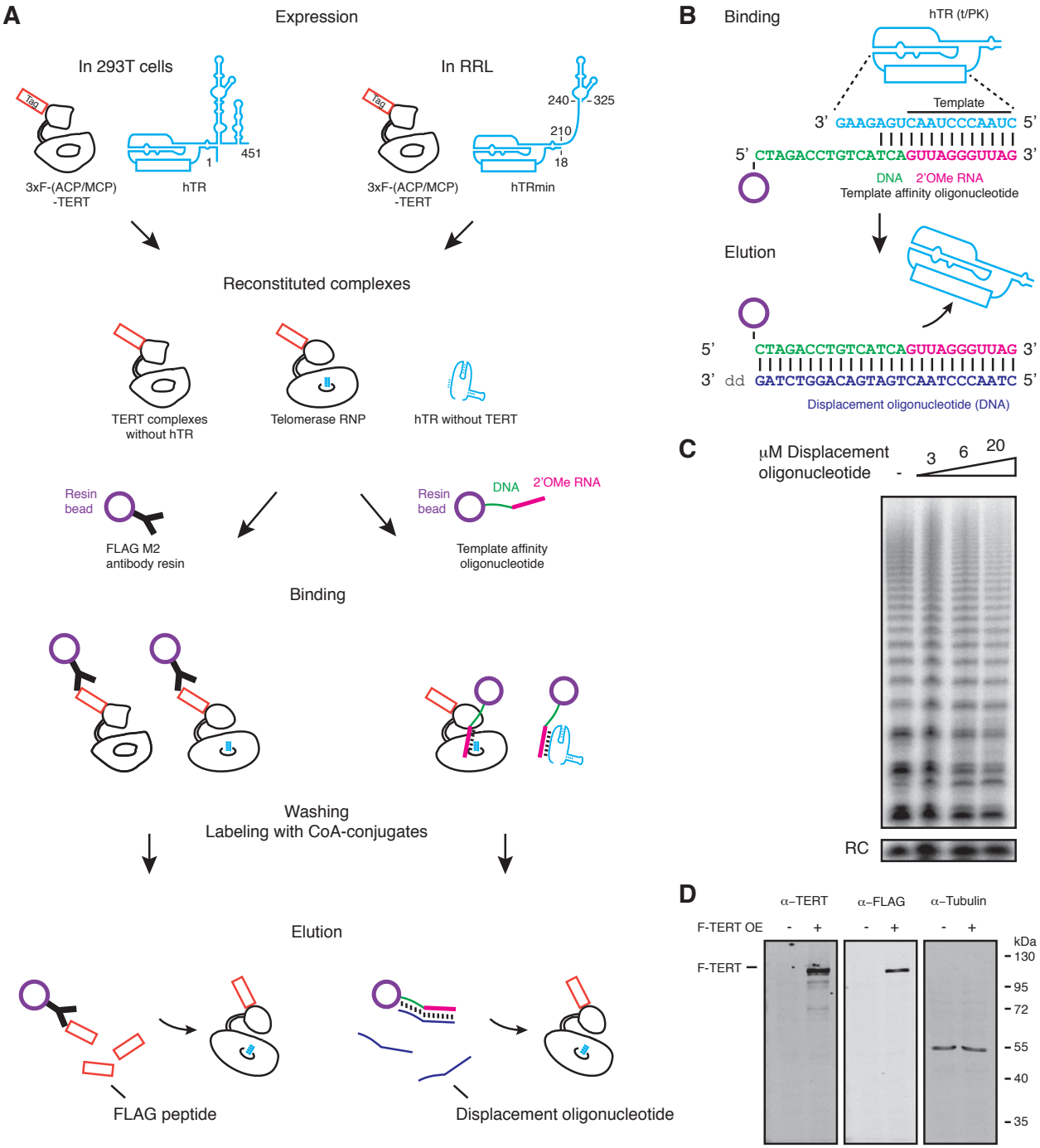
A
Expression
In 293T cells
In RRL
Tag
3xF-(ACP/MCP)
-TERT
hTR
1
451
240
325
210
18
hTRmin
Reconstituted complexes
TERT complexes
without hTR
Telomerase RNP
hTR without TERT
Resin
bead
FLAG M2
antibody resin
DNA
2'OMe RNA
Template affinity
oligonucleotide
Binding
Washing
Labeling with CoA-conjugates
Elution
FLAG peptide
Displacement oligonucleotide
B
Binding
hTR (t/PK)
Template
3' GAAGAGUCAAUCCCAAUC 5'
5' CTAGACCTGTCATCAGUUAGGGUUAG 3'
DNA 2'OMe RNA
Template affinity oligonucleotide
Elution
5' CTAGACCTGTCATCAGUUAGGGUUAG 3'
3' dd GATCTGGACAGTAGTCAATCCCAATC 5'
Displacement oligonucleotide (DNA)
C
μM Displacement
oligonucleotide
3
6
20
RC
D
α–TERT
α–FLAG
α–Tubulin
F-TERT OE
F-TERT
kDa
130
95
72
55
40
35

Figure 2.3 Single-molecule detection of the TERT subunit content in DNA-bound complexes.

(**A**) *Left:* Schematic for detection of TERT content by two-color colocalization. ACP-TERT was labeled with Cy5 (red) and MCP-TERT was labeled with Cy3 (green). PEG indicates polyethylene glycol. *Center:* Example of detection of two-color colocalization indicated by arrowheads, for a 293T-F sample. *Right:* Percentage of two-color colocalization for DNA-bound complexes with coexpressed ACP- and MCP-TERTs, purified by the TERT tag (F) or template-complementary 2'OMe RNA oligonucleotide (O). For this and subsequent quantifications, values are averaged from 3 assays using experimentally independent replicates with standard error of the mean shown. **$p<0.01$ using one-way ANOVA, followed by Tukey's multiple comparison test; n.s. is not significant.
(**B**) *Left:* Schematic for detection of TERT content by steps of photobleaching. MCP-TERT was labeled with Cy5 (red). *Center:* Examples of photobleaching in one or two steps. *Right:* Percentage of MCP-TERT DNA-bound complexes labeled with Cy5 that photobleached in one, two and three or more (3+) steps. Values are the average of triplicate experimental replicates.
(**C**) The predicted relationship between detections of TERT subunit colocalization and two-step photobleaching is shown as the green line (see Equation 3). Data were plotted according to
measured colocalization and photobleaching in two steps only. Error bars represent standard
error of the mean from triplicate experimental replicates of each measured parameter.
(**D**) Measured two-color colocalization and two-step photobleaching as determined by the experiments in (**A)** and (**B)**, respectively.

Figure 2.3

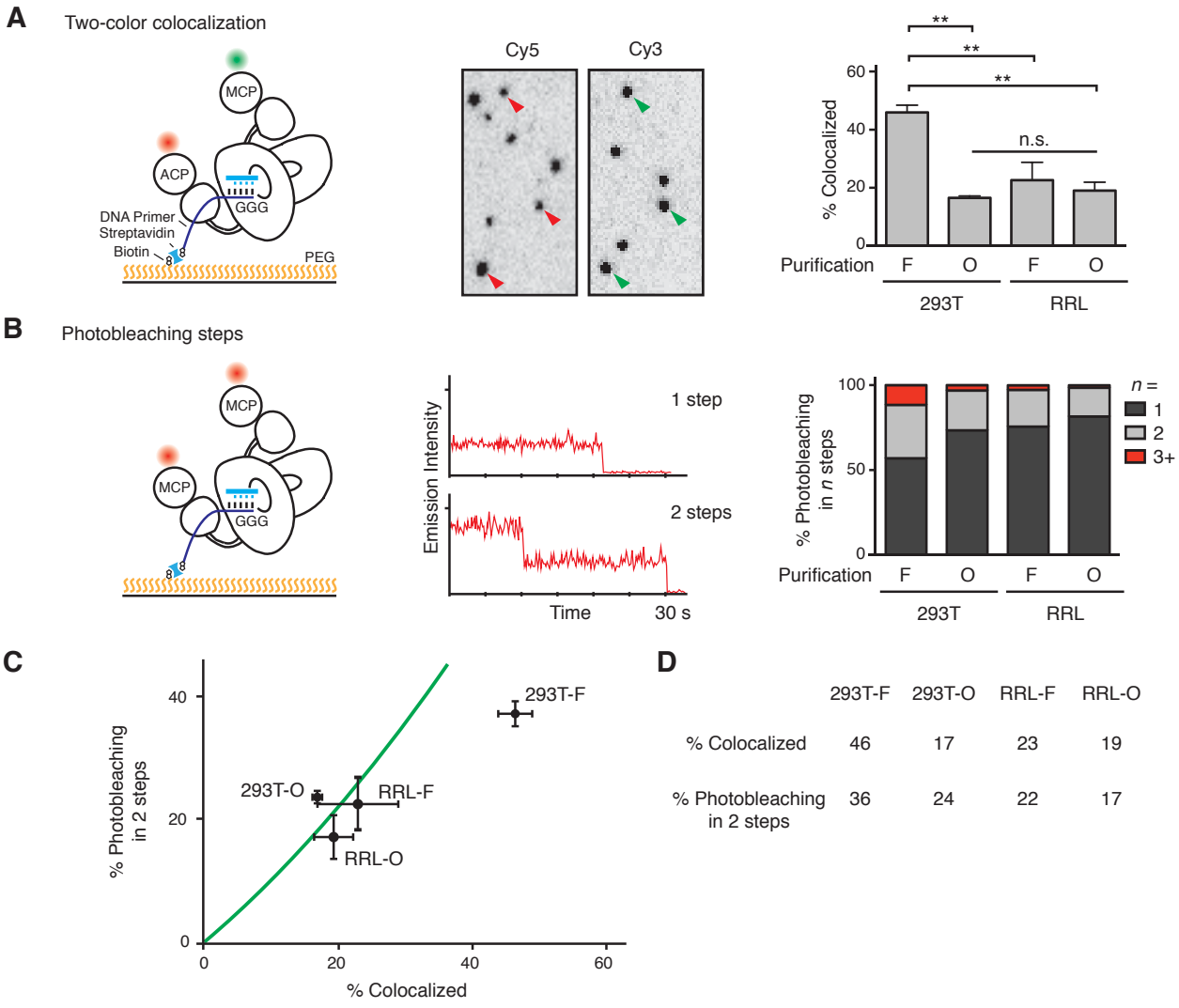

	293T-F	293T-O	RRL-F	RRL-O
% Colocalized	46	17	23	19
% Photobleaching in 2 steps	36	24	22	17

Figure 2.4 Technical robustness of the two-color colocalization assay for TERT subunit content.

Quantification of two-color colocalization for DNA-bound 293T-F and 293T-O TERT complexes was consistent across different spot densities per field (**A**) and using cell extracts from independent transfections of 293T cells (**B**). In (**A**), light blue dots are 293T-F quantification and dark blue dots are 293T-O quantifications from imaging multiple (≥8) fields for each of triplicate experimental replicates. In (**B**), averages are from multiple (≥8) fields counted for each sample.

Figure 2.4

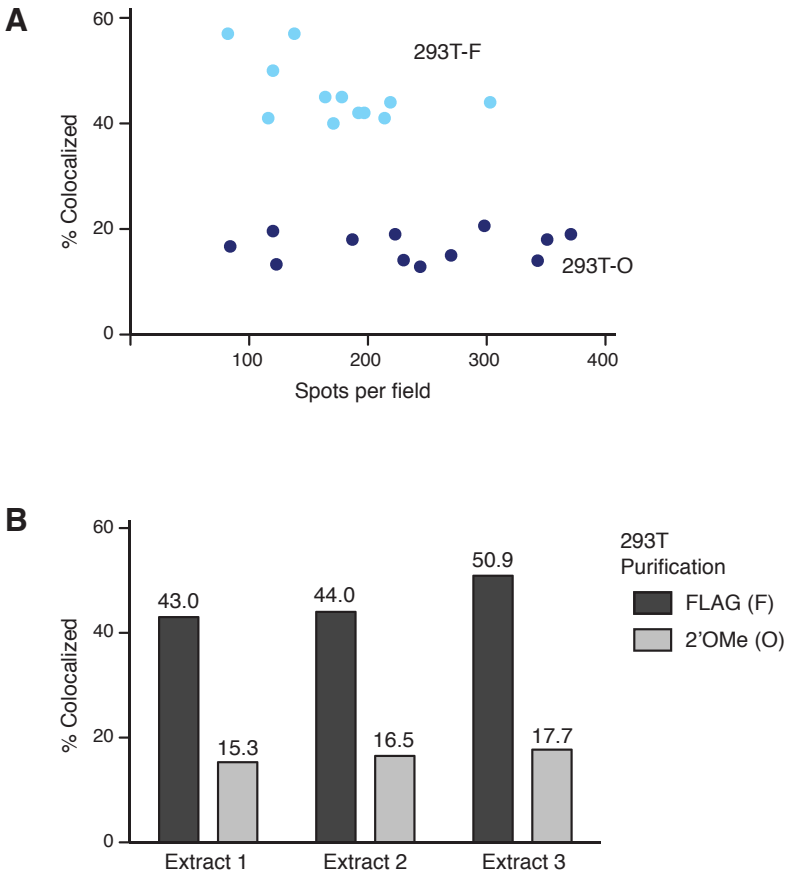
A
60
40
20
0
% Colocalized
293T-F
293T-O
100
200
300
400
Spots per field
B
60
40
20
0
% Colocalized
43.0
15.3
44.0
16.5
50.9
17.7
Extract 1
Extract 2
Extract 3
293T
Purification
FLAG (F)
2'OMe (O)

Figure 2.5 Quantification of the TERT monomer versus multimer content in purified samples based on TERT labeling efficiency.

(**A**) SDS-PAGE analysis of the kinetics of labeling F-purified 293T- or RRL-reconstituted MCP-TERT in reactions with CoA-Cy5 or CoA-Cy3 and SFP synthase. Lines within the panel indicate separate sets of gel lanes. Quantification of labeling intensity was normalized to labeling at the 4 h time point after subtraction of background.
(**B**) Cy5 labeling relative to TERT amount analyzed for telomerase reconstituted and purified as indicated. TERT was detected by TERT immunoblot. Values are the average of triplicate experimental replicates.
(**C**) Validation of equivalent labeling using CoA-dye or CoA-biotin by sequential labeling of F-purified, RRL-expressed MCP-TERT with SFP synthase. Initial TERT labeling using CoA-Cy3 or CoA-biotin competes for subsequent TERT labeling by the other CoA derivative. The biotin label on MCP-TERT was detected by biotin antibody immunoblot.
(**D**) *Left:* Schematic of the biotinylated TERT depletion procedure. *Right:* Quantification of ACP- and/or MCP-TERT remaining after streptavidin agarose depletion, following reconstitution (RRL unless indicated otherwise), F-purification and labeling using CoA-biotin and ACP (A) or SFP (S) synthase. RRL-expressed TERT was ^{35}S-methionine labeled and 293T-expressed TERT was detected by FLAG antibody immunoblot. Samples labeled in reactions lacking CoA-biotin (not Biotin +) were labeled with CoA and those not applied to streptavidin agarose (not Streptavidin depletion +) were mock-depleted on Myc antibody agarose. Lines within the panel indicate separate sets of gel lanes run in parallel. Percentage unbound was calculated as unbound signal normalized to unbound signal of the control depletion. Values are the average of triplicate experimental replicates.
(**E**) Activity of the unbound fraction after streptavidin agarose depletion of biotinylated telomerase labeling using CoA-biotin and SFP synthase, under native binding conditions. Telomerase activity was assayed in reactions with dATP, dGTP, dTTP and α-^{32}P dGTP, followed by denaturing gel electrophoresis; number of 6-nucleotide repeats added to product DNA is indicated. Samples not depleted with streptavidin agarose were mock-depleted on Myc antibody agarose. Lines within the panel indicate separate sets of gel lanes run in parallel. Percentage unbound was normalized to unbound after control depletion. Values are the average of triplicate experimental replicates.
(**F**) *Left:* Schematic of the biotinylated TERT depletion procedure and unbound fraction analysis. *Right:* Quantification of total TERT and biotinylated MCP-TERT in the unbound fraction of 293T-reconstituted, F-purified telomerase, following labeling using CoA-biotin or CoA and depletion by streptavidin agarose or mock-depletion on Myc antibody agarose. MCP-TERT and the biotin label on MCP-TERT were detected by immunoblot. Values are the average of triplicate experimental replicates.
(**G**) Illustration of labeling efficiency determination by comparison of the percent unbound total MCP-TERT and unbound biotinylated MCP-TERT.
(**H**) Calculated percentage of DNA-bound TERT monomer complexes according to fraction TERT subunit colocalization (percentages indicated), assuming the TERT labeling efficiency measured value (82%, blue line; bar graph at *right*), lower bound (51%, green line; Low L numbers at *right*) or upper bound (100%, purple line; High L

numbers at *right*). Vertical dashed lines are the observed fraction of two-color colocalization (from Figure 2.3A).
(**I**) Calculated percentage of DNA-bound TERT monomer complexes according to fraction of one-step photobleaching (percentages indicated), assuming the TERT labeling efficiency measured value (82%, blue line; bar graph at *right*), lower bound (51%, green line; High L numbers at *right*) or upper bound (100%, purple line; Low L numbers at *right*). Vertical dashed lines are the observed fraction of one-step photobleaching (from Figure 2.3B).

Figure 2.5

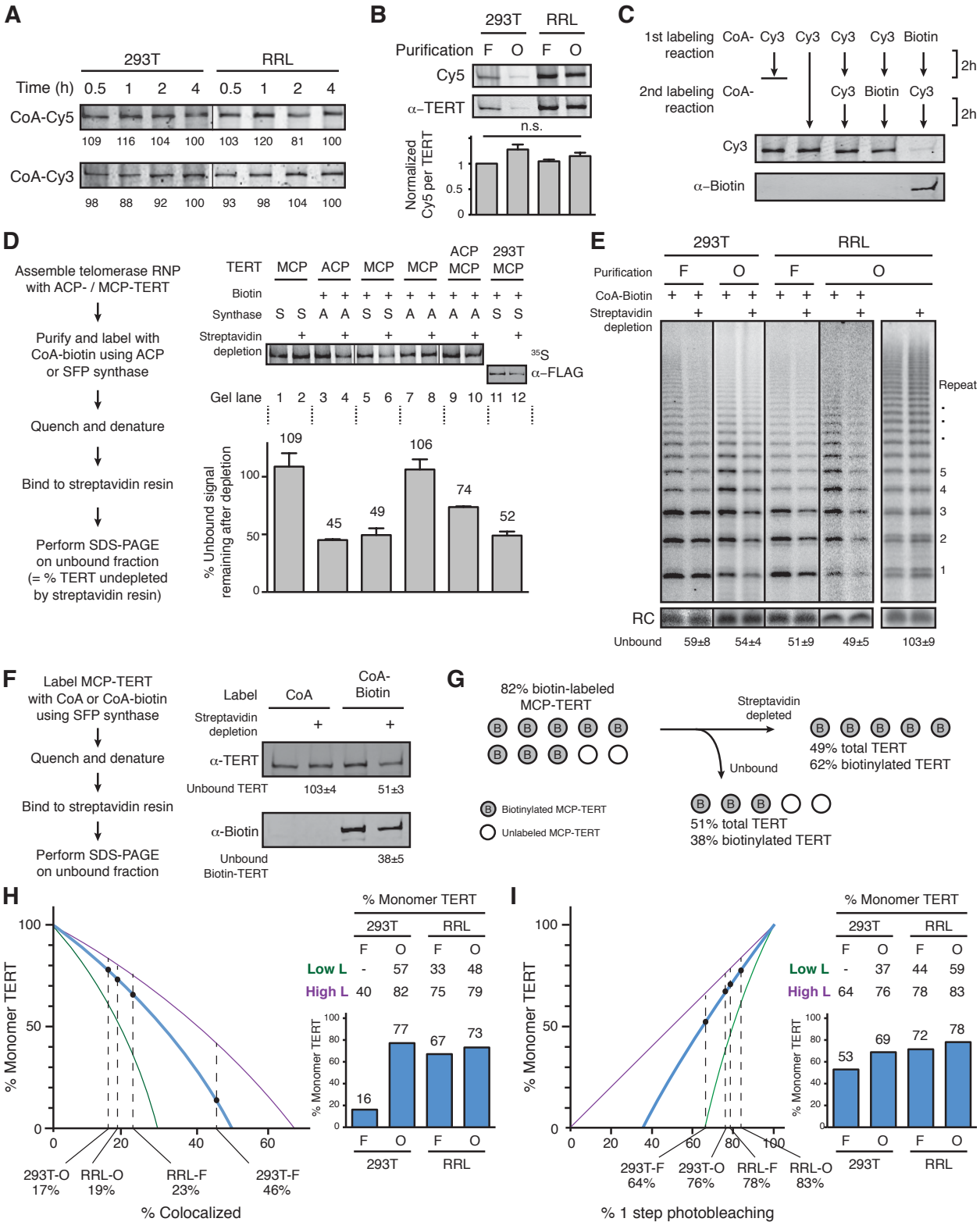
A
293T
RRL
Time (h) 0.5 1 2 4 0.5 1 2 4
CoA-Cy5
109 116 104 100 103 120 81 100
CoA-Cy3
98 88 92 100 93 98 104 100
B
293T RRL
Purification F O F O
Cy5
α–TERT
n.s.
Normalized Cy5 per TERT
C
1st labeling reaction CoA- Cy3 Cy3 Cy3 Cy3 Biotin
2h
2nd labeling reaction CoA- Cy3 Biotin Cy3
2h
Cy3
α–Biotin
D
Assemble telomerase RNP with ACP- / MCP-TERT
Purify and label with CoA-biotin using ACP or SFP synthase
Quench and denature
Bind to streptavidin resin
Perform SDS-PAGE on unbound fraction (= % TERT undepleted by streptavidin resin)
TERT MCP ACP MCP MCP ACP MCP 293T MCP
Biotin
Synthase S S A A S S A A A A S S
Streptavidin depletion
35S
α–FLAG
Gel lane 1 2 3 4 5 6 7 8 9 10 11 12
% Unbound signal remaining after depletion
109 45 49 106 74 52
E
293T RRL
Purification F O F O
CoA-Biotin
Streptavidin depletion
Repeat
RC
Unbound 59±8 54±4 51±9 49±5 103±9
F
Label CoA CoA-Biotin
Streptavidin depletion
α-TERT
Unbound TERT 103±4 51±3
α-Biotin
Unbound Biotin-TERT 38±5
Label MCP-TERT with CoA or CoA-biotin using SFP synthase
Quench and denature
Bind to streptavidin resin
Perform SDS-PAGE on unbound fraction
G
82% biotin-labeled MCP-TERT
Streptavidin depleted
Unbound
49% total TERT
62% biotinylated TERT
51% total TERT
38% biotinylated TERT
Biotinylated MCP-TERT
Unlabeled MCP-TERT
H
% Monomer TERT
293T-O 17%
RRL-O 19%
RRL-F 23%
293T-F 46%
% Colocalized
% Monomer TERT
293T RRL
F O F O
Low L - 57 33 48
High L 40 82 75 79
16 77 67 73
293T RRL
I
% Monomer TERT
293T-F 64%
293T-O 76%
RRL-F 78%
RRL-O 83%
% 1 step photobleaching
% Monomer TERT
293T RRL
F O F O
Low L - 37 44 59
High L 64 76 78 83
53 69 72 78
293T RRL

Figure 2.6 Distinct profiles of activity-dependent elution across populations of TERT complexes.

(**A**) Schematic of TERT complexes' interaction with bound DNA. In the presence of dTTP and dATP, complexes bound productively to primer end GGG-3' would elongate the primer to GGGTTA-3' accompanied by increased likelihood of DNA release (elution, at *top*). Non-productively bound RNP complexes and hTR-free TERT would not elongate the primer and therefore not elute by DNA synthesis, and some productively bound RNP complexes could also fail to elongate primer and/or to release from product DNA. The $t_{1/2}$ values are from published studies using human telomerase holoenzyme (Wallweber et al., 2003).
(**B**) Schematic of the activity-dependent elution procedure.
(**C**) Activity-dependent elution of Cy5-labeled wild-type (WT) or catalytic-dead (D868A) MCP-TERT complexes using buffer containing dATP + dTTP or buffer only. Spot count per field of labeled TERT complexes was normalized to the initial time point. Specific elution was calculated by subtracting the fraction of complexes with buffer-only elution from the fraction eluted with dNTPs. The relative count of DNA-bound complexes from sample pre-treated with RNase A is indicated by shaded gray bars.
(**D**) Schematic of the procedure for post-elution counting and photobleaching of labeled complexes.
(**E**) Number of MCP-TERT DNA-bound complexes labeled with Cy5 per imaging field that photobleached in one, two and three or more steps after elution incubation with or without dNTPs. ***$p<0.001$ by unpaired Student's t-test, n.s. is not significant.
(**F**) Calculated percentage of DNA-bound TERT monomer and dimer complexes after elution according to fractional one-step photobleaching, assuming 82% TERT labeling efficiency.

Figure 2.6

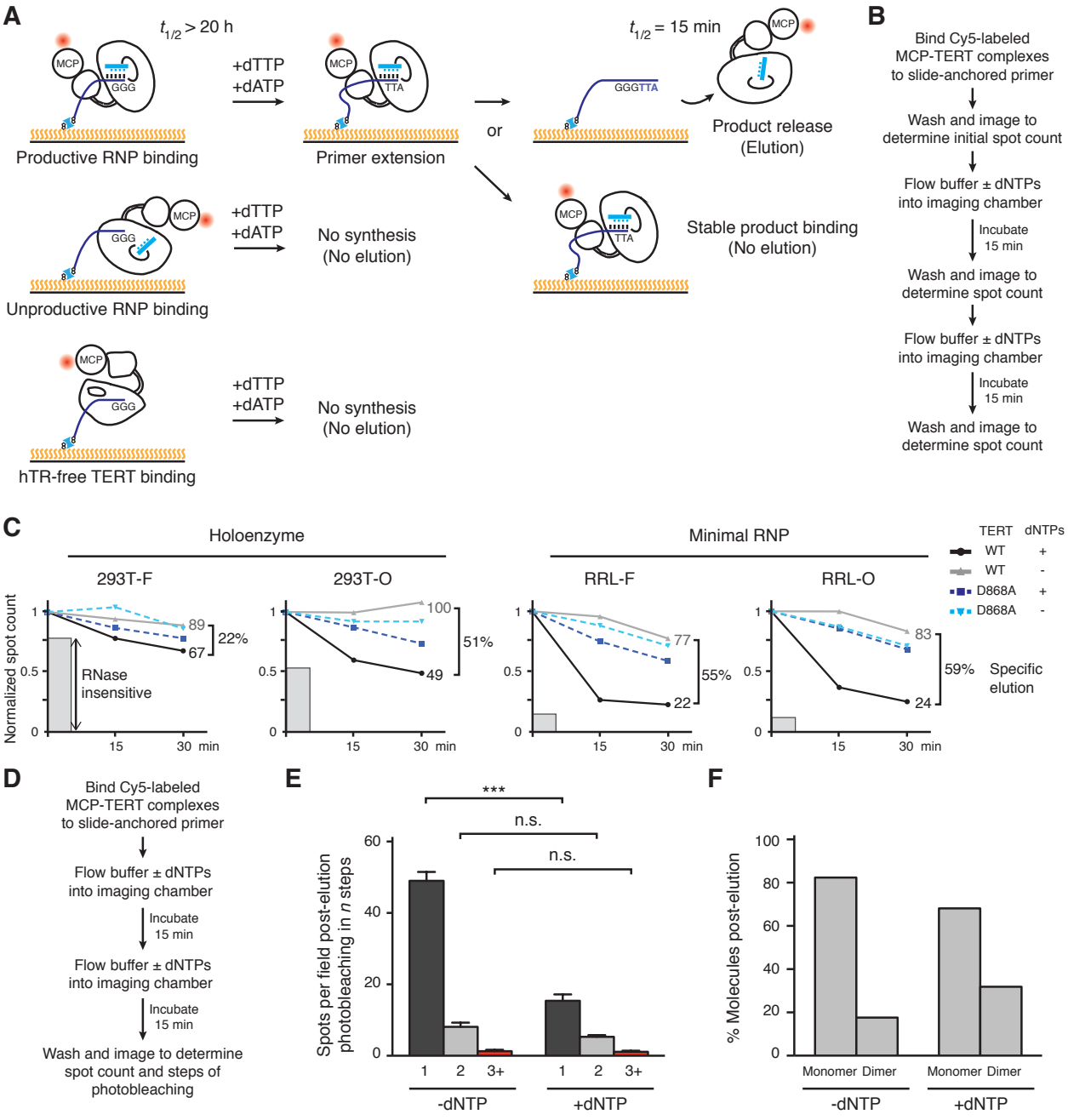
A
$t_{1/2}$ > 20 h
MCP
GGG
Productive RNP binding
+dTTP
+dATP
TTA
Primer extension
or
$t_{1/2}$ = 15 min
GGGTTA
Product release
(Elution)
Unproductive RNP binding
No synthesis
(No elution)
Stable product binding
(No elution)
hTR-free TERT binding
B
Bind Cy5-labeled
MCP-TERT complexes
to slide-anchored primer
Wash and image to
determine initial spot count
Flow buffer ± dNTPs
into imaging chamber
Incubate
15 min
Wash and image to
determine spot count
C
Holoenzyme
Minimal RNP
293T-F
293T-O
RRL-F
RRL-O
TERT
dNTPs
WT
D868A
Normalized spot count
RNase
insensitive
22%
51%
55%
59%
Specific
elution
min
D
Bind Cy5-labeled
MCP-TERT complexes
to slide-anchored primer
Flow buffer ± dNTPs
into imaging chamber
Incubate
15 min
Wash and image to determine
spot count and steps of
photobleaching
E
***
n.s.
Spots per field post-elution
photobleaching in n steps
-dNTP
+dNTP
F
% Molecules post-elution
Monomer
Dimer

Figure 2.7 Direct DNA binding affinity comparison for TERT complexes in bulk purifications.

(**A**) Schematic for detection of Cy5-labeled DNA binding to biotinylated TERT complexes.
(**B**) SDS-PAGE analysis of MCP-TERT complexes labeled using CoA-Cy5. Cy5-labeled MCP-TERT proteolysis products that retain the N-terminal F-MCP tag and are enriched in the 293T-F purification are schematized in comparison to full-length TERT.
(**C**) Concentration dependence of Cy5-labeled DNA retention by slide-anchored TERT complexes across a titration of 0.3, 1, 3, 10 and 30 nM DNA. Spot count per field was normalized to the 30 nM DNA quantification for each sample. Error bars represent standard error of the mean of spot counts of 5 fields per sample per DNA concentration.
(**D**) Graph of the change in Cy5-labeled DNA spot count comparing assays of 30 versus 100 nM DNA, normalized to the 30 nM DNA quantifications for each sample. Error bars represent standard error of the mean of spot counts of 5 fields per sample per DNA concentration.

Figure 2.7

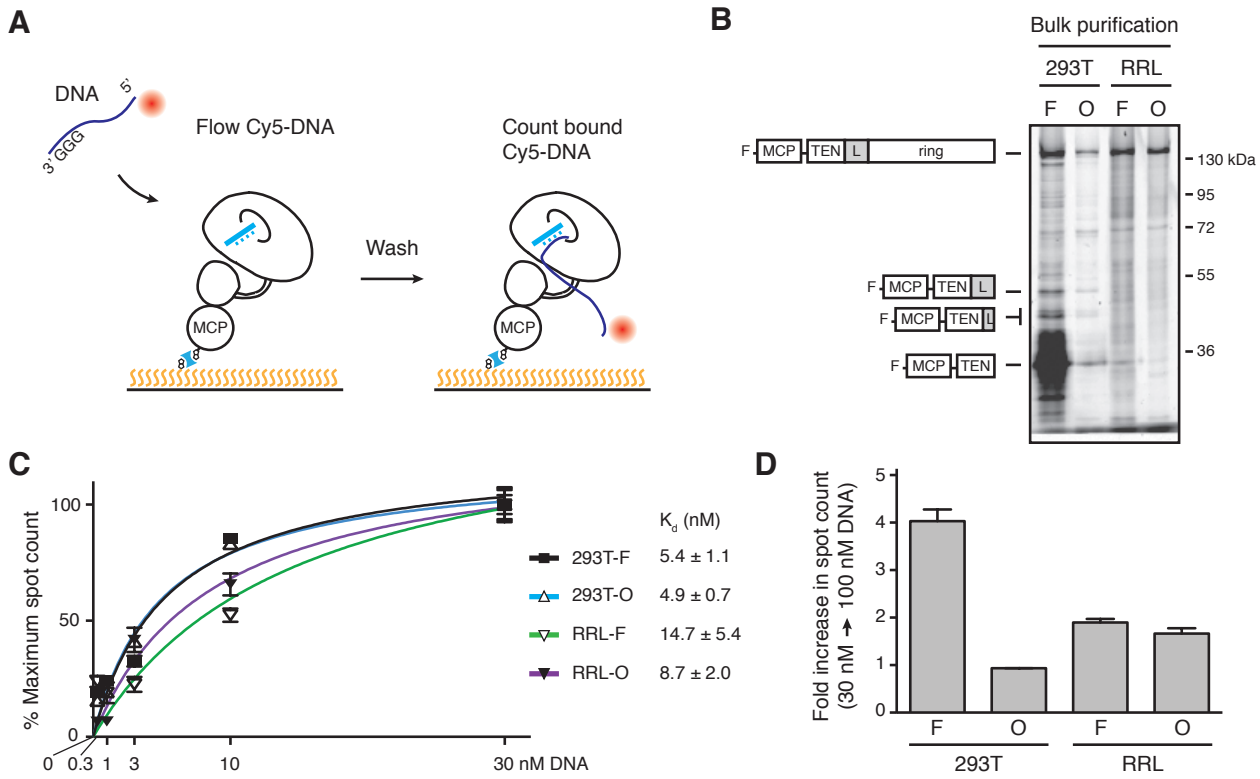
A
DNA
5'
3' GGG
Flow Cy5-DNA
Count bound Cy5-DNA
Wash
MCP
B
Bulk purification
293T
RRL
F O F O
F MCP TEN L ring
F MCP TEN L
F MCP TEN L
F MCP TEN
130 kDa
95
72
55
36
C
% Maximum spot count
100
50
0
0 0.3 1 3 10 30 nM DNA
K_d (nM)
293T-F 5.4 ± 1.1
293T-O 4.9 ± 0.7
RRL-F 14.7 ± 5.4
RRL-O 8.7 ± 2.0
D
Fold increase in spot count (30 nM → 100 nM DNA)
5
4
3
2
1
0
F O F O
293T RRL

Figure 2.8 Telomerase RNP assembly and activity without the TEN domain linker.

(**A**) Schematic representation and expression of N-terminally F-tagged human TERT proteins with the linker replaced by 20, 10 or 5 repeats of the sequence NAAIRS (TERT-20N through 5N) or linker deleted without compensating sequence insertion (TERT-ΔPAL). TERTs expressed in 293T cells were detected by immunoblot with TERT antibody, and TERTs expressed in RRL were detected by ^{35}S-methionine labeling during synthesis.
(**B**) Activity and hTR content of 293T- or RRL-reconstituted, F-purified TERT RNPs with altered linker sequence, bound to FLAG antibody resin. Spot-blot hybridization was used to detect hTR. Relative activity and hTR content were normalized to the WT TERT purification after background subtraction of activity or hTR in the purification of untagged WT TERT. Specific activity was calculated from relative activity and relative hTR.
(**C**) Processive extension of 5'-labeled $(T_2AG_3)_3$ primer by telomerase assembled with WT, ΔPAL or 20N TERT, bound to FLAG antibody resin. The labeled primer was extended for 5 min before chase addition of unlabeled primer for a total extension time of 10, 20 or 40 min.
(**D**) Activity and hTR content of telomerase in 293T input extracts or bound to Myc antibody resin. TPP1 OB-fold domain expression and purification were confirmed by immunoblot detection of the 3xMyc tag. Immunoblot and activity assay with whole cell extract used 2% of the total purification input. Half of the post-purification sample was used for activity assays and half for Myc immunoblot. Spot-blot hybridization was used to detect hTR. Relative activity and hTR content were normalized to the input or bound sample for TPP1 purification of WT TERT, after bound hTR background subtraction using the purification without tagged TPP1 OB-fold domain. Relative percentage enrichment was calculated as relative bound activity adjusted for relative input activity. Specific activity was calculated from relative activity and relative hTR.
(**E**) SDS-PAGE analysis of O-purified 293T MCP-TERT complexes labeled using CoA-Cy5. MCP-TERT fragments resulting from proteolysis within the PAL of WT TERT are schematized, in comparison to full-length TERT.

Figure 2.8

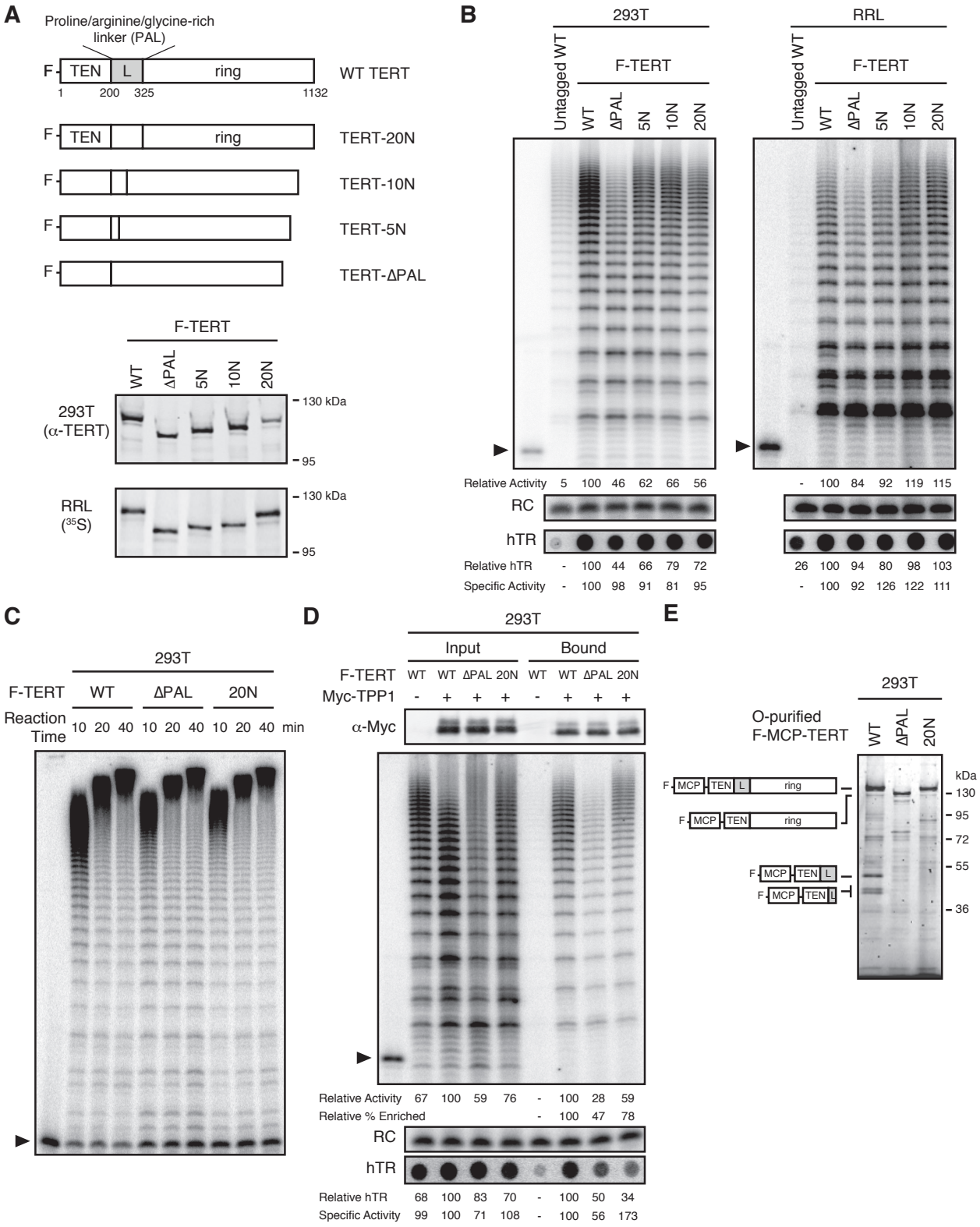
A
Proline/arginine/glycine-rich linker (PAL)
F
TEN
L
ring
1
200
325
1132
WT TERT
TERT-20N
TERT-10N
TERT-5N
TERT-ΔPAL
F-TERT
WT
ΔPAL
5N
10N
20N
293T (α-TERT)
RRL (35S)
130 kDa
95
B
293T
RRL
Untagged WT
F-TERT
Relative Activity
RC
hTR
Relative hTR
Specific Activity
C
293T
F-TERT
Reaction Time
10 20 40 10 20 40 10 20 40 min
D
293T
Input
Bound
Myc-TPP1
α-Myc
Relative Activity
Relative % Enriched
RC
hTR
Relative hTR
Specific Activity
E
293T
O-purified F-MCP-TERT
MCP
kDa
130
95
72
55
36

Figure 2.9 PAL-mediated TERT dimerization.

(**A**) Two-color colocalization quantification for DNA-bound O-purified complexes of coexpressed ACP- and MCP-TERTs. Values are the average of triplicate experimental replicates. ***$p<0.001$ using one-way ANOVA, followed by Tukey's multiple comparison test.
(**B**) Calculated percentage of DNA-bound TERT monomer complexes according to the fraction of two-color TERT colocalization (percentages indicated), assuming the TERT labeling efficiency measured value (82%, blue line; bar graph at *right*), lower bound (51%, green line; Low L numbers at *right*) or upper bound (100%, purple line; High L numbers at *right*).
(**C**) Photobleaching step quantification for DNA-bound O-purified MCP-TERT complexes labeled with Cy5. Values are the average of triplicate experimental replicates.
(**D**) Calculated percentage of DNA-bound TERT monomer complexes according to the fraction of one-step photobleaching (percentages indicated), assuming the TERT labeling efficiency measured value (82%, blue line; bar graph at *right*), lower bound (51%, green line; Low L numbers at *right*) or upper bound (100%, purple line; High L numbers at *right*).
(**E**) Activity-dependent elution of O-purified Cy5-labeled MCP-TERT complexes using buffer containing dATP + dTTP or buffer only. Spot count per field of labeled TERT complexes was normalized to the initial time point of each sample. Specific elution was calculated by subtracting the fraction of complexes with buffer-only elution from the fraction eluted with dNTPs.
(**F**) Illustration presenting the hypothesis of differences in TERT PAL conformation that occur with TERT RNP assembly or dimerization. The PAL is shown with conformations that correlate with catalytically active (red) or inactive (pink) TERT complexes.

Figure 2.9

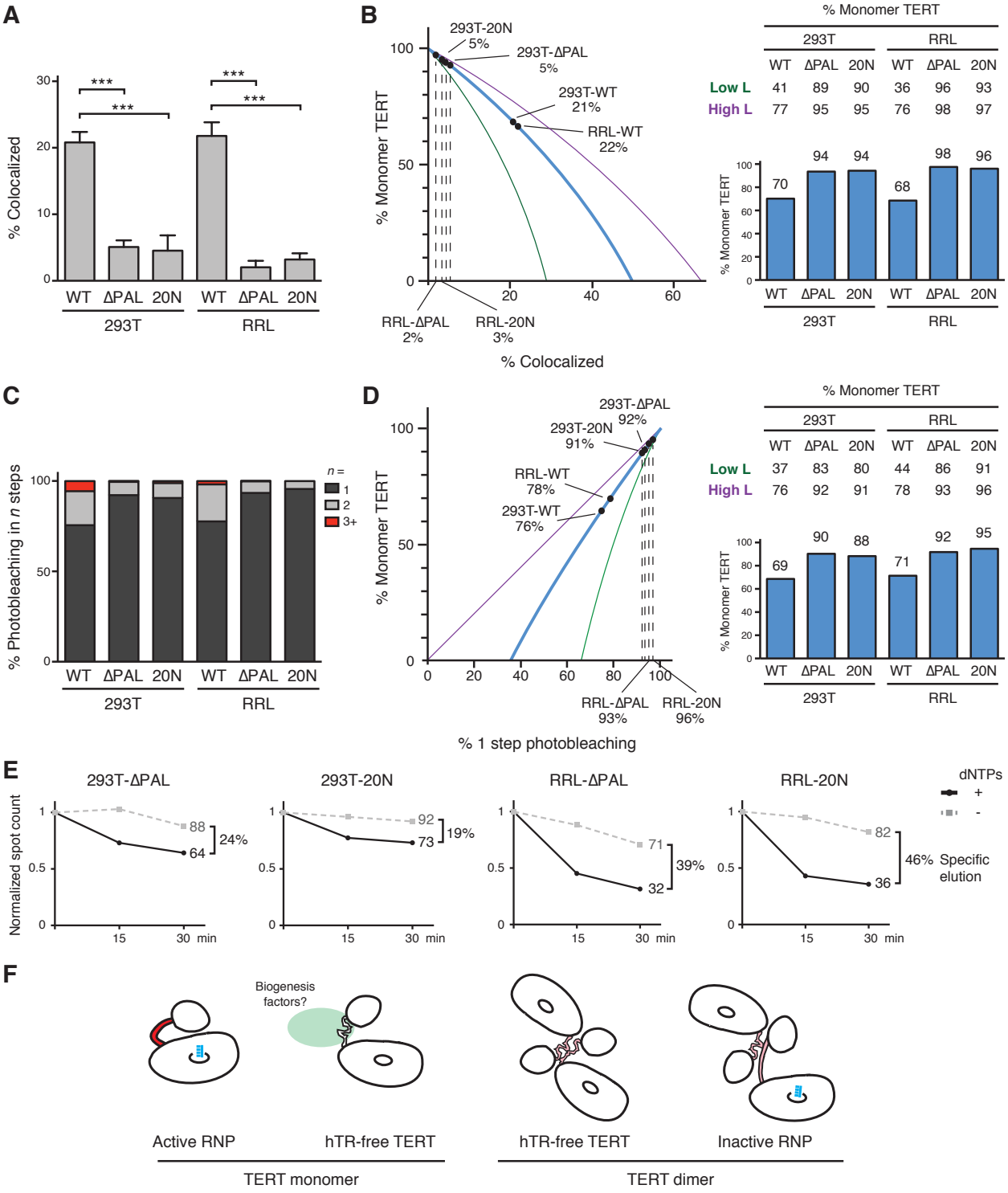
A
% Colocalized
***
***
***
***
WT ΔPAL 20N WT ΔPAL 20N
293T
RRL
B
293T-20N 5%
293T-ΔPAL 5%
293T-WT 21%
RRL-WT 22%
RRL-ΔPAL 2%
RRL-20N 3%
% Monomer TERT
% Colocalized
% Monomer TERT
293T RRL
WT ΔPAL 20N WT ΔPAL 20N
Low L 41 89 90 36 96 93
High L 77 95 95 76 98 97
70 94 94 68 98 96
C
% Photobleaching in n steps
n = 1 2 3+
WT ΔPAL 20N WT ΔPAL 20N
293T
RRL
D
293T-ΔPAL 92%
293T-20N 91%
RRL-WT 78%
293T-WT 76%
RRL-ΔPAL 93%
RRL-20N 96%
% Monomer TERT
% 1 step photobleaching
% Monomer TERT
293T RRL
WT ΔPAL 20N WT ΔPAL 20N
Low L 37 83 80 44 86 91
High L 76 92 91 78 93 96
69 90 88 71 92 95
E
293T-ΔPAL
293T-20N
RRL-ΔPAL
RRL-20N
dNTPs + -
Normalized spot count
88 64 24%
92 73 19%
71 32 39%
82 36 46%
Specific elution
15 30 min
F
Biogenesis factors?
Active RNP
hTR-free TERT
hTR-free TERT
Inactive RNP
TERT monomer
TERT dimer

CHAPTER THREE

Human Telomerase Specialization for Repeat Synthesis by Unique Handling of Primer-Template Duplex

Based on Wu and Collins, *EMBO Journal*, 2014

Abstract

In this chapter, I develop human telomerase domain-complementation assays for TERT and RNA in combination with the first direct footprinting assay for telomerase association with bound DNA. Using these assays, I resolve mechanisms by which TERT domains and RNA motifs direct repeat synthesis. Surprisingly, I find that product-template hybrid is sensed in a length- and sequence-dependent manner to set the template 5' boundary. I demonstrate that the TEN domain determines active-site use of the atypically short primer-template hybrid necessary for telomeric repeat synthesis. Also against expectation, I show that the remainder of TERT (the TERT ring) supports both functional recognition and physical protection of single-stranded DNA adjacent to the template hybrid. These findings establish unprecedented polymerase recognition specificities for DNA-RNA hybrid and single-stranded DNA and change the paradigm for telomerase adaptation to telomeric repeat synthesis.

Introduction

Distinct from other reverse transcriptases, telomerase product DNA is single-stranded rather than a more thermodynamically stable DNA-RNA duplex (Collins, 2011). After primer elongation across the internal TER template to the template 5' boundary, DNA product is released entirely from template base-pairing. Dissociation of the product-template duplex is generally considered rate-limiting for enzyme activity in vitro (Podlevsky and Chen, 2012). Remarkably, most telomerase enzymes can realign the released product 3' end with the template 3' end, forming a limited length of template hybrid that can re-engage within the active site. Product DNA retention during this template repositioning gives rise to telomerase RAP. The RAP quantified for purified telomerase enzymes in vitro is likely to be regulated by coordination with other telomere replication factors in vivo, but the general physiological significance of a telomerase mechanism for RAP is supported by measurements of short telomere extension in yeast (Chang et al., 2007) and telomere length maintenance in human cells (Zhao et al., 2011). Consistent with these observations of RAP in biological context, a chemical inhibitor of human telomerase RAP induces telomere shortening (Pascolo et al., 2002), some disease-associated human TERT mutations primarily affect RAP (Robart and Collins, 2010; Alder et al., 2011) and engineered yeast and human TERTs with decreased RAP do not support telomere maintenance (Wyatt et al., 2010). Telomerase RAP implies atypical polymerase specificities of primer recognition that can discriminate a varying length of primer-template hybrid and also retain single-stranded DNA without base-pairing to the template.

The telomerase protein-nucleic acid interactions that confer specialized template and primer use derive at least in part from TERT-specific domains not shared with other reverse transcriptases (Blackburn and Collins, 2011; Podlevsky and Chen, 2012). TERT has four regions considered to be separate domains: the TEN domain, TERT RNA-binding domain (TRBD), Reverse Transcriptase domain (RT) and C-terminal extension (CTE). While vertebrate TERTs share an unusually long linker between the TEN domain and TRBD, TERTs from some species lack this linker and/or a discernable TEN domain. Unique features of the telomerase catalytic cycle depend on TERT-specific protein motifs and motifs within TER. The vertebrate TER secondary structure established by phylogenetic comparison, nuclease and chemical probing, mutagenesis and high-resolution structures (Podlevsky et al., 2008; Zhang et al., 2011; Egan and Collins, 2012a) includes the conserved template-adjacent pseudoknot (PK) and physically distant conserved regions 4 and 5 (CR4/5; Figure 3.1A), which together are necessary and sufficient for activity reconstitution in vitro. CR4/5 provides the major affinity of vertebrate TER-TERT interaction and stimulates catalytic activity (Mitchell and Collins, 2000). The telomerase PK has less clear function but known structure, with base triples that create a stably folded triple-helix (Theimer et al., 2005). Sequence changes in the extended PK of human TER (hTR), including disease-linked mutations, result in altered catalytic activity (Ly et al., 2003; Chen and Greider, 2005). Resolution of how the PK motif contributes to enzyme function has been complicated by an inability of mutagenesis-based interrogation to distinguish direct PK loss-of-function from indirect consequences of PK misfolding on the positioning of the adjacent TER template.

Telomerase primer binding and extension can be greatly stimulated by a single-stranded region of primer 5' of the primer-template hybrid (Morin, 1991; Collins and Greider, 1993; Lee and Blackburn, 1993). This enhancement is proposed to reflect the presence of a telomerase "anchor site," which, based on activity and primer dissociation assays for the human enzyme, would engage a length of about 2 telomeric repeats of single-stranded DNA (Morin, 1991; Wallweber et al., 2003). An anchor-site groove has been proposed in the atomic-resolution structure of the ciliate *T. thermophila* TERT TEN domain (Jacobs et al., 2006). In support of anchor-site function for the TEN domain, some TEN domain sequence substitutions alter primer K_m or RAP (Moriarty et al., 2004; Romi et al., 2007; Zaug et al., 2008). Also, single-stranded DNA cross-links to the protein linker between the TEN domain and TRBD (Romi et al., 2007) or potentially the TEN domain itself (Lue, 2005; Jacobs et al., 2006). The human TERT TRBD, RT and CTE domains fold together to form a ring encircling the active site (Gillis et al., 2008). RNP assembled in cells with this structural core of TERT (here described as the TERT ring) does not stably bind primer and supports the synthesis of only a single telomeric repeat, but if it is coexpressed with a physically separate TEN domain, the enzyme regains stable primer binding and RAP (Robart and Collins, 2011). These and other findings underlie the widely accepted dogma that the TEN domain mediates single-stranded DNA binding (Wyatt et al., 2010; Lewis and Wuttke, 2012; Podlevsky and Chen, 2012; Nandakumar and Cech, 2013). However, most assays of purified yeast, ciliate and human TERT TEN domains show weak if any specific interaction with single-stranded DNA (Xia et al., 2000; O'Connor et al., 2005; Wyatt et al., 2007; Finger and Bryan, 2008; Sealey et al., 2010; Bairley et al., 2011) and truncation of the TEN domain from full-length TERT does not eliminate DNA binding (Wyatt et al., 2007; Finger and Bryan, 2008). Also, sequence substitutions of mapped and putative DNA contact sites in the TEN domain have surprisingly little impact, and sequence substitutions that reduce RAP can result from slower synthesis rather than a compromised stability of product binding (Romi et al., 2007; Eckert and Collins, 2012). Therefore, the structural specializations that underlie telomerase properties of DNA handling remain poorly understood.

Here, we develop and combine TERT and hTR functional complementation assays and a physical nuclease protection assay to establish how telomerase recognizes primer-template duplex and single-stranded DNA. By requiring the active site to elongate a primer-template duplex structurally unconnected from the rest of the RNP, we could distinguish direct from indirect roles of TERT domains and hTR motifs. We find that the telomerase active site inherently limits product synthesis at the template 5' boundary even without template constraint by flanking RNA motifs. We show that active-site use of a short primer-template hybrid requires the TEN domain, while the TERT ring RNP functionally and physically interacts with single-stranded primer DNA. Our findings provide integrated support for a new structural understanding of telomerase nucleic acid handling, including telomerase adaptation to repeat synthesis by TEN domain-dependent recognition of the short initial primer-template hybrid and active-site discrimination of the sequence and length of product-template hybrid. These insights facilitate future development of small-molecule telomerase inhibition therapies.

Materials and Methods

Telomerase reconstitution in vitro

The hTR RNAs were synthesized from a pUC119 plasmid linearized with EcoRI using in vitro transcription and purified by denaturing gel electrophoresis. Telomerase was reconstituted using the TNT-T7 coupled reticulocyte lysate system (Promega) with reactions containing 40 ng/μl pCITE 3xFLAG-TERT expression construct and 100 ng/μl purified hTRmin incubated at 30°C for 3.5 h. The MBP-TEN domain-His_{10} fusion was expressed using pET28a in *E. coli* BL21 (DE3) RP cells, partially purified on NiNTA resin (Qiagen) with 300 mM imidazole elution and further purified using amylose resin (New England Biolabs) eluted with 10 mM maltose in buffer containing 50 mM Tris-HCl at pH 7.9, 400 mM KCl, 1 mM $MgCl_2$, 10% glycerol, 5 mM DTT and 0.1 mM PMSF.

Telomerase holoenzyme reconstitution

Human U2OS or 293T cells were transiently transfected using calcium phosphate with a pcDNA 3xFLAG-TERT expression construct and full-length hTR or hTRΔtemp construct based on pBSU3hTR500, which contains the U3 small nucleolar RNA promoter and 500 bp of downstream genomic region following the mature hTR 3' end (Fu & Collins, 2003). After 48 hours, cells were lysed by three freeze-thaw cycles in hypotonic lysis buffer (HLB; 20 mM HEPES at pH 8, 2 mM $MgCl_2$, 0.2 mM EGTA, 10% glycerol, 0.1% NP-40, 1 mM DTT and 0.1 mM PMSF). NaCl was added to 400 mM final concentration and the whole-cell extract was cleared by centrifugation. The extract was diluted to bring NaCl concentration to 150 mM before immunopurification with FLAG M2 monoclonal antibody resin (Sigma-Aldrich) by end-over-end rotation at room temperature for two hours. The resin was then washed three times with HLB containing 150 mM NaCl, 0.1% Triton X-100 and 0.2% CHAPS at room temperature.

Activity assays

Activity assays were performed in 20 μl reactions containing extract-purified RNP immobilized on FLAG resin or 2 μl in vitro reconstituted telomerase RNP. Reactions contained 50 mM Tris-acetate at pH 8, 3 mM $MgCl_2$, 1 mM EGTA, 1 mM spermidine, 5 mM DTT, 5% glycerol, 0.1 μM α-^{32}P dGTP (3000 Ci/mmol, 10 mCi/ml, Perkin-Elmer) and if included, 250 μM of other dNTPs and/or 500 μM of ddNTPs. Trans-template assays used 20 μM pre-annealed RNA/DNA hybrid, prepared by mixing and heating to 80°C for 5 min followed by slow cooling to 10°C in buffer containing 10 mM Tris-HCl at pH 7.9, 1 mM EDTA and 200 mM NaCl. Reactions were incubated at room temperature for 60 min. The products were then extracted, precipitated and resolved on 12% or 18% polyacrylamide/7 M urea/0.6X Tris borate-EDTA gels.

Nuclease protection assay

Telomerase enzyme was combined with 1 pmol DNA primer in a total volume of 10 μl and incubated at room temperature for 30 min. The primer extension reaction was

initiated by addition, to final concentration, of 50 mM Tris-acetate at pH 8, 3 mM $MgCl_2$, 1 mM EGTA, 1 mM spermidine, 5 mM DTT, 5% glycerol, 0.1 μM α-^{32}P dGTP and, if included, 250 μM of other dNTPs and/or 500 μM of ddNTPs in a final volume of 20 μl. The reactions were incubated at room temperature for 1 min, followed by addition of 5 units of Exonuclease VII (ExoVII, Affymetrix). The reactions were incubated at room temperature for 5 min then stopped by addition of 80 μl stop buffer (50 mM Tris-HCl at pH 7.9, 20 mM EDTA and 0.2% SDS). The products were extracted, precipitated and resolved on 18% polyacrylamide/7 M urea/0.6X Tris borate-EDTA gels. For heat denaturation, reactions were boiled for 10 min after the initial 1 min elongation, then supplemented with 2.5 μM hTR 46-56 and incubated on ice for 5 min, followed by treatment with 5 units of ExoVII for 5 min. For footprinting during processive synthesis, unlabeled dGTP was added to a final concentration of 5 μM and the reaction was incubated at room temperature for 10 minutes after the initial 1 min elongation, followed by treatment with 5 units of ExoVII for 5 min. Protected products were quantified using Semi-Automated Footprinting Analysis (SAFA) version 11b (Das et al, 2005).

Results

TERT active-site use of a physically autonomous primer-template hybrid

We sought mutagenesis-independent approaches to investigate primer and template handling by human telomerase. We built upon the original trans-template reconstitution for *T. thermophila* TERT and TER (Miller and Collins, 2002) and a recently reported human telomerase trans-template reconstitution used to infer template translocation by active-site release of product-template hybrid (Qi et al., 2012). Telomerase RNPs with 3xFLAG-tagged TERT were assembled by transient transfection of human cells or using rabbit reticulocyte lysate (RRL) expression conditions that stabilize TERT by coassembly with hTR during protein synthesis (see Materials and Methods). RRL reconstitutions used hTRmin, which connects the PK and CR4/5 with a short linker (Figure 3.1A). Enzyme reconstituted with hTRmin was comparable in processivity to enzyme reconstituted with full-length hTR or the two-fragment combination of separated template/PK and CR4/5 fragments (Figure 3.2). Activity reconstitution was better with hTRmin than with the full-length hTR prone to H/ACA domain misfolding (Figure 3.2), but unlike the two-fragment system, hTRmin allows the high-affinity CR4/5-TERT interaction to assemble even a truncated template/PK sequence into RNP.

To assay telomerase active-site use of a template physically autonomous from the PK, we reconstituted a template-less version of full-length hTR RNP (hTRΔtemp) in vivo using telomerase-negative U2OS cells (Figure 3.3) and a template-less version of hTRmin (hTRminΔtemp) in vitro, then supplied TERT RNPs with a trans-template RNA oligonucleotide (hTR 46-56; Figure 3.1A). Both hTRΔtemp and hTRminΔtemp reconstituted robust single-repeat synthesis activity appropriately dependent on the presence of template-cognate dNTPs (Figures 3.1B and 3.3B, lanes 1-2). As additional controls, assays lacking either RNA template or DNA primer did not give radiolabeled product (Figures 3.1B and 3.3B, lanes 3-4). To eliminate the possibility of contaminating co-purified polymerase activities, we assayed RNPs assembled by TERT with the reverse transcriptase motif C substitution D868A, which disrupts catalytic metal ion coordination (Weinrich et al., 1997). As expected, D868A TERT did not support trans-template product synthesis (Figures 3.1B and 3.3B, lanes 5-8) despite RRL expression comparable to wild-type TERT (Figure 3.1C). Notably, these reconstitutions used the native hTR template sequence instead of a previously assayed heterologous template (Qi et al., 2012). The results above firmly establish that a human telomerase RNP containing only hTR PK and CR4/5 can accurately position a physically autonomous primer-template hybrid in the active site.

For these and other assays described below, we used primer with a single-stranded region of poly-thymidine (T), typically in the 27 nt primer T_{21}-GTTAGG (Figure 3.1A, right). The use of a 5' T-tract obliges base-pairing of the primer 3' end with the template, rather than internal regions, and it precludes primer multimerization by guanosine quadruplex formation. Previous studies establish that in the single-stranded region of a primer, non-telomeric sequence increases primer extension comparably to or better than telomeric-repeat sequence (Morin, 1991; Lee and Blackburn, 1993). Also, 5' non-telomeric and

telomeric-repeat sequence extensions both dramatically stabilize primer DNA physical association with human telomerase (Wallweber et al., 2003). A ~12 nt length of single-stranded DNA was sufficient for maximum stimulation of human telomerase catalytic activity or primer binding (Morin, 1991; Wallweber et al., 2003). To validate the use of a non-telomeric single-stranded primer 5' region in our assays, we confirmed that a 5' T-tract enhanced primer use comparably to telomeric-repeat sequence with both TERT assembled with hTRmin in RRL and TERT assembled with full-length hTR as the cellular holoenzyme (Figure 3.4). We also recapitulated major findings below by testing telomeric-repeat as well as non-telomeric 5' extensions from a primer-template hybrid.

Human TERT TEN domain function requires co-folding with the TERT ring and hTR

Sequence substitutions of the TEN domain can alter features of template use (Wyatt et al., 2010; Jurczyluk et al., 2010; Bairley et al., 2011; Eckert and Collins, 2012). To investigate how the TEN domain affects active-site handling of primer and template without the caveats of mutagenesis, we built from the TEN domain trans-complementation developed for human telomerase holoenzyme reconstitution in vivo (Robart and Collins, 2011). We bacterially expressed and purified the human TERT TEN domain (TERT amino acids 1-325) in N-terminal fusion to maltose binding protein (MBP) and C-terminal fusion to a 10-histidine tag (Figure 3.1D). The human TERT ring (amino acids 326-1132) was expressed in RRL under conditions parallel to full-length TERT (Figure 3.1E). Paralleling reconstitutions in vivo (Robart and Collins, 2011), the TERT ring RNP reconstituted in vitro supported single-repeat synthesis (Figure 3.1F, lane 3) and could be complemented by a physically separate TEN domain to attain the RAP of full-length TERT RNP (lanes 8 and 1, respectively).

Curiously, trans-complementation by the purified TEN domain was robust enough to detect by primer extension only if the TEN domain and hTRmin were added to the TERT ring RRL expression reaction before TERT ring synthesis (Figure 3.1F, lanes 2-8). This requirement could not be bypassed by incubating the TEN domain in RRL in parallel with separate TERT ring synthesis (Figure 3.1F, lane 9), suggesting that co-folding of the TEN domain, hTR and TERT ring is necessary to create an active conformation of the TEN domain. Co-folding was stable rather than transient, as judged by the enrichment of high-RAP activity upon repurification of the TEN domain after RNP assembly (Figure 3.2C). Removal of the MBP tag from the TEN domain greatly inhibited TEN domain trans-complementation (unpublished observations). We note that a large fraction of the isolated TEN domain may have inactive conformation, based on the large stoichiometric excess over TERT ring that is required for activity reconstitution. Thus, studies with an isolated recombinant human TEN domain may not fully recapitulate its important functional properties.

Template-flanking motif and TEN domain stimulation of primer-template hybrid use

It is surprisingly unknown how template-flanking single-stranded RNA regions influence template use in vertebrate TERs. A *T. thermophila* TER sequence motif 3' of the template strongly stimulates trans-template use only in cis-linkage to the template (Miller and

Collins, 2002). Also, a *T. thermophila* TER sequence motif 5' of the template enforces the cis-linked template 5' boundary by high-affinity TERT interaction (Lai et al., 2002). Recent mutagenesis and single-molecule FRET studies suggest that these template-flanking RNA elements define the intervening region as template by storing the strain from template stretching and compression (Berman et al., 2011). However, the 5' and 3' template-flanking regions of vertebrate TERs do not have sequence conservation that parallels ciliate TERs or even conservation of a template-flanking stem similar to yeast TERs (Podlevsky et al., 2008). To investigate how cis-linkage to flanking sequences influences human telomerase template use, we assayed hTRminΔtemp RNP for activity with template oligonucleotides extended by the physiological hTR 5' and/or 3' template-flanking sequences (Figure 3.5A).

Repeat synthesis activity was increased 5- to 10-fold by the presence of a 3'-flanking (hTR 46-63) or 5'-flanking (hTR 38-56) hTR template region (Figure 3.5B, lanes 1-3) or both (hTR 38-63, lane 4). This effect was highly reproducible in independent triplicate assays. We next tested whether stimulation of template use by hTR template-flanking regions was sequence-dependent, as is the case for *T. thermophila* TER (Miller and Collins, 2002). Substitution of the wild-type hTR 5' or 3' template-flanking sequences for an equal length of poly-adenosine weakened but did not abolish their stimulatory effects (Figure 3.5B, compare lane 1 to 5 and 3 to 6). The sequence of the template 3'-flanking region also affected the fidelity of template copying: the presence of the wild-type sequence reduced non-templated nucleotide addition after complete repeat synthesis, while the non-native poly-adenosine tract reduced complete template copying (Figure 3.5B, compare product lengths in lanes 1, 2 and 5). Curiously, the presence of template-flanking 5' sequence did not provide additional template: synthesis still predominantly halted at the correct template 5' boundary (Figure 3.5B, compare product lengths in lanes 2, 3 and 6).

We also compared TERT ring RNP activity on minimal versus extended templates. The hTRminΔtemp TERT ring RNP had negligible activity on any trans-template, even if template-flanking 5' and 3' regions were both present (Figure 3.5C, lanes 1-6). However, the same TERT ring RNP complemented with a separate TEN domain could use a trans-template (Figure 3.5C, lanes 7-12). The 3' template-flanking sequence had less stimulatory effect on the RNP with trans-complementing TEN domain than full-length TERT (compare Figure 3.5C, lanes 7 and 8 to Figure 3.5B, lanes 1 and 2), detected reproducibly across independent assays in triplicate. This finding suggests that the hTR 3' template-flanking region is recognized by a coordination of the physically linked TEN domain and TERT ring. Overall, these results indicate that the TEN domain greatly stimulates active-site engagement of a primer-template hybrid even when this hybrid has only RNA template sequence (hTR 46-63) and a fully base-paired 6 nt DNA (Figure 3.5A).

Template 5' boundary definition inherent to the product-template hybrid

The limited change in product length with 5'-extended trans-template RNAs was unexpected, because it implied that template 5' boundary definition could be inherent to

the product-template hybrid rather than steric constraints provided by template-flanking RNA structure or RNA-protein interaction (Berman et al., 2011; Blackburn and Collins, 2011). To test this hypothesis, we performed activity assays with trans-template RNAs harboring sequence substitutions in 5' template positions 47-49 (Figure 3.5D). We tested each template paired to either primer with a fully template-complementary 3' end (T_{21}-GTTAGG) or primer with a template 3'-end mismatch (T_{21}-TATAGG) that would reduce the length of primer-template hybrid to 4 base-pairs (as illustrated in Figure 3.5D).

A shorter initial hybrid length promoted longer product synthesis (Figure 3.5E, lanes 1-2). Also, given the same primer-template base-pairing, some template substitutions also led to longer product synthesis (Figure 3.5E, compare lanes 1 and 9). Combinations of shorter primer-template hybrid length and template sequence substitution decreased the fidelity of synthesis halt at the template 5' boundary to a variable extent, suggesting that product-template hybrid length and sequence each contribute to discrimination of the appropriate template boundary. Extension of the 5' template-flanking region to include the bottom strand of P1 appeared to reduce but not eliminate template 5' boundary bypass induced by shorter initial primer-template hybrid length (Figure 3.5E, compare lanes 1 and 2 to lanes 13 and 14). Taken together, our findings support the conclusion that for human telomerase, the precision of repeat synthesis derives in part from a high specificity of discrimination for the length and sequence of product-template hybrid. Discrimination inherent to features of the product-template hybrid can explain the absence of template-flanking sequence conservation among vertebrate TERs and uncovers an active-site recognition of product DNA-RNA hybrid that is unprecedented in other polymerases.

A PK stem required for productive coupling of the TEN domain and TERT ring for use of primer-template hybrid

The activity inhibition observed in previous PK mutagenesis studies could arise from cis-linked template mis-positioning in the global hTR fold. To discriminate this indirect loss-of-function from a direct PK role such as primer alignment or TEN domain positioning (Qiao and Cech, 2008; Robart and Collins, 2011), we combined the trans-template assay with TEN domain trans-complementation. The entire PK or only the 5' strand of the P2a.1/P2a stem extension was removed from hTRminΔtemp (ΔPK or 91-end; Figure 3.6A). For comparison we introduced substitutions that disrupt PK base triples (illustrated in Figure 3.6B) formed either in the P2b loop (U100C) or in the loop between P2a.1 and P3 (A172U), both of which are critical for enzyme activity (Theimer et al., 2005).

Without the PK, the TERT ring RNP complemented with a TEN domain showed greatly reduced but still detectable trans-template copying activity (Figure 3.6C, lane 2), which was reproducible in more than 3 independent assays. Removal of the P2a.1/P2a bottom strand decreased activity similarly to removal of the entire PK (Figure 3.6C, lane 3). Disruption of the conserved P2b loop triple-helix also strongly decreased activity, more so than disrupting a base triple formed by the P2a.1/P3 loop (Figure 3.6C, lanes 4 and 5). In comparison, for the TERT ring RNP alone, removing the PK decreased activity to a nearly undetectable level, as did disrupting the P2b loop triple-helix (Figure 3.6C, lanes 7

and 9). On the other hand, truncating the bottom strand of P2a.1/P2a had less impact on activity, comparable to disrupting a base triple of the P2a.1/P3 loop (Figure 3.6C, lanes 8 and 10). Thus, the presence of P2a.1/P2a was more critical for activity in the presence versus absence of TEN domain (Figure 3.6C, compare lanes 1 and 3 to lanes 6 and 8). Overall these results suggest that the vertebrate-extended P2a.1/P2a influences coupling of the TEN domain and TERT ring and support important direct function of the PK in active-site engagement of primer-template hybrid (Figure 3.6D).

Functionally sensing of single-stranded primer DNA by a TERT RNP without TEN domain

Current models of telomerase structure and catalytic cycle mechanism predict the TEN domain to be required for activity stimulation by single-stranded DNA 5' of the primer-template hybrid. To test this expectation, we compared the activity of RRL-assembled RNPs containing full-length TERT, TERT ring or TERT ring and trans-complementing TEN domain using primers with or without a 5' single-stranded extension from the primer-template hybrid (Figure 3.7A, E and M primers). We used each primer in combination with the shortest, 11 nt trans-template lacking any non-template sequence or a longer, 5'-extended trans-template RNA (Figure 3.7A, S and L templates).

The full-length TERT RNP used the long or short template paired with either the minimal or extended primer (Figure 3.7B, lanes 1-4). An activity stimulation of more than 10-fold required only extended primer or the longer template, with no additional activity increase from their combination (Figure 3.7B, compare lanes 2-4). The TERT ring RNP with trans-complementing TEN domain also showed activity stimulation by the presence of a single-stranded region of RNA or DNA, with an additional boost from their combination (Figure 3.7B, lanes 9-12). The TERT ring RNP alone was more dependent on the combination of single-stranded RNA and primer regions for robust activity (Figure 3.7B, lanes 5-8). Comparing enzymes with and without the TEN domain, the TEN domain stimulated activity not only with the extended primer but also with the minimal primer, which lacks a single-stranded DNA region for putative TEN domain interaction (Figure 3.7B, compare lanes 6 and 10). Even more surprisingly, the TERT ring RNP was stimulated by the presence of single-stranded DNA (Figure 3.7B, compare lane 6 to 5 and lane 8 to 7). This stimulation was highly reproducible across multiple independent assays. These results suggest that the TEN domain stimulates active-site use of a primer-template hybrid even without single-stranded DNA, and TERT ring RNP senses a single-stranded DNA extension from the primer-template hybrid.

We next explored the length-dependence of TERT ring RNP activity stimulation by single-stranded DNA. Primers of 6, 12 or 18 nt (GTTAGG, T_6-GTTAGG, T_{12}-GTTAGG) progressively stimulated RRL-assembled TERT ring RNP activity on the hTR 18-56 trans-template (Figure 3.7C, lanes 1-3). This stimulation was comparable to or greater than single-stranded DNA stimulation of trans-template copying by the RRL-assembled hTRminΔtemp full-length TERT RNP or TERT ring RNP with a trans-complementing TEN domain (Figure 3.7C, lanes 4-9) or the hTRΔtemp holoenzyme reconstituted in vivo (lanes 10-12). We extended these findings to the TERT ring RNP assembled in vivo on

full-length hTR, which also showed stimulation by single-stranded DNA comparable to or greater than that of full-length TERT RNP assembled in vivo on full-length hTR, each assayed with primers containing a 5' T-tract or telomeric-repeat extension from the primer-template hybrid (Figure 3.8). These results provide strong evidence that the TERT ring RNP can functionally sense single-stranded DNA (Figure 3.7D).

TERT RNP without TEN domain physically protects single-stranded DNA

To parallel the functional assays above, we sought to test telomerase physical association with DNA. Because there is no previously reported benchmark for such an assay, we used holoenzyme with full-length hTR to develop a nuclease protection assay specific for active enzyme complexes (Figure 3.9A). First, the telomerase active site was used to label a productively bound DNA primer by addition of a single radiolabeled dGTP (Figure 3.9B, lanes 1-5). After labeling, bound product was trimmed of accessible single-stranded DNA by brief digestion with Exonuclease VII (ExoVII). The total length of protected product was then assessed by denaturing PAGE, with end-labeled DNA oligonucleotide markers and some undigested product DNA retained for size comparison (Figure 3.9B, lanes 6-10). Because the end-labeled oligonucleotides share the 5' monophosphate of ExoVII products (Chase and Richardson, 1974), they are accurate migration standards. The full-length TERT holoenzyme protected product lengths of ~18 nt, including both the product-template duplex and single-stranded region. Importantly, beyond 18 nt the length range of DNA protection was not dependent on initial primer length (Figure 3.9B, lanes 8-10) and was consistent over a range of nuclease reaction times and amounts (unpublished observations). RRL-reconstituted full-length TERT hTRmin RNP also protected an ~18 nt length of DNA (Figure 3.10), indicating that holoenzyme proteins other than TERT do not associate stably with single-stranded product. The initial and protected product length both increased by 1 nt if dGTP and dideoxythymidine (ddTTP) were added in primer extension (Figure 3.9C, lanes 1-4), and a correspondingly 1 nt longer length of product-template duplex could be detected if product DNA was boiled and annealed with excess template RNA before ExoVII digestion (lanes 5-6).

We next tested physical protection of product DNA by the TERT ring RNP. Remarkably, the TERT ring RNP reconstituted in vivo with full-length hTR protected a product length roughly comparable to the full-length TERT holoenzyme reconstituted in parallel (Figure 3.11A). Product protection by the TERT ring RNP appeared less quantitatively robust than its protection by full-length TERT RNP, based on the lower summed product intensity normalized to the amount of initial product before nuclease digestion (Figure 3.11A, percentage of initial product converted to protected product is indicated). This suggests a higher rate of product dissociation or a more dynamic enzyme-DNA interaction. In addition, the products protected by the TERT ring RNP appeared more evenly spread over a length distribution than the products protected by full-length TERT RNP (Figure 3.11A), with a size range quantified as 14-18 nt (Figure 3.11B). Together with the activity assays described above, the physical nuclease-protection results suggest the surprising conclusion that single-stranded DNA threads from the product-template hybrid along a surface of the TERT ring RNP (Figure 3.11C, open triangles indicate an

anchor site not necessarily localized to one surface of the TERT ring RNP; see Discussion). The TEN domain enhances placement of the initial primer-template hybrid in the active site (Figure 3.11C, left), with or without a direct contribution to the surface and/or stability of single-stranded DNA interaction (Figure 3.11C, right).

To explore how product DNA is protected during repeat synthesis, we performed the nuclease protection assay on products with 3' ends extended to successive positions of the template using combinations of deoxy- and dideoxynucleotides (ddNTPs). In general, the protected products of full-length TERT holoenzyme increased in length with synthesis across the template (Figure 3.12A, lanes 1-4; Figure 3.13). Roughly similar lengths of protection were observed when the primer contained 5' telomeric sequence rather than a T-tract extension (Figure 3.14), with the caveat that the 5' edge of protection of telomeric-repeat product DNA is determined in part by sequence-differential ExoVII cleavage (Chase and Richardson, 1974). Paralleling the results for full-length TERT holoenzyme, protected products of the TERT ring RNP increased in length as synthesis proceeded across the template (Figure 3.12B). This comparison suggests that the TEN domain did not alter the register of telomerase interaction with protected product DNA during repeat synthesis.

Curiously, the register of the 5' end of protected product DNA changed little with active-site progression across the template: product elongation by 4 nt was accompanied by a 3-nt increase in protected product length (Figure 3.12A, lanes 1-4; Figure 3.13). This finding suggests that during repeat synthesis, single-stranded DNA could largely retain its position relative to the active site while the product-template hybrid increases in length (Figure 3.12C). If repeat synthesis was allowed to proceed with RAP before ExoVII digestion using 10 min rather than the standard 1 min interval of primer extension (Figure 3.9A), protected product lengths paralleled those from single-repeat synthesis (Figure 3.12A, lanes 4-6). This result suggests that product DNA threads out of the RNP rather than forming a large loop with retained binding of the original single-stranded primer 5' region. The minority population of longer protected DNA observed upon ExoVII digestion of high-RAP products (Figure 3.12A, lane 5) could reflect ExoVII-resistant guanosine quadruplex structures in enzyme-bound or released product or product elongation after ExoVII cleavage. Overall, these physical and functional assays support a new perspective on telomerase mechanism, including unique polymerase specificities of nucleic acid interaction that discriminate different states of primer-template hybrid as well as single-stranded DNA (Figure 3.15).

Discussion

The telomerase catalytic cycle obliges a distinctive, dynamic positioning of different lengths of primer-template hybrid in the active site. Here we describe new functional and physical assay methods that allowed us to define previously unknown nucleic acid recognition specificities of the TEN domain and TERT ring RNP for primer-template hybrid, template-flanking RNA sequences and primer single-stranded DNA. Our findings provide integrated support for a model in which the TEN domain functions to enhance catalytic activity and confer RAP by increasing active-site use of primer-template hybrid, rather than by binding a 5' single-stranded region of primer distant from the active site (Figure 3.15, state i). This accounts for why even single-repeat primers hybridized entirely with the hTR template are elongated with RAP yet still require the TEN domain for stable binding (Morin, 1991; Robart and Collins, 2011). Upon copying to the template 5' end, additional synthesis is halted by features inherent to the native length and/or sequence of product-template hybrid (Figure 3.15, state ii). Curiously, although template-flanking RNA regions improve human telomerase trans-template use, they are not required for template 5' boundary definition. Active-site release of the product-template hybrid as previously proposed (Qi et al., 2012) would facilitate strand separation (Figure 3.15, states iii-iv). The TEN domain then promotes active-site capture of the product 3' end re-annealed at the template 3' end (Figure 3.15, state v to i). The TEN domain may have evolved to reduce the minimum required base-pairing between primer and template. This would account for why a TEN domain sequence substitution in yeast restricts the registers of primer-template alignment (Bairley et al., 2011) and why TEN domain sequence substitutions in yeast, ciliate or human enzymes can be compromised for synthesis at only template positions that oblige a particularly short primer-template hybrid (Lue, 2005; Jurczyluk et al., 2010; Eckert and Collins, 2012)

Because the active site must release product-template hybrid to complete a catalytic cycle, the TEN domain may favor stable engagement of the primer-template hybrid only for lengths or sequences that do not include the template 5' end. We suggest that functional coordination of the TEN domain with the changing primer-template hybrid could be mediated by the template-proximal PK stem, hTR P2a. Because the P2a stem has a particularly extended length in mammalian TERs (Podlevsky et al., 2008), the mammalian TEN domain may have stronger interaction with TER and/or more stable positioning relative to the active site than the TEN domain of other TERTs. Consistent with this hypothesis, the minimal recombinant human telomerase RNP has more robust TEN domain trans-complementation and higher RAP than does the *T. thermophila* minimal RNP, which requires additional holoenzyme proteins for TEN domain trans-complementation or high RAP (Eckert and Collins, 2012).

Ciliate and yeast telomerases establish the template 5' boundary relative to a template-flanking RNA structure or protein-RNA interactions (Berman et al., 2011; Blackburn and Collins, 2011). For human telomerase, disruption of the hTR P1 stem can reduce template boundary fidelity (Chen and Greider, 2003; Moriarty et al., 2005), as does physical discontinuity of the TEN domain and TERT ring in an RNP reconstituted with full-length hTR in vivo (Robart and Collins, 2011). Results here indicate that at least for human

telomerase, the product-template hybrid itself also plays a major role. Sequence-based discrimination of the product-template hybrid would account for why substitutions of the human template sequence alter the profile and rate of product synthesis (Drosopoulos et al., 2005). Recognition of the product-template hybrid appears more autonomous of template-flanking sequences in the human enzyme than its ciliate or yeast counterparts. To achieve this recognition, we propose that human telomerase retains most or all of the possible product-template base-pairing, rather than a limited length of base-paired duplex as is the precedent from budding yeast (Förstemann and Lingner, 2005). Several lines of evidence support this speculation. First, primer mismatched to a trans-template 3' end induced template 5' boundary bypass, suggesting that the template 3' hybrid influences template 5' boundary fidelity. In addition, for holoenzyme RNP assembled in vivo, the length of product DNA protected from exonuclease digestion increased with synthesis to the template 5' boundary. As illustrated in Figure 3.12C, this is consistent with a constant protection of ~11 nt of single-stranded DNA and an increasing length of product-template hybrid. We note that previous human telomerase trans-template assays are also fully consistent with accommodation of a 10 or 11 base-pair product-template hybrid in the telomerase active site (Qi et al., 2012).

Numerous approaches have attempted to identify physical constituents of the telomerase anchor site. Previous binding and activity assays suggest that human telomerase interacts with a single-stranded primer region of 7-12 nt extending from the primer-template hybrid (Morin, 1989; Wallweber et al., 2003). Using both functional and physical assays, we demonstrate that the TERT ring RNP lacking a TEN domain can account for this inferred length of anchor-site interactions. We propose that anchor-site interactions occur along surfaces that can thread the single-stranded DNA without a specific register of binding other than imposed by distance from the primer-template hybrid. In future studies it will be of high interest to define whether single-stranded DNA has a unique binding site on the TERT ring RNP or instead is occluded from nuclease digestion without the requirement for specific side-chain contacts. Both the TERT ring and TEN domain have a high isoelectric point, reflecting a predominance of basic side chains that could form an electrostatically favorable path or general surface area for anchor-site associations. Electrostatic interactions without a specific binding cleft would account for telomerase activity on primers with base-paired as well as single-stranded 5' extensions (Oganesian et al., 2006). We note that telomerase holoenzyme proteins other than TERT can provide additional anchor-site DNA interactions, such as *T. thermophila* Teb1 (Min and Collins, 2009).

Although active-site stabilization of primer-template hybrid is sufficient to account for TEN domain function, and the TERT ring RNP can account for anchor-site interactions, the TEN domain may contribute to the anchor site as well. Activity assays do not provide evidence for TEN domain interaction with single-stranded DNA, but they are not inconsistent with the possibility. For example, activity with a short trans-template and 5'-extended primer is higher in the presence of the TEN domain (Figure 3.7B, compare lanes 7 and 11), which could reflect TEN domain association with single-stranded DNA in addition to its stabilization of primer-template hybrid in the active site. Physical protection of product DNA differed quantitatively and qualitatively in the presence

versus absence of the TEN domain, which again could reflect TEN domain association with single-stranded DNA. With or without a direct single-stranded DNA interaction surface, the general position of the TEN domain relative to the active site (Jiang et al., 2013) suggests that it could constrain product-template hybrid length or escape of the product single-stranded region from the RNP. Future studies can exploit the new reconstitution systems and assays developed in this work for additional insights about the telomerase structures responsible for DNA handling and how they coordinate with other factors required for telomere replication.

Figure 3.1 Human telomerase reconstituted with hTRmin supports activity on trans-templates and by trans-complementation of the TEN domain.

(**A**) Secondary structures of hTR, hTRmin and hTRminΔtemp with a template oligonucleotide and aligned DNA primer. Nucleotide addition (underlined) extends the primer to form product.
(**B**) Activity of wild-type or D868A TERT RNP reconstituted in RRL with hTRminΔtemp and assayed with or without hTR 46-56 template, T_{21}-GTTAGG primer and the indicated nucleotide substrates. In this and subsequent assay panels, an end-labeled DNA recovery control (RC) was added before product precipitation and unextended primer was 5' end-labeled and run as a size marker (►).
(**C**) SDS-PAGE analysis of TERT expression in RRL by labeling with ^{35}S-methionine.
(**D**) Coomassie-stained SDS-PAGE gel of the bacterially expressed TEN domain after initial partial purification on NiNTA resin and further purification on amylose resin.
(**E**) SDS-PAGE analysis of TERT ring or full-length TERT expression in RRL by labeling with ^{35}S-methionine.
(**F**) Activity of full-length TERT RNP or TERT ring RNP reconstituted in RRL with hTRmin and assayed with $(TTAGGG)_3$ primer. Purified bacterially expressed TEN domain or TEN domain pre-incubated in RRL for 3.5 hours (RRL + TEN) and hTRmin were added before or after TERT ring synthesis as indicated.

Figure 3.1

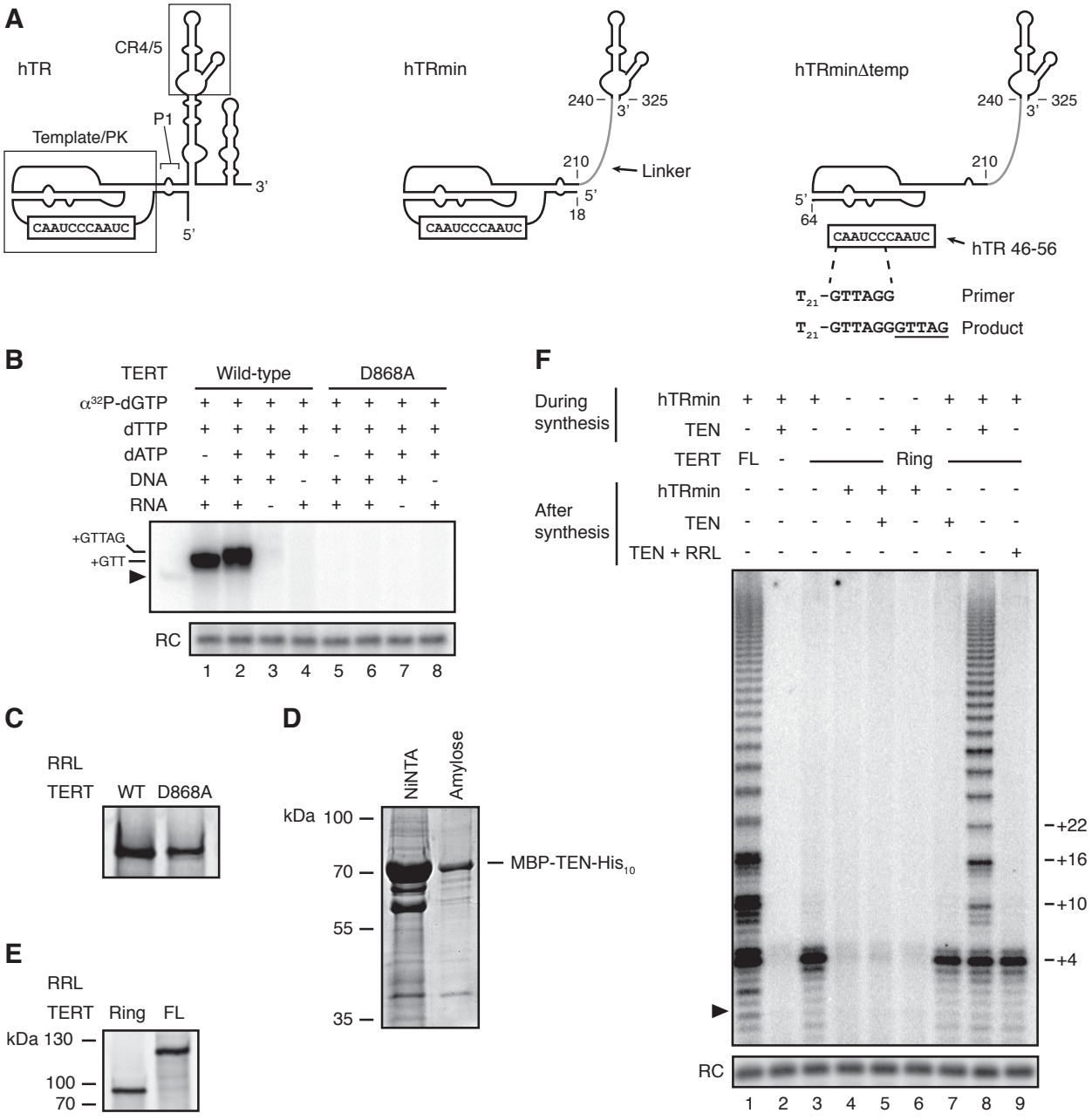
A
hTR
CR4/5
P1
Template/PK
CAAUCCCAAUC
3'
5'
hTRmin
240
325
3'
210
Linker
5'
18
hTRminΔtemp
64
hTR 46-56
T21-GTTAGG
Primer
T21-GTTAGGGTTAG
Product
B
TERT
Wild-type
D868A
α32P-dGTP
dTTP
dATP
DNA
RNA
+GTTAG
+GTT
RC
1 2 3 4 5 6 7 8
C
RRL
TERT
WT
D868A
D
NiNTA
Amylose
kDa
100
70
55
35
MBP-TEN-His10
E
RRL
TERT
Ring
FL
kDa 130
100
70
F
During synthesis
After synthesis
hTRmin
TEN
TERT
FL
Ring
TEN + RRL
+22
+16
+10
+4
RC
1 2 3 4 5 6 7 8 9

Figure 3.2 Telomerase reconstitution in RRL with hTRmin and a trans-complementing TEN domain.

(**A**) Secondary structures of full-length hTR, separated template/PK (t/PK) and CR4/5, and hTRmin.
(**B**) Activity of full-length TERT RNP reconstituted in RRL with the RNAs in (A) and assayed with $(TTAGGG)_3$ primer. An end-labeled DNA recovery control (RC) was added before precipitation and unextended primer was 5' end-labeled and run as a size marker (►). Lane 3 is also shown as lane 1 in Figure 3.1F.
(**C**) Activity and ^{35}S-methionine detection of TERT ring RNP reconstituted with hTRmin and a trans-complementing TEN domain before (Input, lane 1) or after subsequent purification for the TERT ring using FLAG antibody resin or for the TEN domain using amylose or NiNTA resin. Activity was assayed with $(TTAGGG)_3$ primer. Low activity yield with amylose resin purification (lane 3) may be due to resin binding interference by RRL components. Note that NiNTA resin purification enriches high-RAP activity relative to the amount of TERT ring RNP (lane 4).

Figure 3.2

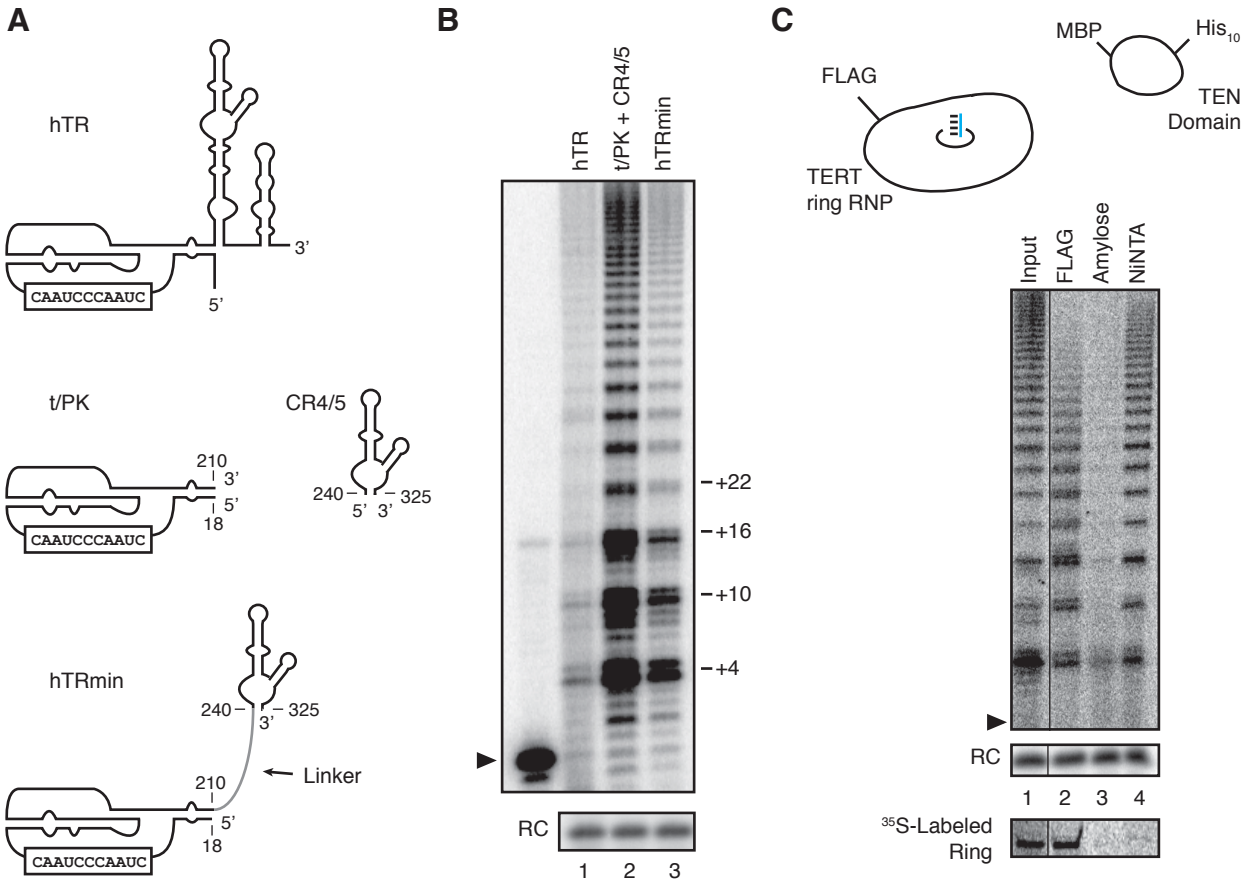
A
hTR
3'
5'
CAAUCCCAAUC
t/PK
210
3'
5'
18
CAAUCCCAAUC
CR4/5
240
325
5'
3'
hTRmin
240
3'
325
Linker
210
5'
18
CAAUCCCAAUC
B
hTR
t/PK + CR4/5
hTRmin
+22
+16
+10
+4
RC
1
2
3
C
MBP
His10
FLAG
TEN
Domain
TERT
ring RNP
Input
FLAG
Amylose
NiNTA
RC
1
2
3
4
35S-Labeled
Ring

Figure 3.3 Template-free holoenzyme activity with a trans-template RNA.

(**A**) Secondary structure of the endogenously assembled template-less hTR (hTRΔtemp) with template RNA oligonucleotide (hTR 46-56) and aligned DNA primer T_{21}-GTTAGG. Nucleotide addition (underlined) extends the primer to form product.
(**B**) Activity of wild-type or D868A TERT holoenzyme reconstituted in U2OS cells with hTRΔtemp and assayed with or without hTR 46-56 template, T21-GTTAGG primer and the indicated nucleotide substrates parallel to the assay in Figure 3.1B.
(**C**) Northern blot detection of hTRΔtemp in transfected U2OS cell extract or following TERT immunopurification (IP) for the activity assay. Note that mature hTRs migrate as multiple species due to partial folding during electrophoresis. An RNA oligonucleotide was added prior to RNA extraction for hybridization detection as a recovery control (RC).

Figure 3.3

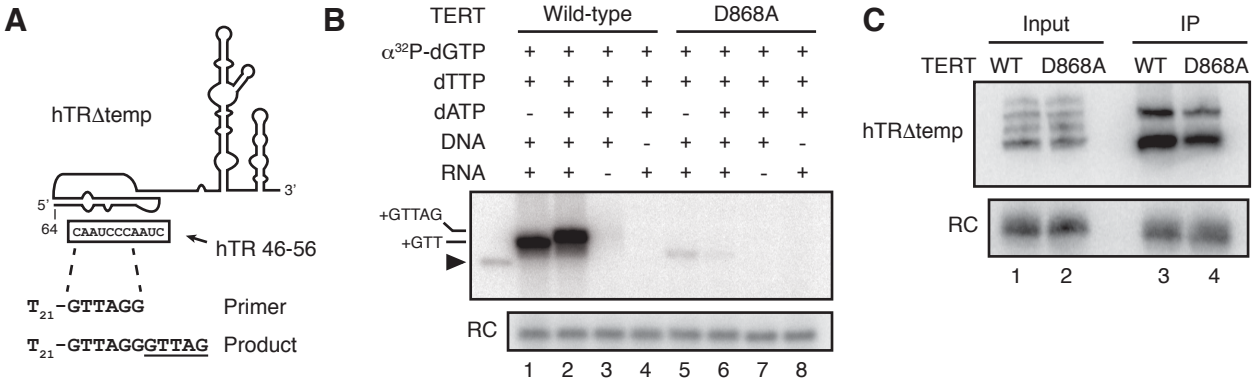
A
hTRΔtemp
5'
3'
64
CAAUCCCAAUC
hTR 46-56
T21-GTTAGG
Primer
T21-GTTAGGGTTAG
Product
B
TERT
Wild-type
D868A
α32P-dGTP + + + + + + + +
dTTP + + + + + + + +
dATP - + + + - + + +
DNA + + + - + + + -
RNA + + - + + + - +
+GTTAG
+GTT
RC
1 2 3 4 5 6 7 8
C
Input
IP
TERT WT D868A WT D868A
hTRΔtemp
RC
1 2 3 4

Figure 3.4 Enhancement of primer use by a 5' region of single-stranded DNA does not depend on single-stranded DNA sequence.

At top, schematic of elongation of the DNA primers. Nucleotides added by primer extension are underlined, with an asterisk denoting ddATP addition. At bottom, activity of full-length TERT RNPs reconstituted either in RRL with hTRmin or in 293T cells with full-length hTR, each assayed with the indicated final concentrations of the minimal 6 nt primer GTTAGG (no 5' extension) or primers 5'-extended with telomeric-repeat sequence [primer AGG$(GTTAGG)_4$] or T-tract sequence (primer T_{21}-GTTAGG). Note that a lower concentration of the longer primers is sufficient for maximal product synthesis, and that product synthesis is comparable or better with the 5' T-tract versus telomeric-repeat extension.

Figure 3.4

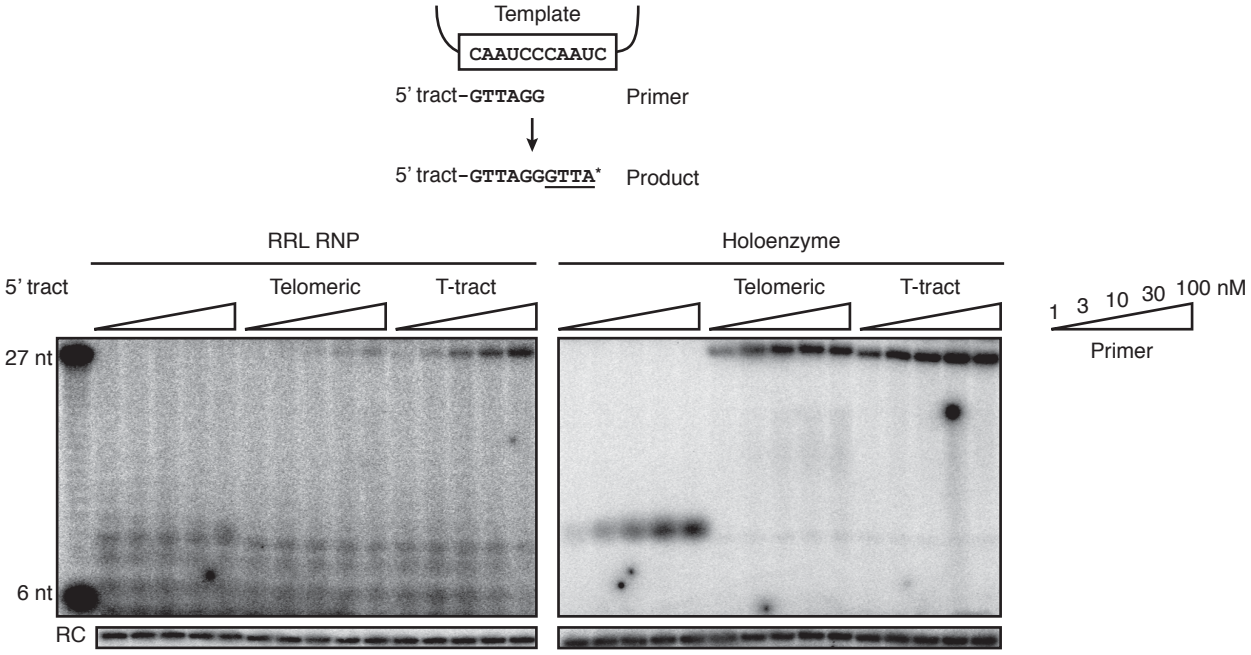
Template
CAAUCCCAAUC
5' tract-GTTAGG
Primer
5' tract-GTTAGGGTTA*
Product
RRL RNP
Holoenzyme
5' tract
Telomeric
T-tract
Telomeric
T-tract
1 3 10 30 100 nM
Primer
27 nt
6 nt
RC

Figure 3.5 Template-flanking RNA sequence and the TEN domain stimulate active-site elongation of an autonomous primer-template hybrid.

(**A**) Schematic of trans-template RNA oligonucleotides containing template-flanking single-stranded regions with aligned DNA primer GTTAGG.
(**B**) Activity from full-length TERT RNP reconstituted in RRL with hTRminΔtemp and assayed with the indicated templates and GTTAGG primer. The 6 nt primer was used to accentuate product size differences. For relative activity (Rel. Act.), product DNA intensities were first subtracted for background signal then normalized to activity from the hTR 38-63 template.
(**C**) Activity from TERT ring RNP or TERT ring RNP with trans-complementing TEN domain reconstituted in RRL with hTRminΔtemp and assayed with the indicated templates and GTTAGG primer. Product DNA intensities were first subtracted for background signal then normalized to activity from the hTR 38-63 template. N.D. is not determined.
(**D**) Schematic of sequence-substituted template RNA oligonucleotides containing 5' template-flanking sequences and aligned primers T_{21}-GTTAGG and T_{21}-TATAGG.
(**E**) Activity of full-length TERT RNP reconstituted in RRL with hTRminΔtemp and assayed with various templates, T_{21}-GTTAGG or T_{21}-TATAGG primer, and dATP, dCTP, dTTP and radiolabeled dGTP. Lanes 13-14 are shown at a higher exposure. Products of template 5' boundary bypass are indicated by an asterisk.

Figure 3.5

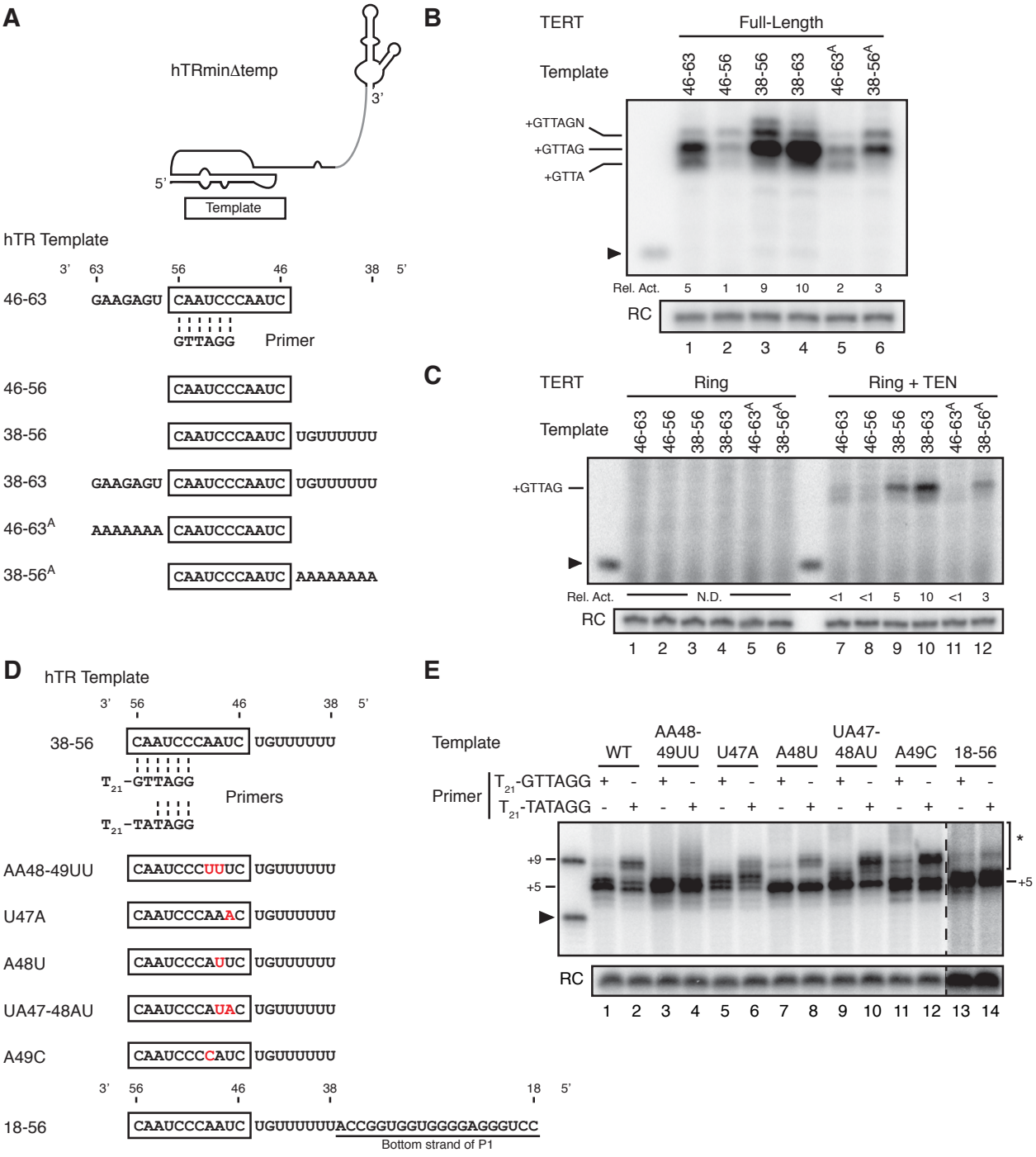
A
hTRminΔtemp
3'
5'
Template
hTR Template
3' 63 56 46 38 5'
46-63 GAAGAGU CAAUCCCAAUC
GTTAGG Primer
46-56 CAAUCCCAAUC
38-56 CAAUCCCAAUC UGUUUUUU
38-63 GAAGAGU CAAUCCCAAUC UGUUUUUU
46-63A AAAAAAA CAAUCCCAAUC
38-56A CAAUCCCAAUC AAAAAAAA
B
TERT
Full-Length
Template
46-63
46-56
38-56
38-63
46-63A
38-56A
+GTTAGN
+GTTAG
+GTTA
Rel. Act. 5 1 9 10 2 3
RC
1 2 3 4 5 6
C
TERT
Ring
Ring + TEN
Template
46-63
46-56
38-56
38-63
46-63A
38-56A
+GTTAG
Rel. Act. N.D. <1 <1 5 10 <1 3
RC
1 2 3 4 5 6 7 8 9 10 11 12
D
hTR Template
3' 56 46 38 5'
38-56 CAAUCCCAAUC UGUUUUUU
T21-GTTAGG
Primers
T21-TATAGG
AA48-49UU CAAUCCCUUUC UGUUUUUU
U47A CAAUCCCAAAC UGUUUUUU
A48U CAAUCCCAUUC UGUUUUUU
UA47-48AU CAAUCCCAUAC UGUUUUUU
A49C CAAUCCCCAUC UGUUUUUU
3' 56 46 38 18 5'
18-56 CAAUCCCAAUC UGUUUUUUACCGGUGGUGGGGAGGGUCC
Bottom strand of P1
E
Template
WT
AA48-49UU
U47A
A48U
UA47-48AU
A49C
18-56
Primer
T21-GTTAGG + - + - + - + - + - + - + -
T21-TATAGG - + - + - + - + - + - + - +
+9
+5
*
+5
RC
1 2 3 4 5 6 7 8 9 10 11 12 13 14

Figure 3.6 The hTR PK has distinct structural requirements for activity of the TERT ring RNP with or without trans-complementing TEN domain.

(**A**) Secondary structures of hTRmin with truncation of the entire PK or the P2a.1/P2a bottom strand (hTRminΔtemp 91-end) and the trans-template RNA hTR 18-56.
(**B**) Sequence and secondary structure within the PK. Dotted lines indicate base-triple pairing. Positions altered by mutagenesis are circled.
(**C**) Activity from TERT ring RNP with or without trans-complementing TEN domain reconstituted in RRL and assayed with template hTR 18-56 and T_{21}-GTTAGG primer. Product DNA intensities were first subtracted for background signal then normalized to activity from unsubstituted hTRminΔtemp (indicated as "WT").
(**D**) The P2a.1/P2a extended stem influences functional coupling of the TEN domain and the TERT ring RNP, and the entire PK increases engagement of primer-template hybrid by the TERT ring RNP.

Figure 3.6

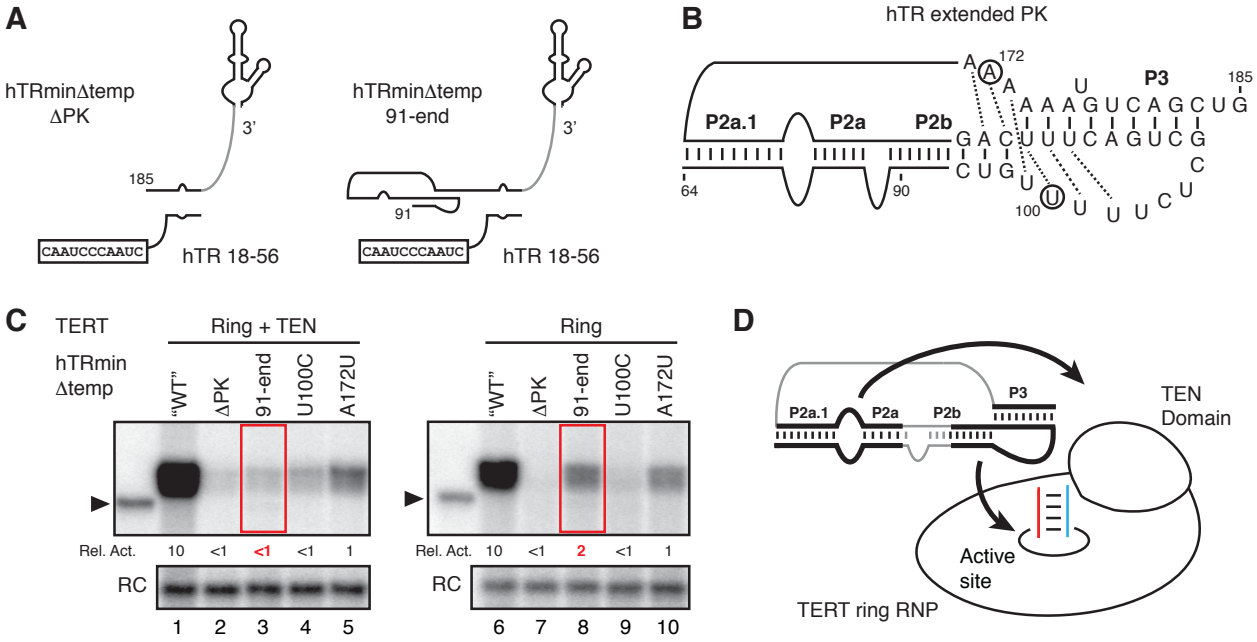
A
hTRminΔtemp
ΔPK
3'
185
CAAUCCCAAUC
hTR 18-56
hTRminΔtemp
91-end
3'
91
CAAUCCCAAUC
hTR 18-56
B
hTR extended PK
A
172
A
U
P3
185
A A A G U C A G C U G
P2a.1
P2a
P2b
G A C U U U C A G U C G
C U G
C
U
64
90
100
U
U U C U
C
TERT
Ring + TEN
hTRmin
Δtemp
"WT"
ΔPK
91-end
U100C
A172U
Rel. Act.
10
<1
<1
<1
1
RC
1 2 3 4 5
Ring
"WT"
ΔPK
91-end
U100C
A172U
Rel. Act.
10
<1
2
<1
1
RC
6 7 8 9 10
D
P2a.1
P2a
P2b
P3
TEN
Domain
Active
site
TERT ring RNP

Figure 3.7 The TEN domain stimulates elongation of an entirely template-paired primer.

(**A**) Secondary structure of hTRminΔtemp with the longest template RNA hTR 18-56 (L) or the shortest template RNA hTR 46-56 (S) aligned with the 5'-extended primer T_{21}-GTTAGG (E) or the minimal template-paired primer GTTAGG (M).
(**B**) Activity of full-length TERT RNP, TERT ring RNP or TERT ring RNP with trans-complementing TEN domain reconstituted in RRL with hTRminΔtemp and assayed with the indicated S or L template and M or E primer. All product intensities were first subtracted for background signal then normalized to activity from the L template and E primer within each set of assays.
(**C**) Activity of TERT ring RNP, TERT ring RNP with trans-complementing TEN domain or full-length TERT RNP reconstituted in RRL with hTRminΔtemp, or full-length TERT RNP reconstituted in U2OS cells with hTRΔtemp, each assayed with hTR 18-56 template and 6 nt (GTTAGG), 12 nt (T_6-GTTAGG) or 18 nt (T_{12}-GTTAGG) primer. Product intensities were first subtracted for background signal then normalized to activity on the 18 nt primer within each set of assays. Unextended 5' end-labeled primers are shown as size markers.
(**D**) The single-stranded region of DNA (DNA shown in red) stimulates activity of the TERT ring RNP, and the TEN domain stimulates activity through the primer-template hybrid (template shown in blue). Not resolved is whether the TEN domain also senses single-stranded DNA (gray arrow).

Figure 3.7

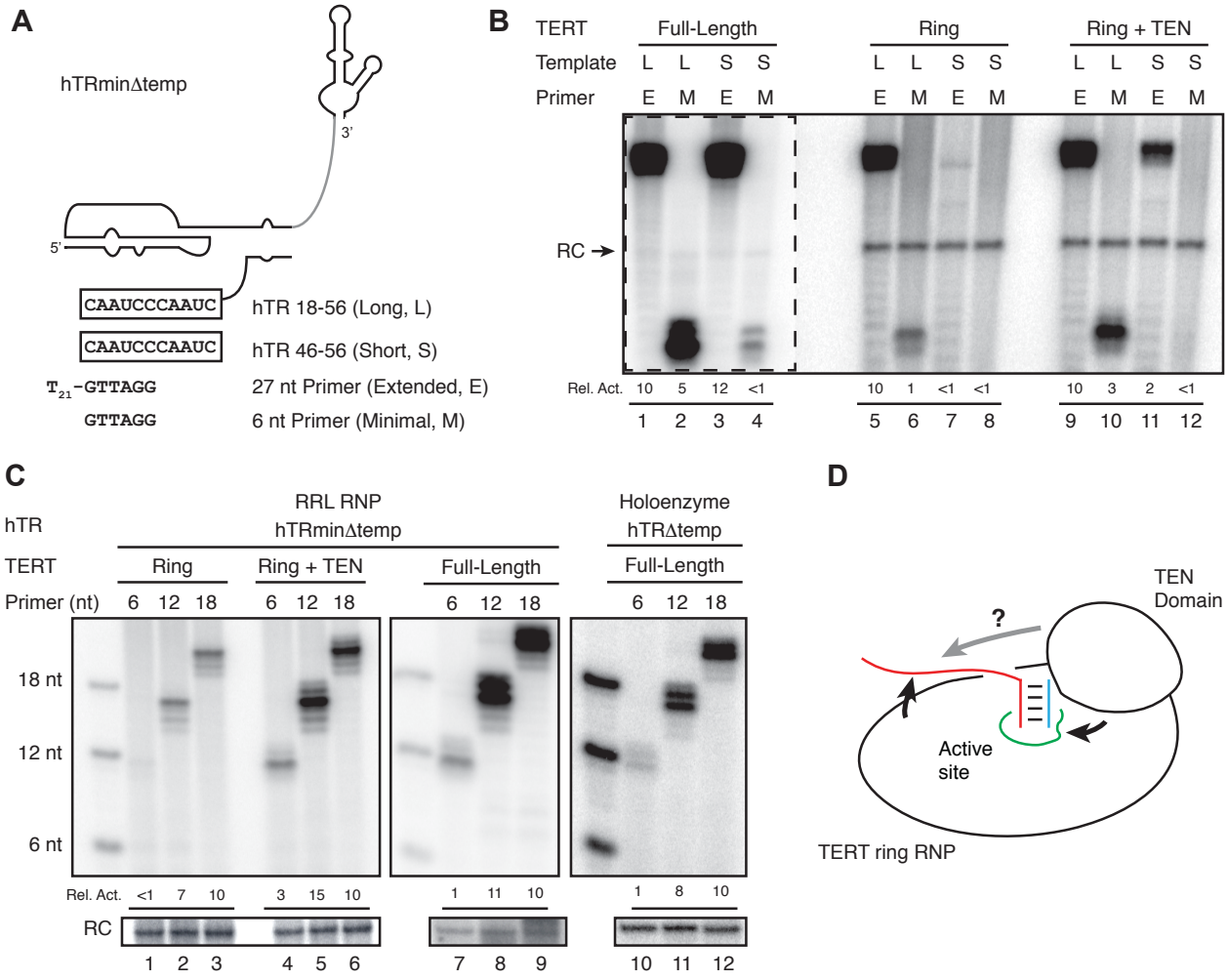
A
hTRminΔtemp
3'
5'
CAAUCCCAAUC
hTR 18-56 (Long, L)
CAAUCCCAAUC
hTR 46-56 (Short, S)
T21-GTTAGG
27 nt Primer (Extended, E)
GTTAGG
6 nt Primer (Minimal, M)
B
TERT
Full-Length
Ring
Ring + TEN
Template
L L S S
Primer
E M E M
RC
Rel. Act.
10 5 12 <1
10 1 <1 <1
10 3 2 <1
1 2 3 4 5 6 7 8 9 10 11 12
C
hTR
RRL RNP
hTRminΔtemp
Holoenzyme
hTRΔtemp
TERT
Ring
Ring + TEN
Full-Length
Full-Length
Primer (nt)
6 12 18
18 nt
12 nt
6 nt
Rel. Act.
<1 7 10
3 15 10
1 11 10
1 8 10
RC
1 2 3 4 5 6 7 8 9 10 11 12
D
TEN
Domain
?
Active
site
TERT ring RNP

Figure 3.8 Primer single-stranded DNA stimulates the activity of TERT ring or full-length TERT assembled as telomerase holoenzyme.

(**A, B**) Activity of TERT ring holoenzyme RNP (**A**) or full-length TERT holoenzyme RNP (**B**) reconstituted in 293T cells with full-length hTR and assayed with 6 nt, 12 nt or 18 nt primers. The 5' single-stranded DNA extensions were either T-tract (T_n with n = 6 or 12) or telomeric-repeat [$(GTTAGG)_n$ with n = 1 or 2] sequence. For relative activity (Rel. Act.), product intensities were first subtracted for background signal then normalized to activity on the 18 nt primer within each set of assays.

Figure 3.8

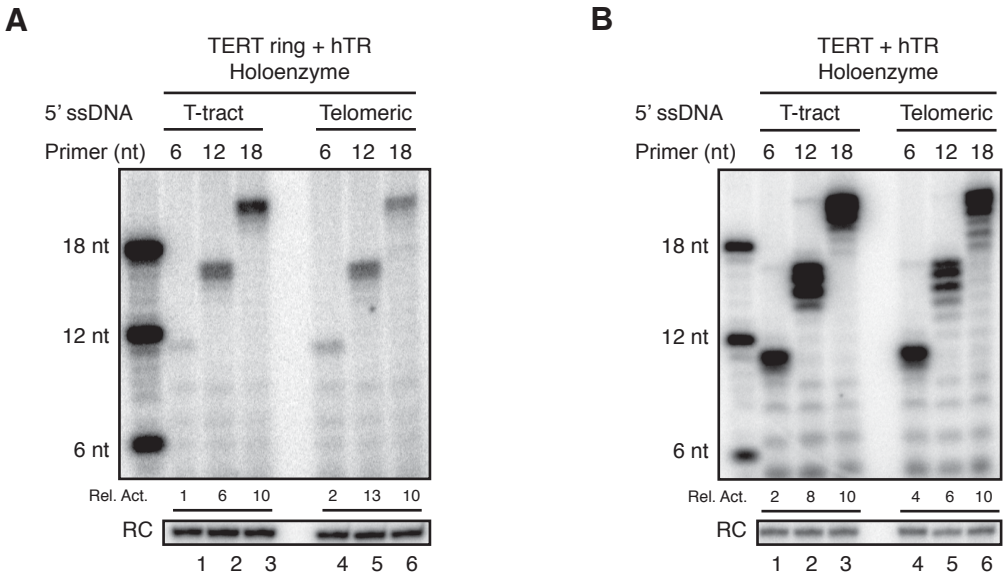
A
TERT ring + hTR
Holoenzyme
5' ssDNA
T-tract
Telomeric
Primer (nt)
6 12 18 6 12 18
18 nt
12 nt
6 nt
Rel. Act.
1 6 10 2 13 10
RC
1 2 3 4 5 6
B
TERT + hTR
Holoenzyme
5' ssDNA
T-tract
Telomeric
Primer (nt)
6 12 18 6 12 18
18 nt
12 nt
6 nt
Rel. Act.
2 8 10 4 6 10
RC
1 2 3 4 5 6

Figure 3.9 A limited length of telomerase product DNA is protected from ExoVII digestion.

(**A**) Schematic of the ExoVII protection assay. Bound DNA is labeled by addition of radiolabeled dGTP for 1 min, followed by treatment with ExoVII for 5 min. The protected, labeled DNA is extracted and resolved by denaturing PAGE.
(**B**) ExoVII protection assay using 12, 18, 24, 30 and 36 nt primers (T_n-GTTAGG with n = 6, 12, 18, 24, 30) with full-length TERT RNP reconstituted in 293T cells with full-length hTR. Unextended 5' end-labeled 6, 12, 18 and 27 nt oligonucleotides are shown as size markers.
(**C**) ExoVII protection assay using full-length TERT RNP reconstituted in 293T cells with full-length hTR and primer T_{21}-GTTAGG extended with radiolabeled dGTP with or without ddTTP (T*). Product DNA was left enzyme-bound or boiled. Boiled samples were supplemented with 2.5 μM hTR 46-56 to re-form the template hybrid. In this and subsequent Figures, undigested telomerase product DNA (U) and ExoVII-digested telomerase products (D) are indicated.

Figure 3.9

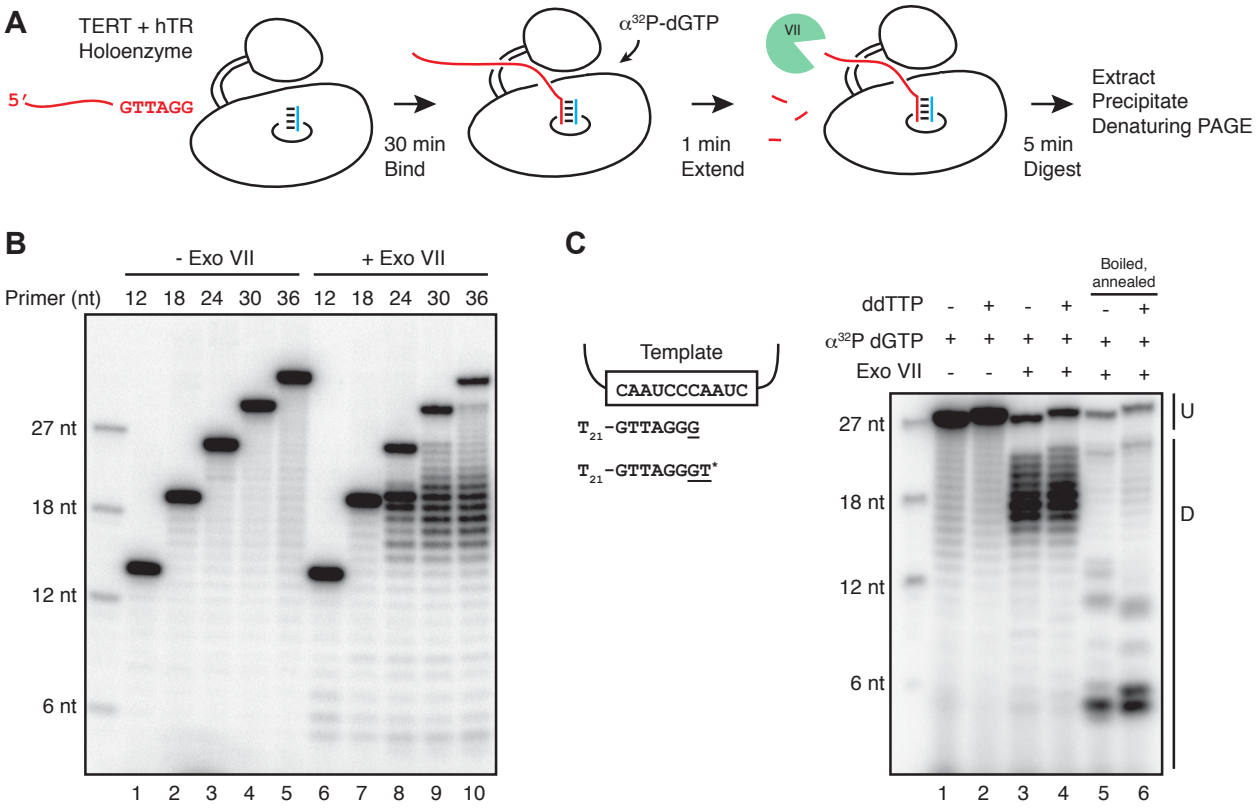
A
TERT + hTR
Holoenzyme
5′
GTTAGG
30 min
Bind
α32P-dGTP
1 min
Extend
VII
5 min
Digest
Extract
Precipitate
Denaturing PAGE
B
- Exo VII
+ Exo VII
Primer (nt) 12 18 24 30 36 12 18 24 30 36
27 nt
18 nt
12 nt
6 nt
1 2 3 4 5 6 7 8 9 10
C
Template
CAAUCCCAAUC
T21-GTTAGGG
T21-GTTAGGGT*
Boiled, annealed
ddTTP - + - + - +
α32P dGTP + + + + + +
Exo VII - - + + + +
27 nt
18 nt
12 nt
6 nt
U
D
1 2 3 4 5 6

Figure 3.10 ExoVII protection of product DNA is similar for holoenzyme and RRL-reconstituted RNPs.

(**A**) ExoVII protection of α-^{32}P dGTP-extended T_{21}-GTTAGG by immunopurified full-length TERT reconstituted in 293T cells with full-length hTR (lanes 1 and 2) or immunopurified full-length TERT RNP reconstituted in RRL with hTRmin (lanes 3 and 4). Unextended 5' end-labeled 6, 12, 18 and 27 nt oligonucleotides are shown as size markers.
(**B**) Product length profiles of ExoVII protection by holoenzyme RNP or RRL-reconstituted RNP from gel lanes in (**A**).

Figure 3.10

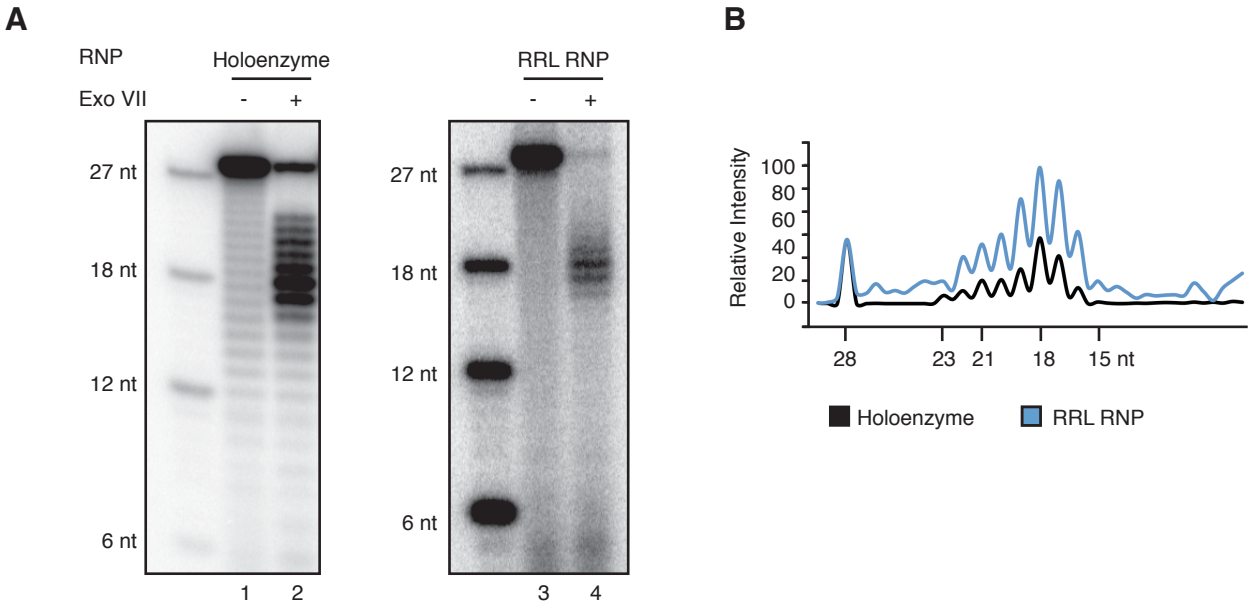
A
RNP
Holoenzyme
RRL RNP
Exo VII
- +
- +
27 nt
18 nt
12 nt
6 nt
27 nt
18 nt
12 nt
6 nt
1 2
3 4
B
Relative Intensity
100
80
60
40
20
0
28
23 21
18
15 nt
Holoenzyme
RRL RNP

Figure 3.11 Exonuclease VII protection of product DNA resolves roles of the TERT ring RNP and TEN domain in DNA handling.

(**A**) ExoVII protection of elongated T_{21}-GTTAGG using full-length TERT RNP or TERT ring RNP reconstituted in 293T cells with full-length hTR. Unextended 5' end-labeled 6, 12, 18 and 27 nt oligonucleotides are shown as size markers. The percentage of cleaved but protected product DNA is quantified relative to the total product amount before ExoVII digestion from a separate reaction shown in the adjacent lane.
(**B**) Protected product profiles for full-length TERT RNP and TERT ring RNP in the gel lanes from (**A**).
(**C**) Telomerase DNA handling includes TERT ring RNP interaction (⊳⊲) with single-stranded DNA and TEN domain stabilization of primer-template hybrid in the active site (i). Unresolved is whether the TEN domain has any contribution to binding of single-stranded DNA, using an interaction site integrated with or separable from DNA interaction by the TERT ring RNP (ii).

Figure 3.11

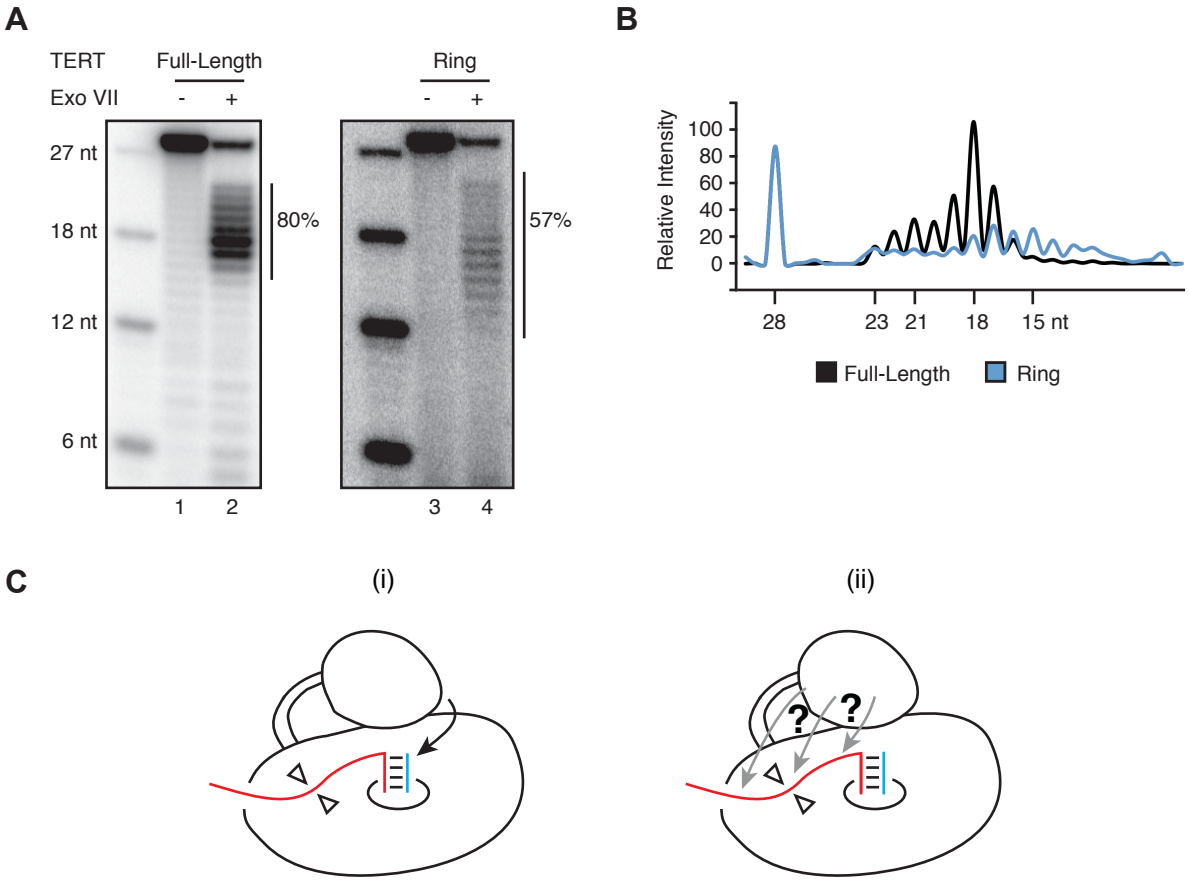
A
TERT
Exo VII
Full-Length
Ring
- +
- +
27 nt
18 nt
12 nt
6 nt
80%
57%
1 2
3 4
B
Relative Intensity
100
80
60
40
20
0
28
23 21
18
15 nt
Full-Length
Ring
C
(i)
(ii)
?
?

Figure 3.12 Changes in ExoVII protection of product DNA during a telomerase catalytic cycle.

(**A, B**) At left, schematic of the extent of DNA primer elongation prior to ExoVII treatment. Nucleotides added by primer extension are underlined, with asterisks denoting ddNTPs. At right, ExoVII footprinting with full-length TERT RNP (**A**) or TERT ring RNP (**B**) reconstituted in 293T cells with full-length hTR. Processive repeat synthesis by full-length TERT RNP was supported by adding unlabeled dGTP (dGTP) and incubating for 10 min before ExoVII digestion. Unextended 5' end-labeled 18 and/or 27 nt oligonucleotides are shown as size markers.
(**C**) Single-stranded DNA register does not change during active-site progression across the template, consistent with the model of a relatively constant length of single-stranded DNA (~11 nt) and an increasing length of product-template hybrid.

Figure 3.12

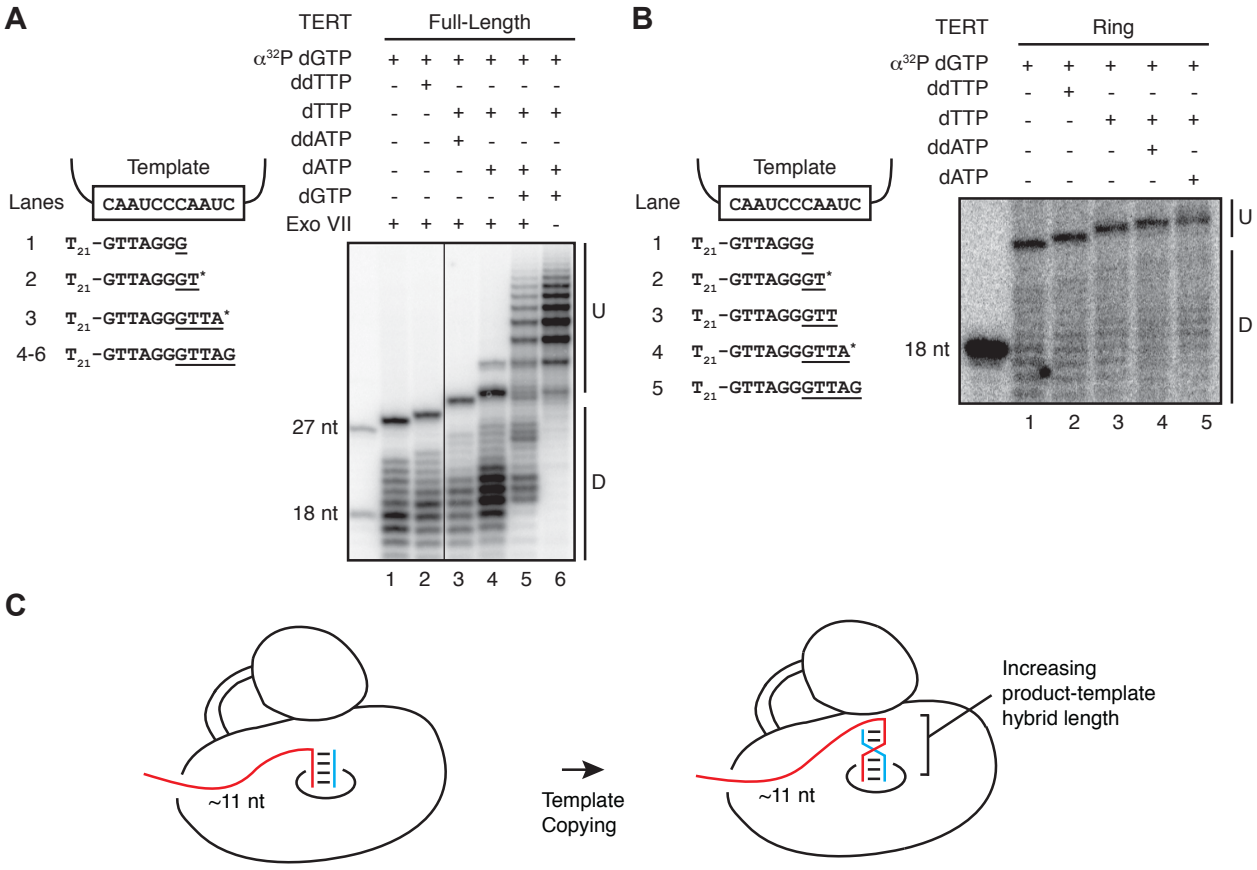
A
TERT
Full-Length
α32P dGTP + + + + + +
ddTTP - + - - - -
dTTP - - + + + +
ddATP - - + - - -
dATP - - - + + +
dGTP - - - - + +
Exo VII + + + + + -
Template
Lanes
CAAUCCCAAUC
1 T21-GTTAGGG
2 T21-GTTAGGGT*
3 T21-GTTAGGGTTA*
4-6 T21-GTTAGGGTTAG
27 nt
18 nt
U
D
1 2 3 4 5 6
B
TERT
Ring
α32P dGTP + + + + +
ddTTP - + - - -
dTTP - - + + +
ddATP - - - + -
dATP - - - - +
Template
Lane
CAAUCCCAAUC
1 T21-GTTAGGG
2 T21-GTTAGGGT*
3 T21-GTTAGGGTT
4 T21-GTTAGGGTTA*
5 T21-GTTAGGGTTAG
18 nt
U
D
1 2 3 4 5
C
~11 nt
Template
Copying
~11 nt
Increasing
product-template
hybrid length

Figure 3.13 The length of product DNA protected from ExoVII increases with synthesis across the template.

Protected products of the full-length TERT RNP are shown from Figure 3.12A. At right, schematics of primer elongation prior to ExoVII treatment. Nucleotides added by primer extension are underlined, with an asterisk denoting a ddNTP. For ease of comparison, the predominant 18 nt length of protection after addition of a single radiolabeled dGTP is marked by the dashed blue line.

Figure 3.13

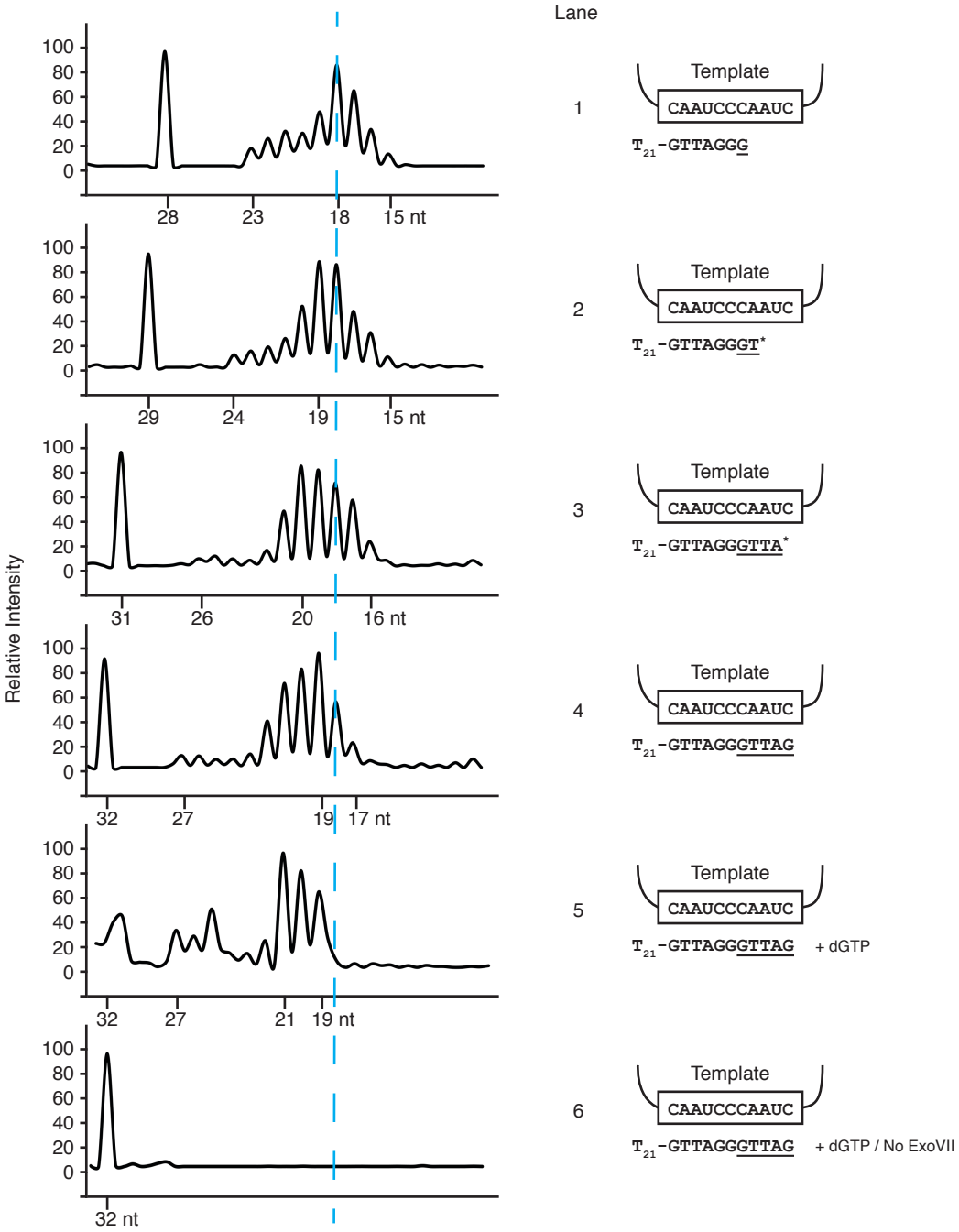
Lane
Relative Intensity
100
80
60
40
20
0
28
23
18
15 nt
1
Template
CAAUCCCAAUC
T21-GTTAGGG
29
24
19
15 nt
2
Template
CAAUCCCAAUC
T21-GTTAGGGT*
31
26
20
16 nt
3
Template
CAAUCCCAAUC
T21-GTTAGGGTTA*
32
27
19
17 nt
4
Template
CAAUCCCAAUC
T21-GTTAGGGTTAG
32
27
21
19 nt
5
Template
CAAUCCCAAUC
T21-GTTAGGGTTAG + dGTP
32 nt
6
Template
CAAUCCCAAUC
T21-GTTAGGGTTAG + dGTP / No ExoVII

Figure 3.14 ExoVII protects telomeric-repeat sequence DNA.

At left, schematic of elongation of the primer 3' end prior to ExoVII treatment. Nucleotides added by primer extension are underlined, with asterisks denoting a ddNTP. At right, ExoVII protection assay using the primer AGG$(GTTAGG)_4$ elongated by immunopurified full-length TERT RNP reconstituted in 293T cells with wild-type hTR. Undigested products (U) and ExoVII-digested products (D) are indicated. Unextended 5' end-labeled 18 nt oligonucleotide was run as a size marker.

Figure 3.14

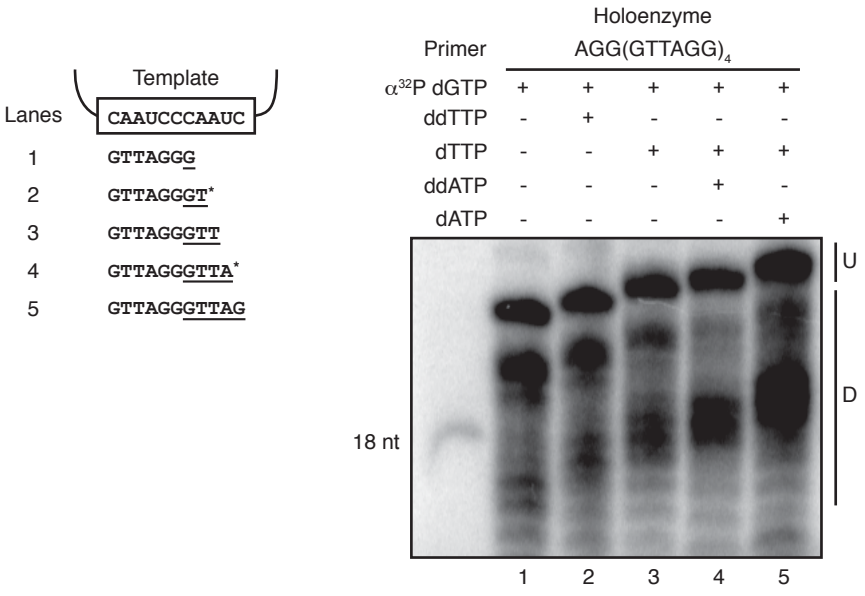
Template
Lanes
CAAUCCCAAUC
1 GTTAGGG
2 GTTAGGGT*
3 GTTAGGGTT
4 GTTAGGGTTA*
5 GTTAGGGTTAG
Holoenzyme
Primer
AGG(GTTAGG)4
α32P dGTP + + + + +
ddTTP - + - - -
dTTP - - + + +
ddATP - - - + -
dATP - - - - +
U
D
18 nt
1 2 3 4 5

Figure 3.15 Multiple specificities of primer-template hybrid recognition provide a new perspective on the telomerase catalytic cycle.

The stop sign indicates product-template hybrid determination of the template 5' boundary. See text for discussion.

Figure 3.15

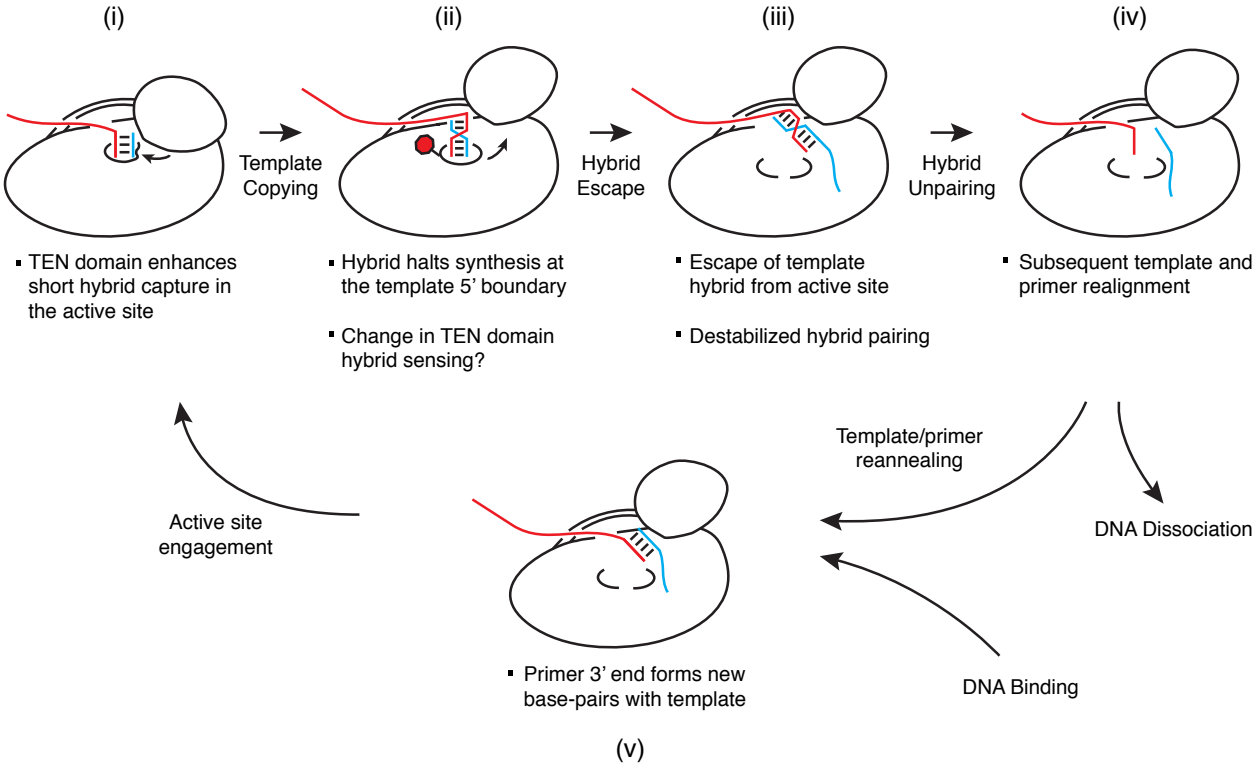
(i)
(ii)
(iii)
(iv)
Template Copying
Hybrid Escape
Hybrid Unpairing
▪ TEN domain enhances short hybrid capture in the active site
▪ Hybrid halts synthesis at the template 5' boundary
▪ Change in TEN domain hybrid sensing?
▪ Escape of template hybrid from active site
▪ Destabilized hybrid pairing
▪ Subsequent template and primer realignment
Template/primer reannealing
DNA Dissociation
Active site engagement
DNA Binding
▪ Primer 3' end forms new base-pairs with template
(v)

CHAPTER FOUR

Conclusions

The function of telomeres is essential for the preservation of genomic integrity in eukaryotes. In this work, we have seen that telomerase, the polymerase that maintains these chromosome ends, accomplishes its unique activity using a specialized catalytic cycle (Figure 4.1). Two important and difficult questions regarding the mechanism of the telomerase catalytic cycle were addressed. Does it require the cooperation of two reverse transcriptase subunits? And what roles do the specialized domains of the reverse transcriptase and RNA subunits play in its mechanism? In this final chapter, I consider some implications of the answers we have found to these questions.

The stoichiometry of the active human telomerase RNP has been challenging to discern using bulk biochemical methods and its resolution required the development of new approaches that interrogate single molecules of telomerase complexes. The observations I made while searching for the active complex explain why the new experimental approaches were necessary in the first place. We now know that human telomerase reconstitution generates heterogeneous mixtures of complexes (Wu et al., 2015). Sample heterogeneity presents challenges for the interpretation of biochemical experiments, and therefore necessitates the development of assays that discriminate for the active enzyme. This is particularly true when physical approaches such as co-purification or crosslinking are used. The presence of many subpopulations also hinders the quest to obtain human telomerase structural models. Armed with a more complete knowledge of how TERT expression, purification and the TERT PAL influence the ratio of these subpopulations, we are much closer to overcoming these challenges.

The most important conclusion from the single-molecule studies is that telomerase RNPs with one TERT molecule are active. This confines the question of how the specialized domains of TERT and hTR function to establish nucleic acid handling specificities involved in the telomerase catalytic cycle to interactions between one TERT and one hTR. Still, these mechanisms are difficult to dissect, in part because telomerase specializations are involved in a network of protein-protein and protein-nucleic acid interactions and approaches other than mutagenesis are required to isolate these functional interactions. We developed assays sensitized to detect these functions using TERT domain trans-complementation in combination with a physically detached template RNA oligonucleotide (Wu and Collins, 2014a). It would not have been surprising to discover that an interaction between the TEN domain and the single-stranded DNA product confers anchor site function, which would have been in agreement with the current models at the time (Wyatt et al., 2010; Lewis and Wuttke, 2012; Podlevsky and Chen, 2012; Nandakumar and Cech, 2013). Instead, we demonstrated using biochemical and physical approaches that the TEN domain is critical for RAP by improving the use of a short primer-template duplex. Since this result has been reported, the conclusion that the TEN domain impacts short primer-template duplex placement in the active site has been corroborated by single-molecule fluorescence resonance energy transfer (FRET) experiments in *T. thermophila* telomerase (Akiyama et al., 2015).

The finding that a TERT domain key for RAP actually acts through short duplex recognition redirects our focus to a previously underappreciated aspect of telomerase specialization – the unique ways in which the active site handles the primer-template duplex contribute importantly to the mechanism of the human telomerase catalytic cycle. Many of the specificities that occur through the catalytic cycle, including the initial engagement of the atypically short primer-template duplex (Figure 4.1, Step 1), the template 5' boundary definition (Figure 4.1, Step 3), and primer-template strand separation (Figure 4.1, Step 5), may in fact be specializations of duplex handling. As one example, Julian Chen's group has reported that a sequence signal within the template specifies when repeat synthesis halts prior to the steps that lead to strand separation and next repeat synthesis (Brown et al., 2014).

Among the remaining questions about the catalytic cycle, one is particularly interesting and difficult: how do the DNA and template strands separate during the progression from a pre-translocation duplex to template translocation (Figure 4.1, Steps 4 through 6)? These states are highly challenging to probe biochemically because the DNA-enzyme interactions involved are quite likely to be highly dynamic. Yet their dynamics also mean that they are unlikely to be captured by structural techniques. Single-molecule FRET studies reveal dynamic interconversion of FRET states when repeat synthesis nears completion (Parks and Stone, 2014). The DNA- and template-position and base-pairing status these states represent are open to interpretation (Wu and Collins, 2014b). We propose that this pre-translocation state represents DNA strand occupation of a nascent product binding site. This protein-DNA interaction is predicted to occur before template translocation and may promote DNA-template strand separation. Atomic resolution models of the translesion DNA polymerase Pol ν reveal a cavity along the protein surface adjacent to the primer strand and a thumb domain capable of rotating to allow primer strand escape from the active site to occupy the cavity (Lee et al., 2015). TERT possesses insertions necessary to form a similar cavity and enable large thumb domain rotations, providing a potential structural basis for the putative nascent product binding site and a mechanism for how it might be filled (Yang and Lee, 2015). The sequence-specified pause in repeat synthesis described by Brown et al. may allow nascent product binding site sampling, or it may be a reflection of the site's sequence specificity. These exciting hypotheses await testing by mutating the important TERT insertions and assaying for their effect on translocation activity, in combination with the DNA nuclease protection assay described in Chapter Three to detect product strand movements and chemical modification protection to assay the state of DNA-template base-pairing.

An important motivation for determining the mechanisms of the telomerase catalytic cycle is understanding how telomerase activity might be regulated. Eukaryotic cells maintain telomere length homeostasis at a length specific to each species and even to specific cell types (Shore and Bianchi, 2009). We do not yet understand the mechanisms by which telomere length-based feedback regulation of telomerase activity at telomeres is accomplished (Hockemeyer and Collins, 2015). An interesting possibility is the modulation of RAP by shelterin (Wang et al., 2007), but surprisingly the significance of RAP in telomere length maintenance is not well understood. Answering these questions

will require knowledge of the determinants of telomerase processivity and observing the effects of their in vivo manipulation on telomere length. Another interesting question is how entry into and exit from the telomerase catalytic cycle is controlled at the telomere. That is, is initial engagement of the telomere overhang regulated by a separate step (e.g. replication fork progression through the telomere)? Is termination of processive synthesis coupled to other complexes or events (e.g. binding of single-stranded products or initiation of C-strand synthesis)? The answers to these questions await our ability to reconstitute increasingly complex reactions coupled to the telomerase catalytic cycle.

Figure 4.1 Model for nucleic acid handling specificities involved in the human telomerase catalytic cycle.

This work has shown that specialized primer-template duplex sensing by a human telomerase complex containing one TERT subunit enables multiple steps of the telomerase catalytic cycle. The TEN domain may be involved in initial duplex formation (Step 1), binding (Step 2) and/or primer extension (Step 3). We also demonstrate that specification of the template 5' boundary relies on sensing of duplex sequence and length (Step 3). After repeat synthesis completes, the single-stranded DNA product could fill a nascent product binding site (Step 4). This site could be analogous to the DNA Pol n cavity that enables primer loop-out (Lee et al., 2015; Yang and Lee, 2015). Nascent product binding may promote DNA-template strand separation (Step 5).

Figure 4.1

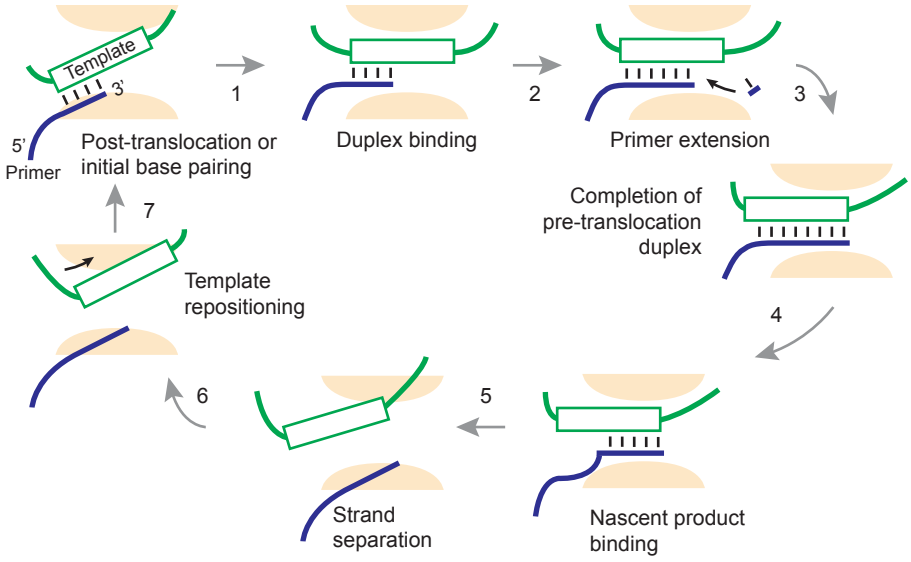
Template
3'
5'
Primer
Post-translocation or
initial base pairing
1
Duplex binding
2
Primer extension
3
Completion of
pre-translocation
duplex
4
Nascent product
binding
5
Strand
separation
6
Template
repositioning
7

REFERENCES

Alder, J. K., Cogan, J. D., Brown, A. F., Anderson, C. J., Lawson, W. E., Lansdorp, P. M., Phillips III, J. A., Loyd, J. E., Chen, J. J. L., & Armanios, M. (2011). Ancestral mutation in telomerase causes defects in repeat addition processivity and manifests as familial pulmonary fibrosis. *PLoS Genetics*, *7*(3), e1001352.

Alves, D., Li, H., Codrington, R., Orte, A., Ren, X., Klenerman, D., & Balasubramanian, S. (2008). Single-molecule analysis of human telomerase monomer. *Nature Chemical Biology*, *4*(5), 287-289.

Akiyama, B. M., Parks, J. W., & Stone, M. D. (2015). The telomerase essential N-terminal domain promotes DNA synthesis by stabilizing short RNA–DNA hybrids. *Nucleic Acids Research*, *43*(11), 5537-5549.

Armanios, M., & Blackburn, E. H. (2012). The telomere syndromes. *Nature Reviews Genetics*, *13*(10), 693-704.

Armanios, M., Chen, J. L., Chang, Y. P. C., Brodsky, R. A., Hawkins, A., Griffin, C. A., Eshleman, J. R., Cohen, A. R., Chakravarti, A., Homosh, A., & Greider, C. W. (2005). Haploinsufficiency of telomerase reverse transcriptase leads to anticipation in autosomal dominant dyskeratosis congenita. *Proceedings of the National Academy of Sciences of the United States of America*, *102*(44), 15960-15964.

Armbruster, B. N., Banik, S. S., Guo, C., Smith, A. C., & Counter, C. M. (2001). N-terminal domains of the human telomerase catalytic subunit required for enzyme activity in vivo. *Molecular and Cellular Biology*, *21*(22), 7775-7786.

Bairley, R. C., Guillaume, G., Vega, L. R., & Friedman, K. L. (2011). A mutation in the catalytic subunit of yeast telomerase alters primer–template alignment while promoting processivity and protein–DNA binding. *Journal of Cell Science*, *124*(24), 4241-4252.

Bajon, E., Laterreur, N., & Wellinger, R. J. (2015). A single templating RNA in yeast telomerase. *Cell Reports*, *12*(3), 441-448.

Belshaw, P. J., Walsh, C. T., & Stachelhaus, T. (1999). Aminoacyl-CoAs as probes of condensation domain selectivity in nonribosomal peptide synthesis. *Science*, *284*(5413), 486-489.

Berman, A. J., Akiyama, B. M., Stone, M. D., & Cech, T. R. (2011). The RNA accordion model for template positioning by telomerase RNA during telomeric DNA synthesis. *Nature Structural & Molecular Biology*, *18*(12), 1371-1375.

Bernards, A., Michels, P. A., Lincke, C. R., & Borst, P. (1983). Growth of chromosome ends in multiplying trypanosomes. *Nature*, *303*(5918), 592-597.

Biessmann, H., & Mason, J. M. (1997). Telomere maintenance without telomerase. *Chromosoma*, *106*(2), 63-69.

Blackburn, E. H. (1990). Telomeres: structure and synthesis. *Journal of Biological Chemistry*, *265*(11), 5919-5921.

Blackburn, E. H., Budarf, M. L., Challoner, P. B., Cherry, J. M., Howard, E. A., Katzen, A. L., Pan, W. C., & Ryan, T. (1983). DNA termini in ciliate macronuclei. In *Cold Spring Harbor Symposia on Quantitative Biology* (Vol. 47, pp. 1195-1207). Cold Spring Harbor Laboratory Press.

Blackburn, E. H., & Collins, K. (2011). Telomerase: an RNP enzyme synthesizes DNA. *Cold Spring Harbor Perspectives in Biology*, *3*(5), a003558.

Blackburn, E. H., & Gall, J. G. (1978). A tandemly repeated sequence at the termini of the extrachromosomal ribosomal RNA genes in *Tetrahymena*. *Journal of Molecular Biology*, *120*(1), 33-53.

Bodnar, A. G., Ouellette, M., Frolkis, M., Holt, S. E., Chiu, C. P., Morin, G. B., Harley, C. B., Shay, J. W., Lichtsteiner, S., & Wright, W. E. (1998). Extension of life-span by introduction of telomerase into normal human cells. *Science*, *279*(5349), 349-352.

Brown, A. F., Podlevsky, J. D., Qi, X., Chen, Y., Xie, M., & Chen, J. J. L. (2014). A self-regulating template in human telomerase. *Proceedings of the National Academy of Sciences of the United States of America*, *111*(31), 11311-11316.

Bryan, T. M., Englezou, A., Dalla-Pozza, L., Dunham, M. A., & Reddel, R. R. (1997). Evidence for an alternative mechanism for maintaining telomere length in human tumors and tumor-derived cell lines. *Nature Medicine*, *3*(11), 1271-1274.

Bryan, T. M., Goodrich, K. J., & Cech, T. R. (2003). *Tetrahymena* telomerase is active as a monomer. *Molecular Biology of the Cell*, *14*(12), 4794-4804.

Byers, D. M., & Gong, H. (2007). Acyl carrier protein: structure-function relationships in a conserved multifunctional protein family. *Biochemistry and Cell Biology*, *85*(6), 649-662.

Chan, D. I., & Vogel, H. J. (2010). Current understanding of fatty acid biosynthesis and the acyl carrier protein. *Biochemical Journal*, *430*(1), 1-19.

Chang, M., Arneric, M., & Lingner, J. (2007). Telomerase repeat addition processivity is increased at critically short telomeres in a Tel1-dependent manner in *Saccharomyces cerevisiae*. *Genes & Development*, *21*(19), 2485-2494.

Chapman, J. R., Taylor, M. R., & Boulton, S. J. (2012). Playing the end game: DNA double-strand break repair pathway choice. *Molecular Cell*, *47*(4), 497-510.

Chase, J. W., & Richardson, C. C. (1974). Exonuclease VII of *Escherichia coli*. Mechanism of Action. *Journal of Biological Chemistry*, *249*(14), 4553-4561.

Chen, J. L., & Greider, C. W. (2003). Template boundary definition in mammalian telomerase. *Genes & Development*, *17*(22), 2747-2752.

Chen, J. L., & Greider, C. W. (2005). Functional analysis of the pseudoknot structure in human telomerase RNA. *Proceedings of the National Academy of Sciences of the United States of America*, *102*(23), 8080-8085.

Chen, J. L., Opperman, K. K., & Greider, C. W. (2002). A critical stem–loop structure in the CR4–CR5 domain of mammalian telomerase RNA. *Nucleic Acids Research*, *30*(2), 592-597.

Ciccia, A., & Elledge, S. J. (2010). The DNA damage response: making it safe to play with knives. *Molecular Cell*, *40*(2), 179-204.

Cohen, S. B., Graham, M. E., Lovrecz, G. O., Bache, N., Robinson, P. J., & Reddel, R. R. (2007). Protein composition of catalytically active human telomerase from immortal cells. *Science*, *315*(5820), 1850-1853.

Coletta, A., Pinney, J. W., Solís, D. Y. W., Marsh, J., Pettifer, S. R., & Attwood, T. K. (2010). Low-complexity regions within protein sequences have position-dependent roles. *BMC Systems Biology*, *4*(1), 1.

Collins, K. (2011). Single-stranded DNA repeat synthesis by telomerase. *Current Opinion in Chemical Biology*, *15*(5), 643-648.

Collins, K., & Greider, C. W. (1993). *Tetrahymena* telomerase catalyzes nucleolytic cleavage and nonprocessive elongation. *Genes & Development*, *7*(7b), 1364-1376.

Counter, C. M., Avilion, A. A., LeFeuvre, C. E., Stewart, N. G., Greider, C. W., Harley, C. B., & Bacchetti, S. (1992). Telomere shortening associated with chromosome instability is arrested in immortal cells which express telomerase activity. *EMBO Journal*, *11*(5), 1921-1929.

Counter, C. M., Hahn, W. C., Wei, W., Caddle, S. D., Beijersbergen, R. L., Lansdorp, P. M., Sedivy, J. M., & Weinberg, R. A. (1998). Dissociation among in vitro telomerase activity, telomere maintenance, and cellular immortalization. *Proceedings of the National Academy of Sciences of the United States of America*, *95*(25), 14723-14728.

Cunningham, D. D., & Collins, K. (2005). Biological and biochemical functions of RNA in the *Tetrahymena* telomerase holoenzyme. *Molecular and Cellular Biology*, *25*(11), 4442-4454.

Damm, K., Hemmann, U., Garin-Chesa, P., Hauel, N., Kauffmann, I., Priepke, H., Niestroj, C., Daiber, C., Enenkel, B., Guilliard, B., & Lauritsch, I. (2001). A highly selective telomerase inhibitor limiting human cancer cell proliferation. *EMBO Journal*, *20*(24), 6958-6968.

Darzacq, X., Kittur, N., Roy, S., Shav-Tal, Y., Singer, R. H., & Meier, U. T. (2006). Stepwise RNP assembly at the site of H/ACA RNA transcription in human cells. *Journal of Cell Biology*, *173*(2), 207-218.

Das, R., Laederach, A., Pearlman, S. M., Herschlag, D., & Altman, R. B. (2005). SAFA: semi-automated footprinting analysis software for high-throughput quantification of nucleic acid footprinting experiments. *RNA*, *11*(3), 344-354.

di Fagagna, F. D. A., Teo, S. H., & Jackson, S. P. (2004). Functional links between telomeres and proteins of the DNA-damage response. *Genes & Development*, *18*(15), 1781-1799.

Doksani, Y., & de Lange, T. (2014). The role of double-strand break repair pathways at functional and dysfunctional telomeres. *Cold Spring Harbor Perspectives in Biology*, *6*(12), a016576.

Drosopoulos, W. C., DiRenzo, R., & Prasad, V. R. (2005). Human telomerase RNA template sequence is a determinant of telomere repeat extension rate. *Journal of Biological Chemistry*, *280*(38), 32801-32810.

Eckert, B., & Collins, K. (2012). Roles of telomerase reverse transcriptase N-terminal domain in assembly and activity of *Tetrahymena* telomerase holoenzyme. *Journal of Biological Chemistry*, *287*(16), 12805-12814.

Egan, E. D., & Collins, K. (2010). Specificity and stoichiometry of subunit interactions in the human telomerase holoenzyme assembled in vivo. *Molecular and Cellular Biology*, *30*(11), 2775-2786.

Egan, E. D., & Collins, K. (2012a). Biogenesis of telomerase ribonucleoproteins. *RNA*, *18*(10), 1747-1759.

Egan, E. D., & Collins, K. (2012b). An enhanced H/ACA RNP assembly mechanism for human telomerase RNA. *Molecular and Cellular Biology*, *32*(13), 2428-2439.

Eickbush, T. H., & Jamburuthugoda, V. K. (2008). The diversity of retrotransposons and the properties of their reverse transcriptases. *Virus Research*, *134*(1), 221-234.

Emery, H. S., & Weiner, A. M. (1981). An irregular satellite sequence is found at the termini of the linear extrachromosomal rDNA in *Dictyostelium discoideum*. *Cell*, *26*(3), 411-419.

Errington, T. M., Fu, D., Wong, J. M., & Collins, K. (2008). Disease-associated human telomerase RNA variants show loss of function for telomere synthesis without dominant-negative interference. *Molecular and Cellular Biology*, *28*(20), 6510-6520.

Finger, S. N., & Bryan, T. M. (2008). Multiple DNA-binding sites in *Tetrahymena* telomerase. *Nucleic Acids Research*, *36*(4), 1260-1272.

Förstemann, K., & Lingner, J. (2005). Telomerase limits the extent of base pairing between template RNA and telomeric DNA. *EMBO Reports*, *6*(4), 361-366.

Fu, D., & Collins, K. (2003). Distinct biogenesis pathways for human telomerase RNA and H/ACA small nucleolar RNAs. *Molecular Cell*, *11*(5), 1361-1372.

Gall, J. G. (1990). Telomerase RNA: tying up the loose ends. *Nature*, *344*(6262), 108-109.

Gallardo, F., Laterreur, N., Cusanelli, E., Ouenzar, F., Querido, E., Wellinger, R. J., & Chartrand, P. (2011). Live cell imaging of telomerase RNA dynamics reveals cell cycle-dependent clustering of telomerase at elongating telomeres. *Molecular Cell*, *44*(5), 819-827.

George, N., Pick, H., Vogel, H., Johnsson, N., & Johnsson, K. (2004). Specific labeling of cell surface proteins with chemically diverse compounds. *Journal of the American Chemical Society*, *126*(29), 8896-8897.

Gilley, D., & Blackburn, E. H. (1996). Specific RNA residue interactions required for enzymatic functions of *Tetrahymena* telomerase. *Molecular and Cellular Biology*, *16*(1), 66-75.

Gillis, A. J., Schuller, A. P., & Skordalakes, E. (2008). Structure of the *Tribolium castaneum* telomerase catalytic subunit TERT. *Nature*, *455*(7213), 633-637.

Goldbach, R. W., Bollen-de Boer, J. E., Van Bruggen, E. F. J., & Borst, P. (1979). Replication of the linear mitochondrial DNA of *Tetrahymena pyriformis*. *Biochimica et Biophysica Acta (BBA)-Nucleic Acids and Protein Synthesis*, *562*(3), 400-417.

Greider, C. W. (1991). Telomerase is processive. *Molecular and Cellular Biology*, *11*(9), 4572-4580.

Greider, C. W., & Blackburn, E. H. (1985). Identification of a specific telomere terminal transferase activity in *Tetrahymena* extracts. *Cell*, *43*(2), 405-413.

Greider, C. W., & Blackburn, E. H. (1987). The telomere terminal transferase of *Tetrahymena* is a ribonucleoprotein enzyme with two kinds of primer specificity. *Cell*, *51*(6), 887-898.

Greider, C. W., & Blackburn, E. H. (1989). A telomeric sequence in the RNA of *Tetrahymena* telomerase required for telomere repeat synthesis. *Nature*, *337*(6205), 331-337.

Griffith, J. D., Comeau, L., Rosenfield, S., Stansel, R. M., Bianchi, A., Moss, H., & De Lange, T. (1999). Mammalian telomeres end in a large duplex loop. *Cell*, *97*(4), 503-514.

Hansen, D. T., Thiyagarajan, T., Larson, A. C., & Hansen, J. L. (2016). Telomerase repeat amplification protocol (TRAP) activity upon recombinant expression and purification of human telomerase in a bacterial system. *Protein Expression and Purification*, *123*, 6-13.

Harbi, D., Kumar, M., & Harrison, P. M. (2011). LPS-annotate: complete annotation of compositionally biased regions in the protein knowledgebase. *Database*, *2011*, baq031.

Hardy, C. D., Schultz, C. S., & Collins, K. (2001). Requirements for the dGTP-dependent Repeat Addition Processivity of Recombinant *Tetrahymena* Telomerase. *Journal of Biological Chemistry*, *276*(7), 4863-4871.

Henderson, E. R., & Blackburn, E. H. (1989). An overhanging 3'terminus is a conserved feature of telomeres. *Molecular and Cellular Biology*, *9*(1), 345-348.

Heumann, J. M. (1976). A model for replication of the ends of linear chromosomes. *Nucleic Acids Research*, *3*(11), 3167-3172.

Hockemeyer, D., & Collins, K. (2015). Control of human telomerase action at telomeres. *Nature Structural & Molecular Biology*, *22*(11), 848-852.

Hong, K., Upton, H., Miracco, E. J., Jiang, J., Zhou, Z. H., Feigon, J., & Collins, K. (2013). *Tetrahymena* telomerase holoenzyme assembly, activation, and inhibition by domains of the p50 central hub. *Molecular and Cellular Biology*, *33*(19), 3962-3971.

Ishikawa, F., & Naito, T. (1999). Why do we have linear chromosomes? A matter of Adam and Eve. *Mutation Research/DNA Repair*, *434*(2), 99-107.

Jacobs, S. A., Podell, E. R., & Cech, T. R. (2006). Crystal structure of the essential N-terminal domain of telomerase reverse transcriptase. *Nature Structural & Molecular Biology*, *13*(3), 218-225.

Jiang, J., Miracco, E. J., Hong, K., Eckert, B., Chan, H., Cash, D. D., Min, B., Zhou, Z. H., Collins, K., & Feigon, J. (2013). The architecture of *Tetrahymena* telomerase holoenzyme. *Nature*, *496*(7444), 187-192.

Johnson, E. M. (1980). A family of inverted repeat sequences and specific single-strand gaps at the termini of the *Physarum* rDNA palindrome. *Cell*, *22*(3), 875-886.

Jurczyluk, J., Nouwens, A. S., Holien, J. K., Adams, T. E., Lovrecz, G. O., Parker, M. W., Cohen, S. B., & Bryan, T. M. (2010). Direct involvement of the TEN domain at the active site of human telomerase. *Nucleic Acids Research*, *39*(5), 1774-1788.

Kato, M., Han, T. W., Xie, S., Shi, K., Du, X., Wu, L. C., Mirzaei H., Goldsmith, E. J., Longgood, J., Pei, J., & Grishin, N. V. (2012). Cell-free formation of RNA granules: low complexity sequence domains form dynamic fibers within hydrogels. *Cell*, *149*(4), 753-767.

Kohlstaedt, L. A., Wang, J., Friedman, J. M., Rice, P. A., & Steitz, T. A. (1992). Crystal structure at 3.5 Å resolution of HIV-1 reverse transcriptase complexed with an inhibitor. *Science*, *256*(5065), 1783-1790.

Lai, C. K., Miller, M. C., & Collins, K. (2002). Template boundary definition in *Tetrahymena* telomerase. *Genes & Development*, *16*(4), 415-420.

Lai, C. K., Mitchell, J. R., & Collins, K. (2001). RNA binding domain of telomerase reverse transcriptase. *Molecular and Cellular Biology*, *21*(4), 990-1000.

Lee, M. S., & Blackburn, E. H. (1993). Sequence-specific DNA primer effects on telomerase polymerization activity. *Molecular and Cellular Biology*, *13*(10), 6586-6599.

Lee, Y. S., Gao, Y., & Yang, W. (2015). How a homolog of high-fidelity replicases conducts mutagenic DNA synthesis. *Nature Structural & Molecular Biology*, *22*(4), 298-303.

Lewis, K. A., & Wuttke, D. S. (2012). Telomerase and telomere-associated proteins: structural insights into mechanism and evolution. *Structure*, *20*(1), 28-39.

Lin, J., Smith, D. L., & Blackburn, E. H. (2004). Mutant telomere sequences lead to impaired chromosome separation and a unique checkpoint response. *Molecular Biology of the Cell*, *15*(4), 1623-1634.

Lingner, J., Hughes, T. R., Shevchenko, A., Mann, M., Lundblad, V., & Cech, T. R. (1997). Reverse transcriptase motifs in the catalytic subunit of telomerase. *Science*, *276*(5312), 561-567.

Linger, B. R., & Price, C. M. (2009). Conservation of telomere protein complexes: shuffling through evolution. *Critical Reviews in Biochemistry and Molecular Biology*, *44*(6), 434-446.

Livengood, A. J., Zaug, A. J., & Cech, T. R. (2002). Essential regions of *Saccharomyces cerevisiae* telomerase RNA: separate elements for Est1p and Est2p interaction. *Molecular and Cellular Biology*, *22*(7), 2366-2374.

Lue, N. F. (2005). A physical and functional constituent of telomerase anchor site. *Journal of Biological Chemistry*, *280*(28), 26586-26591.

Lue, N. F., Yu, E. Y., & Lei, M. (2013). A popular engagement at the ends. *Nature Structural & Molecular Biology*, *20*(1), 10-12.

Lundblad, V., & Blackburn, E. H. (1993). An alternative pathway for yeast telomere maintenance rescues *est1*− senescence. *Cell*, *73*(2), 347-360.

Ly, H., Blackburn, E. H., & Parslow, T. G. (2003). Comprehensive structure-function analysis of the core domain of human telomerase RNA. *Molecular and Cellular Biology*, *23*(19), 6849-6856.

Mason, D. X., Goneska, E., & Greider, C. W. (2003). Stem-loop IV of *Tetrahymena* telomerase RNA stimulates processivity in trans. *Molecular and Cellular Biology*, *23*(16), 5606-5613.

McClintock, B. (1941). The stability of broken ends of chromosomes in *Zea mays*. *Genetics*, *26*(2), 234-282.

McClintock, B. (1942). The fusion of broken ends of chromosomes following nuclear fusion. *Proceedings of the National Academy of Sciences of the United States of America*, *28*(11), 458-463.

McElligott, R., & Wellinger, R. J. (1997). The terminal DNA structure of mammalian chromosomes. *EMBO Journal*, *16*(12), 3705-3714.

Miller, M. C., & Collins, K. (2002). Telomerase recognizes its template by using an adjacent RNA motif. *Proceedings of the National Academy of Sciences of the United States of America*, *99*(10), 6585-6590.

Mimitou, E. P., & Symington, L. S. (2009). DNA end resection: many nucleases make light work. *DNA Repair*, *8*(9), 983-995.

Min, B., & Collins, K. (2009). An RPA-related sequence-specific DNA-binding subunit of telomerase holoenzyme is required for elongation processivity and telomere maintenance. *Molecular Cell*, *36*(4), 609-619.

Min, B., & Collins, K. (2010). Multiple mechanisms for elongation processivity within the reconstituted *Tetrahymena* telomerase holoenzyme. *Journal of Biological Chemistry*, *285*(22), 16434-16443.

Mitchell, J. R., Cheng, J., & Collins, K. (1999). A box H/ACA small nucleolar RNA-like domain at the human telomerase RNA 3′ end. *Molecular and Cellular Biology*, *19*(1), 567-576.

Mitchell, J. R., & Collins, K. (2000). Human telomerase activation requires two independent interactions between telomerase RNA and telomerase reverse transcriptase. *Molecular Cell*, *6*(2), 361-371.

Moriarty, T. J., Marie-Egyptienne, D. T., & Autexier, C. (2004). Functional organization of repeat addition processivity and DNA synthesis determinants in the human telomerase multimer. *Molecular and Cellular Biology*, *24*(9), 3720-3733.

Moriarty, T. J., Marie-Egyptienne, D. T., & Autexier, C. (2005). Regulation of 5′ template usage and incorporation of noncognate nucleotides by human telomerase. *RNA*, *11*(9), 1448-1460.

Morin, G. B. (1989). The human telomere terminal transferase enzyme is a ribonucleoprotein that synthesizes TTAGGG repeats. *Cell*, *59*(3), 521-529.

Morin, G. B. (1991). Recognition of a chromosome truncation site associated with α-thalassaemia by human telomerase. *Nature, 353*(6343), 454-456

Moyzis, R. K., Buckingham, J. M., Cram, L. S., Dani, M., Deaven, L. L., Jones, M. D., Meyne J., Ratliff, R. L., & Wu, J. R. (1988). A highly conserved repetitive DNA sequence, $(TTAGGG)_n$, present at the telomeres of human chromosomes. *Proceedings of the National Academy of Sciences of the United States of America*, *85*(18), 6622-6626.

Muller, H. J. (1938). The remaking of chromosomes. *Collecting Net*, *13*(198), 181-195.

Murnane, J. P. (2012). Telomere dysfunction and chromosome instability. *Mutation Research/Fundamental and Molecular Mechanisms of Mutagenesis*, *730*(1), 28-36.

Nakamura, T. M., & Cech, T. R. (1998). Reversing time: origin of telomerase. *Cell*, *92*(5), 587-590.

Nandakumar, J., & Cech, T. R. (2013). Finding the end: recruitment of telomerase to telomeres. *Nature Reviews Molecular Cell Biology*, *14*(2), 69-82.

O'Connor, C. M., Lai, C. K., & Collins, K. (2005). Two purified domains of telomerase reverse transcriptase reconstitute sequence-specific interactions with RNA. *Journal of Biological Chemistry*, *280*(17), 17533-17539.

Oganesian, L., Moon, I. K., Bryan, T. M., & Jarstfer, M. B. (2006). Extension of G-quadruplex DNA by ciliate telomerase. *EMBO Journal*, *25*(5), 1148-1159.

Olovnikov, A. M. (1973). A theory of marginotomy: the incomplete copying of template margin in enzymic synthesis of polynucleotides and biological significance of the phenomenon. *Journal of Theoretical Biology*, *41*(1), 181-190.

Palm, W., & de Lange, T. (2008). How shelterin protects mammalian telomeres. *Annual Review of Genetics*, *42*, 301-334.

Parks, J. W., & Stone, M. D. (2014). Coordinated DNA dynamics during the human telomerase catalytic cycle. *Nature Communications*, *5*.

Pascolo, E., Wenz, C., Lingner, J., Hauel, N., Priepke, H., Kauffmann, I., Garin-Chesa, P., Rettig, W. J., Damm, K., & Schnapp, A. (2002). Mechanism of human telomerase inhibition by BIBR1532, a synthetic, non-nucleosidic drug candidate. *Journal of Biological Chemistry*, *277*(18), 15566-15572.

Podlevsky, J. D., Bley, C. J., Omana, R. V., Qi, X., & Chen, J. J. L. (2008). The telomerase database. *Nucleic Acids Research*, *36*(suppl 1), D339-D343.

Podlevsky, J. D., & Chen, J. J. L. (2012). It all comes together at the ends: telomerase structure, function, and biogenesis. *Mutation Research/Fundamental and Molecular Mechanisms of Mutagenesis*, *730*(1), 3-11.

Qi, X., Xie, M., Brown, A. F., Bley, C. J., Podlevsky, J. D., & Chen, J. J. L. (2012). RNA/DNA hybrid binding affinity determines telomerase template-translocation efficiency. *EMBO Journal*, *31*(1), 150-161.

Qiao, F., & Cech, T. R. (2008). Triple-helix structure in telomerase RNA contributes to catalysis. *Nature Structural & Molecular Biology*, *15*(6), 634-640.

Rambo, R. P., & Doudna, J. A. (2004). Assembly of an active group II intron-maturase complex by protein dimerization. *Biochemistry*, *43*(21), 6486-6497.

Robart, A. R., & Collins, K. (2010). Investigation of human telomerase holoenzyme assembly, activity, and processivity using disease-linked subunit variants. *Journal of Biological Chemistry*, *285*(7), 4375-4386.

Robart, A. R., & Collins, K. (2011). Human telomerase domain interactions capture DNA for TEN domain-dependent processive elongation. *Molecular Cell*, *42*(3), 308-318.

Romi, E., Baran, N., Gantman, M., Shmoish, M., Min, B., Collins, K., & Manor, H. (2007). High-resolution physical and functional mapping of the template adjacent DNA binding site in catalytically active telomerase. *Proceedings of the National Academy of Sciences of the United States of America*, *104*(21), 8791-8796.

Sauerwald, A., Sandin, S., Cristofari, G., Scheres, S. H., Lingner, J., & Rhodes, D. (2013). Structure of active dimeric human telomerase. *Nature Structural & Molecular Biology*, *20*(4), 454-460.

Schmidt, J. C., & Cech, T. R. (2015). Human telomerase: biogenesis, trafficking, recruitment, and activation. *Genes & Development*, *29*(11), 1095-1105.

Schmidt, J. C., Dalby, A. B., & Cech, T. R. (2014). Identification of human TERT elements necessary for telomerase recruitment to telomeres. *eLife*, *3*, e03563.

Schnapp, G., Rodi, H. P., Rettig, W. J., Schnapp, A., & Damm, K. (1998). One-step affinity purification protocol for human telomerase. *Nucleic Acids Research*, *26*(13), 3311-3313.

Sealey, D. C., Zheng, L., Taboski, M. A., Cruickshank, J., Ikura, M., & Harrington, L. A. (2009). The N-terminus of hTERT contains a DNA-binding domain and is required for telomerase activity and cellular immortalization. *Nucleic Acids Research*, *38*(6), 2019-2035.

Sexton, A. N., Regalado, S. G., Lai, C. S., Cost, G. J., O'Neil, C. M., Urnov, F. D., Jaenisch, R., Collins, K., & Hockemeyer, D. (2014). Genetic and molecular identification of three human TPP1 functions in telomerase action: recruitment, activation, and homeostasis set point regulation. *Genes & Development*, *28*(17), 1885-1899.

Sexton, A. N., Youmans, D. T., & Collins, K. (2012). Specificity requirements for human telomere protein interaction with telomerase holoenzyme. *Journal of Biological Chemistry*, *287*(41), 34455-34464.

Shampay, J., Szostak, J. W., & Blackburn, E. H. (1983). DNA sequences of telomeres maintained in yeast. *Nature*, *310*(5973), 154-157.

Shippen-Lentz, D., & Blackburn, E. H. (1990). Functional evidence for an RNA template in telomerase. *Science*, *247*(4942), 546-552.

Shore, D., & Bianchi, A. (2009). Telomere length regulation: coupling DNA end processing to feedback regulation of telomerase. *EMBO Journal*, *28*(16), 2309-2322.

Soudet, J., Jolivet, P., & Teixeira, M. T. (2014). Elucidation of the DNA end-replication problem in *Saccharomyces cerevisiae*. *Molecular Cell*, *53*(6), 954-964.

Steitz, T. A. (1999). DNA polymerases: structural diversity and common mechanisms. *Journal of Biological Chemistry*, *274*(25), 17395-17398.

Steitz, T. A., & Steitz, J. A. (1993). A general two-metal-ion mechanism for catalytic RNA. *Proceedings of the National Academy of Sciences of the United States of America*, *90*(14), 6498-6502.

Szostak, J. W., & Blackburn, E. H. (1982). Cloning yeast telomeres on linear plasmid vectors. *Cell*, *29*(1), 245-255.

Theimer, C. A., Blois, C. A., & Feigon, J. (2005). Structure of the human telomerase RNA pseudoknot reveals conserved tertiary interactions essential for function. *Molecular Cell*, *17*(5), 671-682.

Tusell, L., Pampalona, J., Soler, D., Frías, C., & Genescà, A. (2010). Different outcomes of telomere-dependent anaphase bridges. *Biochemical Society Transactions*, *38*(6), 1698-1703.

Tzfati, Y., Fulton, T. B., Roy, J., & Blackburn, E. H. (2000). Template boundary in a yeast telomerase specified by RNA structure. *Science*, *288*(5467), 863-867.

Volff, J. N., & Altenbuchner, J. (2000). A new beginning with new ends: linearisation of circular chromosomes during bacterial evolution. *FEMS Microbiology Letters*, *186*(2), 143-150.

Wallweber, G., Gryaznov, S., Pongracz, K., & Pruzan, R. (2003). Interaction of human telomerase with its primer substrate. *Biochemistry*, *42*(2), 589-600.

Wang, F., Podell, E. R., Zaug, A. J., Yang, Y., Baciu, P., Cech, T. R., & Lei, M. (2007). The POT1–TPP1 telomere complex is a telomerase processivity factor. *Nature*, *445*(7127), 506-510.

Watson, J. D. (1972). Origin of concatemeric T7 DNA. *Nature*, *239*(94), 197-201.

Weinrich, S. L., Pruzan, R., Ma, L., Ouellette, M., Tesmer, V. M., Holt, S. E., Bodnar, A. G., Lichtsteiner, S., Kim, N. W., & Trager, J. B., Taylor, R. D., Carlos, R., Andrews, W. H., Wright, W. E., Shay, J. W., Harley, C. B., & Morin, G. B. (1997). Reconstitution of human telomerase with the template RNA component hTR and the catalytic protein subunit hTRT. *Nature Genetics*, *17*(4), 498-502.

Wellinger, R. J., Wolf, A. J., & Zakian, V. A. (1993). *Saccharomyces* telomeres acquire single-strand TG 1–3 tails late in S phase. *Cell*, *72*(1), 51-60.

Wenz, C., Enenkel, B., Amacker, M., Kelleher, C., Damm, K., & Lingner, J. (2001). Human telomerase contains two cooperating telomerase RNA molecules. *EMBO Journal*, *20*(13), 3526-3534.

Witkin, K. L., & Collins, K. (2004). Holoenzyme proteins required for the physiological assembly and activity of telomerase. *Genes & Development*, *18*(10), 1107-1118.

Wong, J. M., & Collins, K. (2006). Telomerase RNA level limits telomere maintenance in X-linked dyskeratosis congenita. *Genes & Development*, *20*(20), 2848-2858.

Wootton, J. C., & Federhen, S. (1993). Statistics of local complexity in amino acid sequences and sequence databases. *Computers & Chemistry*, *17*(2), 149-163.

Wu, R. A., & Collins, K. (2014a). Human telomerase specialization for repeat synthesis by unique handling of primer-template duplex. *EMBO Journal*, *33*(8), 921-935.

Wu, R. A., & Collins, K. (2014b). Sequence specificity of human telomerase. *Proceedings of the National Academy of Sciences of the United States of America*, *111*(31), 11234-11235.

Wu, R. A., Dagdas, Y. S., Yilmaz, S. T., Yildiz, A., & Collins, K. (2015). Single-molecule imaging of telomerase reverse transcriptase in human telomerase holoenzyme and minimal RNP complexes. *eLife*, *4*, e08363.

Wyatt, H. D., Lobb, D. A., & Beattie, T. L. (2007). Characterization of physical and functional anchor site interactions in human telomerase. *Molecular and Cellular Biology*, *27*(8), 3226-3240.

Wyatt, H. D., West, S. C., & Beattie, T. L. (2010). InTERTpreting telomerase structure and function. *Nucleic Acids Research*, *38*(17), 5609-5622.

Xi, L., & Cech, T. R. (2014). Inventory of telomerase components in human cells reveals multiple subpopulations of hTR and hTERT. *Nucleic Acids Research*, *42*(13), 8565-8577.

Xi, L., & Cech, T. R. (2015). Protein-RNA interaction restricts telomerase from running through the stop sign. *Nature Structural & Molecular Biology*, *22*(11), 835-836.

Xia, J., Peng, Y., Mian, I. S., & Lue, N. F. (2000). Identification of functionally important domains in the N-terminal region of telomerase reverse transcriptase. *Molecular and Cellular Biology*, *20*(14), 5196-5207.

Xin, H., Liu, D., Wan, M., Safari, A., Kim, H., Sun, W., O'Connor, M. S., & Songyang, Z. (2007). TPP1 is a homologue of ciliate TEBP-beta and interacts with POT1 to recruit telomerase. *Nature*, *445*(7127), 559-562.

Yang, J., & Eickbush, T. H. (1998). RNA-induced changes in the activity of the endonuclease encoded by the R2 retrotransposable element. *Molecular and Cellular Biology*, *18*(6), 3455-3465.

Yang, W., & Lee, Y. S. (2015). A DNA-hairpin model for repeat-addition processivity in telomere synthesis. *Nature Structural & Molecular Biology*, *22*(11), 844-847.

Yin, J., Lin, A. J., Golan, D. E., & Walsh, C. T. (2006). Site-specific protein labeling by Sfp phosphopantetheinyl transferase. *Nature Protocols*, *1*(1), 280-285.

Yin, J., Straight, P. D., McLoughlin, S. M., Zhou, Z., Lin, A. J., Golan, D. E., Kelleher, N. L., Kolter, R., & Walsh, C. T. (2005). Genetically encoded short peptide tag for versatile protein labeling by Sfp phosphopantetheinyl transferase. *Proceedings of the National Academy of Sciences of the United States of America*, *102*(44), 15815-15820.

Yu, G. L., Bradley, J. D., Attardi, L. D., & Blackburn, E. H. (1990). In vivo alteration of telomere sequences and senescence caused by mutated *Tetrahymena* telomerase RNAs. *Nature*, *344*(6262), 126-132.

Zaug, A. J., Crary, S. M., Fioravanti, M. J., Campbell, K., & Cech, T. R. (2013). Many disease-associated variants of hTERT retain high telomerase enzymatic activity. *Nucleic Acids Research*, *41*(19), 8969-8978.

Zaug, A. J., Podell, E. R., & Cech, T. R. (2008). Mutation in TERT separates processivity from anchor-site function. *Nature Structural & Molecular Biology*, *15*(8), 870-872.

Zaug, A. J., Podell, E. R., Nandakumar, J., & Cech, T. R. (2010). Functional interaction between telomere protein TPP1 and telomerase. *Genes & Development*, *24*(6), 613-622.

Zhang, Q., Kim, N. K., & Feigon, J. (2011). Architecture of human telomerase RNA. *Proceedings of the National Academy of Sciences of the United States of America*, *108*(51), 20325-20332.

Zhao, Y., Abreu, E., Kim, J., Stadler, G., Eskiocak, U., Terns, M. P., Terns, R. M., Shay, J. W., & Wright, W. E. (2011). Processive and distributive extension of human telomeres by telomerase under homeostatic and nonequilibrium conditions. *Molecular Cell*, *42*(3), 297-307.

Zhou, Z., Cironi, P., Lin, A. J., Xu, Y., Hrvatin, S., Golan, D. E., Silver, P. A., Walsh, C. T., & Yin, J. (2007). Genetically encoded short peptide tags for orthogonal protein labeling by Sfp and AcpS phosphopantetheinyl transferases. *ACS Chemical Biology*, *2*(5), 337-346.